Ellipsoidal figures of equilibrium – Compressible models

Article *in* The Astrophysical Journal Supplement Series · October 1993

DOI: 10.1086/191822 · Source: NTRS

3 authors, including:

Dong Lai
Cornell University
298 PUBLICATIONS **9,365** CITATIONS

SEE PROFILE

THE ASTROPHYSICAL JOURNAL SUPPLEMENT SERIES, 88:205–252, 1993 September

ELLIPSOIDAL FIGURES OF EQUILIBRIUM: COMPRESSIBLE MODELS

DONG LAI,[1] FREDERIC A. RASIO,[2,3] AND STUART L. SHAPIRO[1,4]
Center for Radiophysics and Space Research, Cornell University, Ithaca, NY 14853
Received 1992 September 21; accepted 1992 December 18

ABSTRACT

We present a new analytic study of ellipsoidal figures of equilibrium for compressible, self-gravitating Newtonian fluids. Using an energy variational method, we construct approximate hydrostatic equilibrium solutions for rotating polytropes, either isolated or in binary systems. Both uniformly and nonuniformly rotating configurations are considered. Compressible generalizations are given for most classical incompressible objects, such as Maclaurin spheroids, Jacobi, Dedekind, and Riemann ellipsoids, and Roche, Darwin, and Roche-Riemann binaries. The validity of our approximations is established by presenting detailed comparisons of our results to those of recent three-dimensional computational studies. Although our treatment is quite different, the presentation of our results follows closely that of Chandrasekhar in his work on the incompressible solutions using the tensor virial method. In the incompressible limit, our equilibrium solutions reduce exactly to those of Chandrasekhar. For binary systems, however, our analysis improves on previous results even in the incompressible limit. Our energy variational method can also be used to study the stability properties of the equilibrium solutions. Both secular and dynamical instability limits can be identified. For an isolated rotating star, we find that, when expressed in terms of the ratio $T/|W|$ of kinetic energy of rotation to gravitational binding energy, the stability limits for axisymmetric configurations to nonaxisymmetric perturbations are independent of compressibility in our approximation. We also study the effects of rotation and tidal forces on the radial stability of stars against gravitational collapse. Our most significant new results concern the stability properties of binary configurations. Along a Roche sequence parameterized by binary separation, we demonstrate the existence of a point where the total energy and angular momentum of the system simultaneously attain a *minimum*. A similar minimum exists for Darwin binaries when the polytropic index n of both components is below a critical value $n_{\rm crit} \approx 2$. We show that such a turning point along an equilibrium sequence marks the onset of secular instability. The instability occurs before the Roche limit is reached in Roche binaries, and before the surfaces of the two components come into contact in Darwin binaries. We point out the critical importance of this instability in determining the final evolution of coalescing binary systems.

Subject headings: binaries: close — hydrodynamics — stars: rotation

1. INTRODUCTION

Computers now make it possible to explore stellar hydrodynamic equilibria in more than one dimension. Examples of multidimensional stellar equilibria include uniformly rotating stars, stars with nonuniform internal motions, and stars in binary systems. Each of these fluid systems requires two or three spatial dimensions for a complete mathematical description.

While computer modeling of such configurations is a rapidly advancing science, it is useful to find simple analytic counterparts to the detailed results of numerical simulations. Simple and physically intuitive analytic results, even those based on crude approximations, are invaluable aids in interpreting the very large sets of numerical data produced by multidimensional computations. They are very helpful in reducing these data sets to simple, meaningful conclusions of astrophysical relevance. Often, however, adequate analytic models are not available in the literature.

In our recent work on hydrodynamic stellar interactions (e.g., Rasio & Shapiro 1992) we have frequently felt the need for approximate solutions for the equilibrium structure and stability properties of stars perturbed by rotation or tidal fields in close binary systems. By far the most complete source of information is the authoritative monograph by Chandrasekhar (1969, hereafter Ch69), *Ellipsoidal Figures of Equilibrium*. Unfortunately, this monograph treats solely the case of *incompressible* matter, whereas current numerical work deals mostly with *compressible* fluids and, in particular, polytropes.

The work presented here is our attempt at generalizing the results of Ch69 to polytropes, using a formalism as simple and physically intuitive as possible. Our approach is based on the use of an ellipsoidal energy variational principle to construct approximate stellar equilibrium solutions and study their stability. An energy variational technique very similar to ours was introduced at least as early as 1860 by Riemann (Riemann 1860; see also Lebovitz 1966, and Ch69, chap. 7) for exploring the properties of incompressible rotating configurations. Recently, ellipsoidal energy variational methods have been applied by Zel'dovich & Novikov (1971, hereafter ZN), Shapiro & Teukolsky (1983, hereafter ST), and others, to compressible (polytropic) configurations. In all of these recent applications,

[1] Department of Physics, Cornell University.
[2] Hubble Fellow.
[3] Current address: Institute for Advanced Study, Princeton, NJ 08540.
[4] Department of Astronomy, Cornell University.

the emphasis was on determining the effects of perturbations such as rotation, magnetic fields, or general relativity, on the stability of a star against gravitational collapse. In all cases, the equilibrium configurations considered were axisymmetric. In this paper we extend the method to study the equilibrium structure and stability properties of compressible, fully triaxial configurations. Single rotating stars, the compressible analogues of the classical Maclaurin, Jacobi, Dedekind, and Riemann-S ellipsoids, as well as stars in binary systems, generalizations of the Roche, Darwin, and Roche-Riemann problems, are all considered.

Exact solutions for all the equilibrium configurations considered here can be obtained in the *incompressible limit* (although for binaries, "exact" applies only to a truncated tidal interaction potential). Much of our modern knowledge about these exact triaxial solutions comes from the pioneering work of Chandrasekhar and his colleagues (see Ch69 and references therein) using the tensor virial (TV) method. In the incompressible limit, our energy variational method reproduces these exact equilibrium solutions. For compressible configurations, the method yields an approximate solution, equivalent to the use of an ellipsoidal trial function when extremizing the energy functional of the system. As in the TV treatment, our method replaces the full set of coupled hydrodynamic equilibrium equations—partial-differential equations in two or three dimensions—with two or three coupled *algebraic equations* for the principal axes of the configuration. Our discussion for compressible configurations makes extensive use of results derived in Ch69 for incompressible configurations. Hence we will frequently cite that reference for comparisons throughout this paper.

In the opposite limit of *highly compressible configurations* (polytropes with indices $n \geq 3$), the first-order perturbation technique of Monaghan & Roxburgh (1965) has been used successfully to calculate semianalytic equilibrium solutions (see, e.g., Martin 1970; Naylor & Anand 1970). In this technique the polytrope is divided into two regions. In the inner region the perturbing tidal and centrifugal forces are assumed to be small, and a linear perturbation of the Lane-Emden solution is used. In the outer region the density is assumed to be negligible so that the potential can be written as a solution of the Laplace equation. The two solutions are then matched at some critical radius. Clearly this method is only applicable to highly compressible, centrally condensed stars for which the two-region approximation is valid. An extreme version of the same approximation consists in replacing the stars by point masses embedded in gaseous envelopes of negligible density. This leads to the well-known Roche-type models for rotating stars and binary systems (Kopal 1959; Paczyński 1971; ST, §§ 7.4 and 13.7). Because they are essentially analytic, these models are widely employed, even for configurations which do not meet the criterion of high compressibility.

Little has been done analytically about the intermediate category of stars that are neither very centrally condensed nor quasi-homogeneous (effective polytropic index $0.5 \lesssim n \lesssim 2$). Many rotating and binary configurations of astrophysical relevance contain stars which belong precisely to this category. In particular, all low-mass white dwarf and main-sequence stars have $n \approx 1.5$, and all observed neutron stars (which have masses $M \approx 1.4\ M_\odot$) may very well have $n \approx 0.5$–1.0 (see ST, chap. 9, and Chau, Cheng, & Zhang 1992). The ellipsoidal approximation we adopt here is ideally suited to this mildly compressible regime.

Our ellipsoidal energy variational method to obtain equilibrium solutions is formally equivalent to the hydrostatic limit of the affine model developed by Carter & Luminet (1985; see also Luminet & Carter 1986). In that model a linear transformation matrix with time-dependent coefficients is introduced to approximate the Langrangian displacement of the fluid in a perturbed configuration. The model has been used to study a number of time-dependent problems, such as the tidal disruption of a star by a massive black hole (Carter & Luminet 1985) and the evolution of tidal-capture binaries in globular clusters (Kochanek 1992a). The ellipsoidal trial function which characterizes our approximation can be obtained as the static limit of the linear transformation used in the affine model. However, our treatment in this paper remains much closer to that of Ch69, and the language of the affine model is never introduced.

Fully numerical studies of rotating compressible stars, isolated or in binary systems, have become possible in recent years. The original treatments of rotating equilibria (see Tassoul 1978 for a comprehensive summary and references) have been considerably improved and can now be used to handle highly eccentric, rapidly rotating stars as well as nonaxisymmetric configurations (see Hachisu 1986a, b; Cook, Shapiro, & Teukolsky 1992, and references therein). The new methods are capable in principle of providing equilibrium solutions of great accuracy, even for very compressible configurations, provided of course that sufficient computer resources are available. Unfortunately, it is often difficult to derive physical insight from purely numerical data, especially in three dimensions. The recent numerical studies are very useful, however, in providing a reference against which the validity of our approximations can be tested.

The advantages of our energy variational approach come from its simplicity. All results are analytic or quasi-analytic, and usually lend themselves to straightforward physical interpretation. This is in part because the method deals directly with the global quantities of interest in most astrophysical problems, such as the various energies in the system. Moreover, once quantities like the total energy and angular momentum (conserved by the hydrodynamic equations for a perfect gas) are determined along an equilibrium sequence, the future evolution of the system can be tracked as it loses energy and angular momentum by some quasi-static dissipative process. Such an evolution can lead to the spin-up or spin-down of a rotating star due to radiation, viscosity, or gravitational-wave emission, and to the coalescence of close binary systems undergoing orbital decay by some similar mechanism. Astrophysical applications of great current interest include the spin evolution of millisecond pulsars (Shapiro, Teukolsky, & Nakamura 1990; Chau et al. 1992), the coalescence of neutron-star binaries and neutron-star-black-hole binaries (Clark & Eardley 1977; Nakamura & Oohara 1989; Kochanek 1992b; Rasio & Shapiro 1992, 1993), and the formation of blue stragglers and other binary mergers in globular cluster cores (Bailyn 1993; Rasio 1993).

Our paper is organized as follows. In § 2 we review briefly the energy variational method and describe our approximations.

We also establish several equivalent stability conditions and discuss secular versus dynamical instabilities. In §§ 3–5 we derive the equilibrium structure equations for isolated, rotating polytropes. Axisymmetric configurations (compressible Maclaurin spheroids) are considered briefly in § 3, but our efforts focus on triaxial configurations, either in a state of uniform rotation (generalizing the classical Jacobi ellipsoids), in § 4, or with internal fluid motions of uniform vorticity (the compressible analogues of Riemann-S ellipsoids), in § 5. The stability properties of these single star configurations are discussed in § 6. Secular stability against both axisymmetric and nonaxisymmetric perturbations is considered, as well as dynamical stability. In §§ 7 and 8 we solve the compressible generalizations of the Roche and Roche-Riemann problems for a polytrope in orbit about a point-mass companion. The stability of our binary equilibrium solutions is studied in § 9. Finally, in § 10 we consider the generalized Darwin problem for two identical polytropes in a binary.

2. METHOD AND APPROXIMATIONS

2.1. *The Energy Variational Method*

We consider an isolated, self-gravitating fluid system in steady state. The specific entropy is assumed to be constant throughout the fluid. The system is specified by conserved global quantities such as its total mass M, entropy S, and angular momentum J. The total energy of such a system, *not necessarily in equilibrium,* can always be written as a functional of the fluid density and velocity fields $\rho(\boldsymbol{x})$ and $\boldsymbol{v}(\boldsymbol{x})$,

$$E = E[\rho(\boldsymbol{x}), \boldsymbol{v}(\boldsymbol{x}); M, S, J, \ldots] . \tag{2.1}$$

It is well known that the equilibrium configuration of the system can be determined by extremizing this functional with respect to all variations of $\rho(\boldsymbol{x})$ and $\boldsymbol{v}(\boldsymbol{x})$ that leave the conserved quantities unchanged. The direct application of such a general variational principle to solve for multidimensional equilibrium configurations is in general a very difficult and computationally intensive task.

Great simplification is achieved if we can replace the infinite number of degrees of freedom contained in $\rho(\boldsymbol{x})$ and $\boldsymbol{v}(\boldsymbol{x})$ by a limited number of parameters $\alpha_1, \alpha_2, \ldots$, so that the total energy becomes a function of these parameters,

$$E = E(\alpha_1, \alpha_2, \ldots; M, S, J, \cdots) . \tag{2.2}$$

For sufficiently simple systems, it is often possible to write down directly an expression of this type for the energy, based on a set of simplifying assumptions. We will follow that approach in this paper. Our set of simplifying assumptions is described in § 2.2. Equivalently, an expression of the type (2.2) can be obtained by inserting *trial functions* with parameters α_i for $\rho(\boldsymbol{x})$ and $\boldsymbol{v}(\boldsymbol{x})$ in the general functional (2.1). We will not, however, refer explicitly to trial functions in our treatment.

Given an expression of the type (2.2), the equilibrium configuration of the system is determined by extremizing the energy according to

$$\frac{\partial E}{\partial \alpha_i} = 0, \quad i = 1, 2, \cdots \quad \text{(equilibrium)} , \tag{2.3}$$

where the partial derivatives are taken holding $M, S, J, \cdots$ constant.

A trivial example clearly illustrates the method (see ST, chap. 6 for other examples). Consider a spherical (nonrotating) configuration with mass M and radius R. Assume that the density and pressure profiles are those of a polytrope of index n, where

$$P = K\rho^{\Gamma}, \quad \Gamma = 1 + \frac{1}{n} , \tag{2.4}$$

but that R *is not necessarily the equilibrium radius* corresponding to the mass M and polytropic constant K. In place of R, we can introduce the central density

$$\rho_c = \frac{1}{3}\frac{\xi_1}{|\theta_1'|}\bar{\rho} = \frac{\xi_1}{4\pi|\theta_1'|}\frac{M}{R^3} , \tag{2.5}$$

where θ and ξ are the usual Lane-Emden variables for a polytrope (see, e.g., Chandrasekhar 1939). The total energy of such a configuration can be written in the form (2.2) as[5]

$$E(\rho_c; M) = U + W , \tag{2.6}$$

where U is the internal energy,

$$U = k_1 K \rho_c^{1/n} M , \tag{2.7}$$

W is the gravitational potential energy,

$$W = -\frac{3}{5-n}\frac{GM^2}{R} = -k_2 \rho_c^{1/3} G M^{5/3} , \tag{2.8}$$

and we have introduced two dimensionless constants (cf. ST § 6.10)

$$k_1 \equiv \frac{n(n+1)}{5-n}\xi_1|\theta_1'| , \tag{2.9}$$

$$k_2 \equiv \frac{3}{5-n}\left(\frac{4\pi|\theta_1'|}{\xi_1}\right)^{1/3} . \tag{2.10}$$

In equilibrium, ρ_c (or R) must be such that E is minimum. This implies

$$\frac{\partial E}{\partial \rho_c} = \frac{1}{n}\frac{U}{\rho_c} + \frac{1}{3}\frac{W}{\rho_c} = 0 , \tag{2.11}$$

which gives immediately the *virial relation,*

$$\frac{3}{n}U + W = 0 , \tag{2.12}$$

[5] The polytropic constant K is a function the entropy S. Since we consider only polytropes in this paper, we will henceforth omit S from the list of conserved quantities.

and, using equations (2.7) and (2.8), the equilibrium $M(\rho_c)$ relation for spherical polytropes,

$$M(\rho_c) = \left(\frac{3k_1K}{nk_2}\right)^{3/2} \rho_c^{(3-n)/2n}, \tag{2.13}$$

as well as the total *equilibrium* energy,

$$E_{\rm eq} = \frac{3-n}{3} W = -\frac{3-n}{5-n}\frac{GM^2}{R}. \tag{2.14}$$

2.2. *The Ellipsoidal Approximation*

To arrive at an expression of the type (2.2) for the energy of a rotating polytrope, we make two simplifying assumptions (ZN, chap. 11; ST, chap. 7). First, we assume that the surfaces of constant density (and constant pressure, since $P = K\rho^{\Gamma}$) are *self-similar ellipsoids*. The geometry of the configuration is then completely specified by the three principal axes of the outer surface (where $P = \rho = 0$), which we denote by a_1, a_2, and a_3. Under this assumption, the axis ratios a_2/a_1 and a_3/a_1 are the same for all interior isodensity surfaces. Our second assumption is that the density profile $\rho(m)$ (and the specific energy profile $u(m)$, since $u = nK\rho^{1/n}$), where m is the mass interior to an isodensity surface, is identical to that of a spherical polytrope of same K and n, but with radius $R = (a_1a_2a_3)^{1/3}$, that is, a spherical polytrope of same volume as the rotating configuration. It is important to note that R is *not*, in general, the equilibrium radius of that spherical polytrope (cf. the example at the end of § 2.1).[6] Both assumptions are strictly valid only in the incompressible ($n = 0$) limit (see Tassoul 1978, § 4.4). In this limit, our method can provide the *exact* equilibrium solution for any particular problem (as does the TV method of Ch69). In the general case where $n \neq 0$, it provides an approximation to the true equilibrium solution. Clearly we expect this approximation to be best for slowly rotating, nearly incompressible configurations, but we will see in this paper that our method yields, in fact, very good numerical results in all cases.

The ellipsoidal approximation adopted here is closely related to the "affine model" developed by Carter & Luminet (1985). In that model the positions of all fluid elements are linearly related to their initial positions in the spherical star through a time-dependent matrix. Deformation of the spherical star into an ellipsoidal configuration of the type described above is accomplished by such a linear transformation. Equivalently, we can think in terms of a density trial function $\rho_{\rm trial}(\boldsymbol{x}) = \rho_0(|\boldsymbol{Q}\cdot\boldsymbol{x}|)$, where $\rho_0(r)$ is the density profile of a spherical equilibrium polytrope, and $\boldsymbol{Q}$ is the matrix of an affine transformation. In the affine model a set of ordinary differential equations is derived for the evolution of the matrix elements $Q_{ij}(t)$. The static limit of these evolution equations is equivalent to the equilibrium structure equations obtained with our method. While the affine model is very useful for calculating numerically the approximate dynamical evolution of stellar models, our approach based on energy considerations is both simpler and more convenient for studying equilibrium configurations and identifying their stability limits.

[6] Both ZN and ST state this assumption incorrectly, indicating that a spherical surface of constant density in the (equilibrium) nonrotating star transforms into an ellipsoidal surface enclosing the same volume. This would imply that the central density ρ_c of all rotating configurations is the same as that of the nonrotating star. Instead, both ZN and ST proceed, as we do here, to vary ρ_c when extremizing the energy.

2.3. *Stability Conditions*

In general, stability requires that an equilibrium configuration correspond to a true *minimum* of the total energy $E(\alpha_1, \alpha_2, \ldots; M, J, \cdots)$, that is, that all eigenvalues of the matrix $(\partial^2 E/\partial\alpha_i\partial\alpha_j)_{eq}$ be positive. Here and throughout this paper, a subscript "*eq*" indicates a quantity evaluated in equilibrium (with all conditions [2.3] satisfied). The onset of instability along any one-parameter sequence of equilibrium configurations can be determined from the condition

$$\det\left(\frac{\partial^2 E}{\partial\alpha_i\partial\alpha_j}\right)_{\rm eq} = 0, \quad i,j = 1, 2, \cdots \quad \text{(onset of instability)}. \tag{2.15}$$

When this condition is first satisfied along the sequence, one of the eigenvalues must change sign. It may then become possible for the system to further minimize its energy by evolving away from the equilibrium configuration considered. In the space of the parameters α_i, the evolution should be in the direction of the eigenvector associated to the eigenvalue responsible for the realization of condition (2.15). Whether the instability actually arises depends on the presence of a dissipation mechanism which preserves the conservation laws built into the equilibrium model (see § 2.4). Moreover, since the approximations leading to expression (2.2) are equivalent to the use of a trial function to evaluate the general functional (2.1), the condition (2.15) is in general a *sufficient but not necessary* condition for instability (Hunter 1977).

It is easy to show that condition (2.15) is equivalent to the more familiar "turning point" or "static" method for locating the onset of instability (see Tassoul 1978, chap. 6, and ST, chap. 6). In this method a turning point along a certain equilibrium curve indicates the onset of instability along a one-parameter sequence of models. Consider, for example, an energy function of the form $E(\alpha_i; M, J)$. Differentiating the equilibrium conditions (2.3), we get

$$0 = \sum_j \left(\frac{\partial^2 E}{\partial\alpha_i\partial\alpha_j}\right) d\alpha_j + \left(\frac{\partial^2 E}{\partial\alpha_i\partial M}\right) dM + \left(\frac{\partial^2 E}{\partial\alpha_i\partial J}\right) dJ, \quad i = 1, 2, \ldots. \tag{2.16}$$

Now construct the one-parameter equilibrium sequence obtained by allowing the mass M to vary, but keeping J constant. Let us use α_1 as parameter along that sequence. The equilibrium conditions (2.3) then give M and $\alpha_j, j \neq 1$, as functions of α_1 only. Evaluating equations (2.16) along this equilibrium sequence gives

$$\sum_{j\neq 1}\left(\frac{\partial^2 E}{\partial\alpha_i\partial\alpha_j}\right)_{\rm eq}\left(\frac{d\alpha_j}{d\alpha_1}\right)_{\rm eq} + \left(\frac{\partial^2 E}{\partial\alpha_i\partial M}\right)_{\rm eq}\left(\frac{dM}{d\alpha_1}\right)_{\rm eq} = -\left(\frac{\partial^2 E}{\partial\alpha_i\partial\alpha_1}\right)_{\rm eq}, \quad i = 1, 2, \ldots. \tag{2.17}$$

We can solve this set of linear equations for the derivatives $(da_j/d\alpha_1)_{eq}$, $j \neq 1$ and $(dM/d\alpha_1)_{eq}$. We see immediately that

$$\left(\frac{dM}{d\alpha_1}\right)_{eq} = 0 \Leftrightarrow \det\left(\frac{\partial^2 E}{\partial\alpha_i \partial\alpha_j}\right)_{eq} = 0 . \tag{2.18}$$

A similar result can be written for $(dM/d\alpha_i)_{eq}$, $i = 2, \ldots$, as well as for $(dJ/d\alpha_i)_{eq}$ along a sequence with constant M.

Consider next the variation of the total equilibrium energy $E_{eq}(\alpha_1)$ along the same one-parameter sequence considered above. We have along that sequence

$$\begin{aligned}\frac{dE_{eq}}{d\alpha_1} &= \left(\frac{\partial E}{\partial\alpha_1}\right)_{eq} + \sum_{j\neq 1}\left(\frac{\partial E}{\partial\alpha_j}\right)_{eq}\left(\frac{d\alpha_j}{d\alpha_1}\right)_{eq} \\ &\quad + \left(\frac{\partial E}{\partial M}\right)_{eq}\left(\frac{dM}{d\alpha_1}\right)_{eq} + \left(\frac{\partial E}{\partial J}\right)_{eq}\left(\frac{dJ}{d\alpha_1}\right)_{eq} \\ &= \left(\frac{\partial E}{\partial M}\right)_{eq}\left(\frac{dM}{d\alpha_1}\right)_{eq} ,\end{aligned} \tag{2.19}$$

where we have used the equilibrium conditions (2.3) and the constancy of J to obtain the second equality. Clearly,

$$\frac{dE_{eq}}{d\alpha_1} = 0 \Leftrightarrow \left(\frac{dM}{d\alpha_1}\right)_{eq} = 0 . \tag{2.20}$$

Thus a turning point on the equilibrium energy curve also identifies the onset of instability.

Note that the determinant condition (2.15) and the turning point conditions (2.18) or (2.20) are equivalent only for instabilities that do not involve new degrees of freedom besides those considered explicitly in the equilibrium model. Condition (2.15) can be used more generally to study instabilities involving new degrees of freedom if these can be included in the construction of the energy function (see §§ 6.2, 6.3, and 9.2 for examples). Note also that all of the conditions for instability given above are applicable to very general equilibrium configurations, including uniformly and nonuniformly rotating single stars (see § 6), as well as binary configurations (see § 9).

As a trivial example, consider again the nonrotating spherical model introduced in § 2.1. We see immediately from equation (2.13) that along a one-parameter sequence with constant $J = 0$, $(dM/d\rho_c)_{eq} \propto (3 - n)$, with a positive constant of proportionality. It is easy to show from equations (2.6)–(2.14) that $(d^2E/d\rho_c^2)_{eq}$ and $dE_{eq}/d\rho_c$ are also proportional to $(3 - n)$. Thus we recover the well-known result that a spherical polytrope is radially unstable when $\Gamma < \frac{4}{3}$. The determinant condition and turning point criteria are equivalent here since the instability preserves the spherical symmetry of the configuration.

2.4. *Secular versus Dynamical Instabilities*

We now specialize our discussion to the two particular types of velocity fields considered in this paper. For stars in *uniform rotation,* the conserved quantities appearing in the energy function (2.2) are the mass M and angular momentum J. We will also consider nonuniformly rotating stars, with internal fluid motions of *uniform vorticity.* For these stars, the conserved *circulation* $\mathscr{C}$ along the stellar equator will also be introduced in the energy function.

The conditions for onset of instability given in § 2.3 are based on the existence of a neighboring configuration with lower total energy. The equilibrium system can evolve into this neighboring configuration provided that a suitable dissipation mechanism is operating. Clearly the evolution will take place over the time scale of the dissipation. The conditions given in § 2.3 are therefore in general for the onset of *secular instability.* Note that, by construction, all conserved quantities appearing in the energy function (2.2) are constant for all configurations near the equilibrium state. For the secular instability to arise, a dissipation mechanism which conserves these quantities must be present. For example, viscosity conserves M and J, but not $\mathscr{C}$, while gravitational radiation reaction forces conserve M and $\mathscr{C}$, but not J (see Miller 1974).

When the conservation of M, J, *and* $\mathscr{C}$ is built into the equilibrium model, the conditions given in § 2.3 cannot be interpreted in terms of a secular instability, since no physically realistic dissipation mechanism is compatible with all three conservation laws. However, these conditions may then signal the onset of *dynamical* instability. Indeed, conservation of M, J, and $\mathscr{C}$ is a property of the Euler equations of motion for an ideal (dissipationless) fluid. For spherical models (with $J = \mathscr{C} = 0$), it is well known that a turning point (conditions [2.18] or [2.20]) marks the location along an equilibrium sequence where the frequency of the radial pulsation mode changes from real to imaginary, that is, the onset of dynamical instability (see, e.g., ZN, chap. 10, or ST, § 6.8). This is because there exists a Lagrangian displacement which carries the equilibrium configuration into a neighboring configuration along the sequence, with no second-order variation of the energy.[7] The same cannot be concluded, in general, for turning points along sequences of uniformly rotating models, since viscous transfer of angular momentum is needed to maintain the uniform rotation during a perturbation. If we relax the assumption of uniform rotation, a turning point could mark the onset of dynamical instability, provided that enough degrees of freedom have been incorporated into the equilibrium model (see § 6.3 for a particularly clear example). By *convention* in this paper, we will label as "dynamical" an instability point determined by one of the conditions given § 2.3 for any equilibrium model that was constructed without imposing uniform rotation. Specifically, instability points are presumed dynamical whenever M, J, *and* $\mathscr{C}$ are held fixed in all first- and second-order variations of the energy function. We emphasize that no rigorous proof can be given that a dynamical instability will in fact arise at those points (but see § 6.3). This problem may be of little astrophysical relevance since we expect that secular instability, which is less restrictive, always occurs before a dynamical instability point is reached along an equilibrium sequence. For more detailed discussions about secular versus dynamical instabilities in rotating stars, see Bardeen et al. (1977), Friedman, Ipser & Sorkin (1988), and references therein.

[7] We assume implicitly here that the adiabatic index Γ_1 governing dynamical perturbations is equal to $\Gamma = 1 + 1/n$.

3. COMPRESSIBLE MACLAURIN SPHEROIDS

We begin by treating the simplest case of a uniformly rotating polytrope in axial symmetry, constructing the compressible analogue of a classical Maclaurin spheroid (see Ch69, chap. 5, and ST, § 7.3). Some of the results obtained in this section were first derived in ZN (§ 11.13) and ST (§ 7.4), where post-Newtonian correction terms were also included. More sophisticated models of uniformly rotating polytropes based on a more general variational calculation were constructed by Roberts (1963a, b) and Hurley & Roberts (1964, 1965). While our method is somewhat more approximate, it leads to purely algebraic equations. In addition, our results agree well with those of detailed numerical models (see § 3.4) and can be easily extended to nonaxisymmetric and binary configurations.

3.1. *Equilibrium Conditions*

Consider an axisymmetric, uniformly rotating polytrope of mass M, index $n = 1/(\Gamma - 1)$, and entropy constant $K \equiv P/\rho^{\Gamma}$. Its equilibrium configuration is uniquely determined once the total angular momentum J is specified. We denote the central density by ρ_c and the principal axes of the outer surface by a_1 $(=a_2)$, and a_3, with a_3 measured along the rotation axis and a_1 in the equatorial plane. It is easy to write down the expression for the total energy E of such a configuration as the sum of an internal energy U, gravitational potential energy W, and rotational kinetic energy T. We treat each contribution in turn.

In the ellipsoidal approximation (§ 2.2), the specific internal energy profile $u(m)$ of the rotating star is identical to that of a spherical polytrope of same central density. The same must be true of the total internal energy U. Therefore we can write, as in § 2.1,

$$U = k_1 K \rho_c^{1/n} M , \tag{3.1}$$

where k_1 is given by equation (2.9). Thus U is a function of ρ_c alone, independent of the shape of the configuration.

When compared to that of a spherical polytrope with the same central density, the gravitational potential energy W is modified by rotation in the same way as it is modified for a homogeneous star. This follows from Newton's theorem that the potential inside an ellipsoidal shell of constant density is constant (see Ch69, § 17), together with our assumption that the density profile $\rho(m)$ remains unchanged (§ 2.2). For a sphere of constant density ρ we have

$$W(\text{Sphere}) = -\frac{3}{5}\frac{GM^2}{R} = -\frac{3}{5}\left(\frac{4\pi}{3}\right)^{1/3} GM^{5/3}\rho^{1/3} . \tag{3.2}$$

Compare this to the result for a homogeneous spheroid of density ρ (Ch69, chap. 3),

$$W(\text{Spheroid}) = -\frac{3}{5}\frac{GM^2}{a_1}\frac{\sin^{-1} e}{e} = -\frac{3}{5}\left(\frac{4\pi}{3}\right)^{1/3} GM^{5/3}\rho^{1/3}\frac{\sin^{-1} e}{e}(1 - e^2)^{1/6} , \tag{3.3}$$

where the eccentricity e is defined by

$$e^2 \equiv 1 - \left(\frac{a_3}{a_1}\right)^2 . \tag{3.4}$$

Given expression (2.8) for the potential energy of a spherical polytrope, it follows that for our compressible spheroid we must have

$$W = -k_2 GM^{5/3}\rho_c^{1/3}\frac{\sin^{-1} e}{e}(1 - e^2)^{1/6} . \tag{3.5}$$

Following ZN and ST, we introduce for convenience (especially when taking derivatives) the oblateness parameter

$$\lambda \equiv \left(\frac{a_3}{a_1}\right)^{2/3} = (1 - e^2)^{1/3} . \tag{3.6}$$

In terms of this quantity we have

$$W = -k_2 GM^{5/3}\rho_c^{1/3} g(\lambda) , \tag{3.7}$$

where we have defined the function

$$g(\lambda) \equiv \lambda^{1/2}(1 - \lambda^3)^{-1/2}\cos^{-1}(\lambda^{3/2}) = \frac{\sin^{-1} e}{e}(1 - e^2)^{1/6} . \tag{3.8}$$

It is also often convenient to introduce, instead of the central density ρ_c, the mean radius R of the spheroid,

$$R \equiv (a_1^2 a_3)^{1/3} = a_1(1 - e^2)^{1/6} = a_1\lambda^{1/2} . \tag{3.9}$$

This is not to be confused with the radius of the nonrotating, spherical equilibrium configuration with the same mass and entropy, which we denote by R_0 (see § 3.2 below). Either R or ρ_c can be used as an independent variable, and we will often switch from one to the other. Using the definition of k_2, equation (2.10), and the relation between the central and mean density for a polytrope,

$$\bar{\rho} \equiv \frac{3M}{4\pi R^3} = 3\rho_c\frac{|\theta_1'|}{\xi_1} , \tag{3.10}$$

we find that expression (3.7) can be rewritten in terms of R as

$$W = -\frac{3}{5 - n}\frac{GM^2}{R} g(\lambda) . \tag{3.11}$$

Not surprisingly, this is just the first of the two expressions in equation (2.8) multiplied by the same factor $g(\lambda)$ that corrects for rotation.

Now turn to the kinetic energy of rotation. For a spheroid, the moment of inertia $I \propto Ma_1^2$. Therefore, if we define I_s to be the moment of inertia of the sphere of same volume, we must have

$$\frac{I}{I_s} = \frac{a_1^2}{R^2} = \frac{a_1^2}{(a_1^2 a_3)^{2/3}} = \frac{1}{\lambda} . \tag{3.12}$$

For the spherical polytrope of same volume we have

$$I_s = \tfrac{2}{5}\kappa_n M R^2 , \tag{3.13}$$

where we have defined (cf. ST, eq. [7.4.9])

$$\kappa_n \equiv \frac{5}{3}\frac{\int_0^{\xi_1} \theta^n \xi^4 d\xi}{\xi_1^4 |\theta_1'|} , \tag{3.14}$$

so that $\kappa_n = 1$ for $n = 0$. Combining equations (3.12) and (3.13), we see that for our compressible spheroid

$$I = \frac{I_s}{\lambda} = \frac{2}{5}\kappa_n M a_1^2 , \tag{3.15}$$

and the kinetic energy of rotation can be written

$$T = \frac{J^2}{2I} = k_3 \lambda J^2 M^{-5/3} \rho_c^{2/3} , \tag{3.16}$$

where

$$k_3 \equiv \frac{5}{4}\frac{(4\pi)^{2/3}}{\kappa_n}\left(\frac{|\theta_1'|}{\xi_1}\right)^{2/3} \tag{3.17}$$

is a constant (independent of λ).[8] For convenience, we have listed in Table 1 the values of all the structure constants, k_1, k_2, k_3, and κ_n, for polytropes of various indices.

The total energy of a configuration with given mass M and angular momentum J, *not necessarily in equilibrium,* is obtained by summing equations (3.1), (3.7), and (3.16),

$$E(\rho_c, \lambda; M, J) = U + W + T . \tag{3.18}$$

In equilibrium we must have

$$\frac{\partial E}{\partial \rho_c} = \frac{\partial E}{\partial \lambda} = 0 . \tag{3.19}$$

The first condition gives immediately the virial relation,

$$\frac{3}{n} U + W + 2T = 0 , \tag{3.20}$$

[8] Note that k_3 defined here is called k_5 in ST.

TABLE 1

POLYTROPIC STRUCTURE CONSTANTS[a]

n	κ_n	k_1	k_2	k_3
0.0	1.	0.	0.96720	3.2481
0.1	0.96064	0.041374	0.94627	3.1083
0.2	0.92257	0.085269	0.92714	2.9815
0.3	0.88562	0.13139	0.90949	2.8656
0.4	0.84973	0.17950	0.89310	2.7587
0.5	0.81482	0.22939	0.87777	2.6594
1.0	0.65345	0.50000	0.81289	2.2472
1.5	0.51149	0.79586	0.76077	1.9252
2.0	0.38712	1.1078	0.71618	1.6562
2.5	0.27951	1.4295	0.67623	1.4202
3.0	0.18839	1.7558	0.63899	1.2041
3.5	0.11387	2.0817	0.60294	0.99766
4.0	0.05643	2.4008	0.56640	0.78954
4.5	0.01724	2.7019	0.52676	0.55896

[a] κ_n is defined by eq. (3.14); k_1, k_2, k_3 by eqs. (2.9), (2.10), and (3.17).

while the second can be used to derive an equilibrium relation between λ (or e) and the ratio $T/|W|$. We find

$$\frac{T}{|W|} = \frac{1}{2}\left[1 + \frac{3\lambda^3}{1-\lambda^3} - \frac{3\lambda^{3/2}}{(1-\lambda^3)^{1/2}\cos^{-1}\lambda^{3/2}}\right] = \frac{3}{2e^2}\left(1 - \frac{e(1-e^2)^{1/2}}{\sin^{-1} e}\right) - 1 . \tag{3.21}$$

This is the same relation between e (or λ) and $T/|W|$ as that found for a *homogeneous* Maclaurin spheroid (ST, eq. [7.3.24]). Using the virial relation (3.20), together with expressions (3.1) for U and (3.11) for W, we can now determine the equilibrium relation between M and ρ_c for fixed J (cf. ST eq. [7.4.40]),

$$M(\rho_c; J) = M(\rho_c; 0)\left[g(\lambda)\left(1 - 2\frac{T}{|W|}\right)\right]^{-3/2} , \tag{3.22}$$

where $M(\rho_c; 0)$ is given by equation (2.13), as well as the total equilibrium energy

$$E_{\rm eq} = \frac{3-n}{3} W\left(1 - \frac{3-2n}{3-n}\frac{T}{|W|}\right) . \tag{3.23}$$

Equations (3.11) and (3.20)–(3.23) completely determine the equilibrium configuration corresponding to a given eccentricity e. The angular momentum and rotation frequency can be calculated from equations (3.15) and (3.16) as $J = (2IT)^{1/2}$ and $\Omega = (2T/I)^{1/2}$.

3.2. *Constructing the Equilibrium Sequences*

Consider a one-parameter sequence of equilibrium models where the stars have a fixed mass M, polytropic index n, and entropy constant K. Each model along the sequence is completely determined by specifying just one other quantity, such as the angular momentum J or the eccentricity e. As an illustration, Figures 1 and 2 show the behavior of E and Ω along

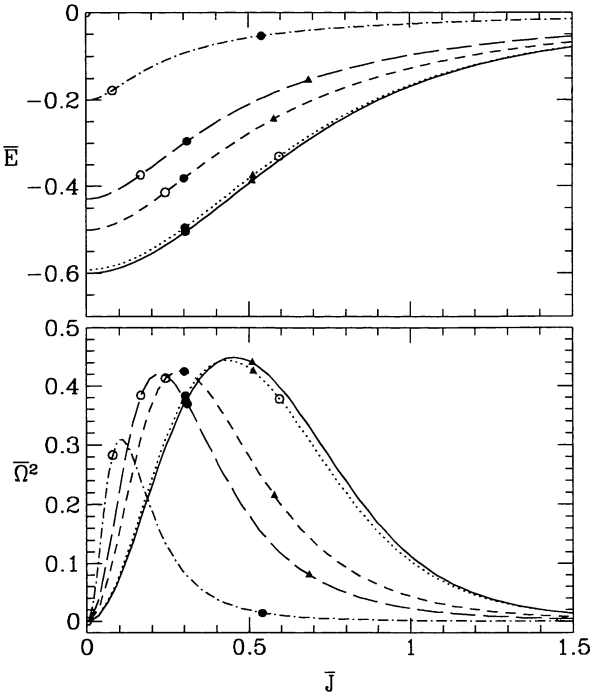

FIG. 1.—Plots of the equilibrium energy and angular frequency of rotation as a function of angular momentum along compressible Maclaurin sequences with polytropic index $n = 0$ (*solid lines*), $n = 0.1$ (*dotted lines*), $n = 1$ (*short-dashed lines*), $n = 1.5$ (*long-dashed lines*), and $n = 2.5$ (*dotted-dashed lines*). The secular instability limits (*filled circles*), dynamical instability limits (*triangles*), and mass-shedding limits (*open circles*) are also indicated. The units are defined in eq. (3.26).

equilibrium sequences corresponding to different polytropic indices. The curves corresponding to $n = 0$ are identical to those shown in Ch69 (chap. 5). All numerical values are given in units referring to the nonrotating, spherical equilibrium polytrope of same mass M, entropy constant K, and polytropic index n. The radius of this spherical polytrope is

$$R_0 \equiv \xi_1(\xi_1^2|\theta_1'|)^{-(1-n)/(3-n)}\left(\frac{M}{4\pi}\right)^{(1-n)/(3-n)}\left[\frac{(n+1)K}{4\pi G}\right]^{n/(3-n)}. \tag{3.24}$$

It is important to note that for $n \neq 0$, R_0 is *not* equal to the mean radius $R \equiv (a_1^2 a_3)^{1/3}$ of a rotating spheroidal polytrope along the sequence. Combining equations (3.22) and (3.24), we find that R and R_0 are related by

$$R = R_0\left[g(\lambda)\left(1 - 2\frac{T}{|W|}\right)\right]^{-n/(3-n)}. \tag{3.25}$$

Since, in contrast to R_0, the quantity R varies along a compressible equilibrium sequence, it should not be used to define the units. The rotation frequency, angular momentum, and energy have been made dimensionless by introducing the ratios

$$\bar{\Omega} \equiv \frac{\Omega}{(\pi G\bar{\rho}_0)^{1/2}}, \quad \bar{J} \equiv \frac{J}{(GM^3R_0)^{1/2}}, \quad \bar{E} \equiv \frac{E}{GM^2/R_0}, \tag{3.26}$$

where $\bar{\rho}_0 \equiv M/(4\pi R_0^3/3)$. Note from Figures 1 and 2 that, as in the incompressible case, Ω attains a maximum along all compressible sequences. The values of e and J at the maximum clearly depend on the polytropic index. In contrast, both E and J increase monotonically as a function of e. The mass-shedding limit (see § 3.3) and stability limits (see § 6) along each sequence are also indicated in Figures 1 and 2. Stellar models past the maximum of Ω tend to spin-*up* as they lose angular momentum. For stars in strictly uniform rotation, this behavior seems possible only for nearly incompressible models. Indeed, we find that when $n \gtrsim 0.5$, mass shedding occurs before the maximum of Ω is reached along an equilibrium sequence with increasing J. However, although this is not shown in Figure 1, for n very close to 3, once again the mass-shedding limit is reached beyond the point where Ω is maximum, making spin-up possible again (Shapiro et al. 1990).

The results of § 3.1 can also be presented as a single equilibrium sequence described in terms of universal dimensionless quantities that are functions of e only (independent of the polytropic index n). One such quantity is the ratio $T/|W|$. Others are

$$\begin{aligned}
\hat{\Omega}^2 &\equiv \kappa_n(1 - n/5)\left(\frac{\Omega^2}{\pi G\bar{\rho}}\right), \\
\hat{J}^2 &\equiv \frac{1}{\kappa_n}(1 - n/5)\left(\frac{J^2}{GM^3R}\right), \\
\hat{W} &\equiv \frac{5-n}{3}\left(\frac{W}{GM^2/R}\right), \\
\hat{R} &\equiv \left(\frac{R}{R_0}\right)^{(3-n)/n}.
\end{aligned} \tag{3.27}$$

Table 2 presents the variation of these quantities along the universal equilibrium sequence. The equilibrium energy $E_{\rm eq}$

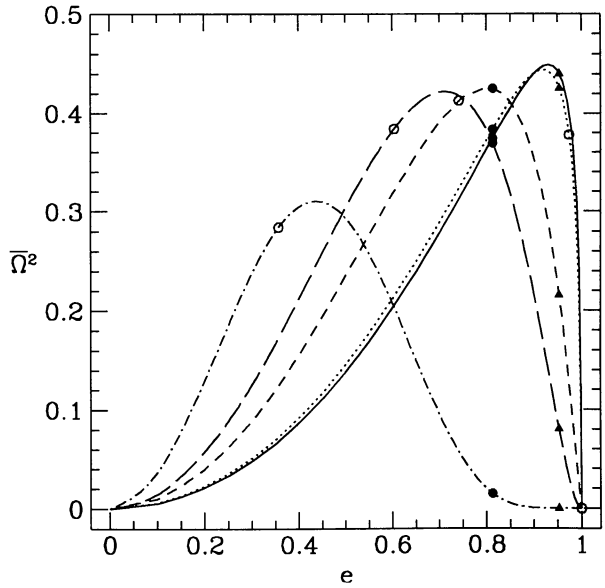

FIG. 2.—Variation of the angular frequency with eccentricity along the same compressible Maclaurin sequences as in Fig. 1. Conventions are as in Fig. 1.

TABLE 2

COMPRESSIBLE MACLAURIN SEQUENCE[a]

e [b]	$T/\|W\|$	$\hat{\Omega}^2$	$\hat{J}$	$\hat{W}$	$\hat{R}$
0.	0.	0.	0.	1.	1.
0.1000	0.1340(-2)	0.5341(-2)	0.2540(-1)	1.0000	1.003
0.2000	0.5437(-2)	0.2146(-1)	0.5144(-1)	0.99996	1.011
0.3000	0.1254(-1)	0.4862(-1)	0.7882(-1)	0.9998	1.026
0.4000	0.2314(-1)	0.8727(-1)	0.1085	0.9993	1.049
0.4500	0.2998(-1)	0.1111	0.1245	0.9989	1.065
0.5000	0.3804(-1)	0.1380	0.1416	0.9982	1.084
0.5500	0.4751(-1)	0.1681	0.1601	0.9971	1.108
0.6000	0.5867(-1)	0.2014	0.1804	0.9956	1.138
0.6500	0.7187(-1)	0.2378	0.2029	0.9934	1.176
0.7000	0.8765(-1)	0.2773	0.2283	0.9901	1.225
0.7500	0.1068	0.3195	0.2579	0.9852	1.291
0.8000	0.1305	0.3632	0.2935	0.9776	1.384
0.8127*	0.1375	0.3742	0.3038	0.9751	1.415
0.8500	0.1611	0.4058	0.3383	0.9653	1.528
0.9000	0.2031	0.4405	0.3999	0.9434	1.785
0.9529**	0.2738	0.4402	0.5091	0.8903	2.483
0.9800	0.3396	0.3780	0.6249	0.8164	3.818
0.9900	0.3809	0.3103	0.7121	0.7515	5.587
0.9950	0.4127	0.2437	0.7945	0.6858	8.355
0.9990	0.4590	0.1254	0.9738	0.5422	22.50
0.9999	0.4867	0.4286(-1)	1.2263	0.3765	99.64
1.	0.5	0.	∞	0.	∞

[a] $\hat{\Omega}$, $\hat{J}$, $\hat{W}$, and $\hat{R}$ are defined in eq. (3.27).
[b] One asterisk marks the secular instability limit, two the dynamical instability limit.

can be calculated easily for any n from equation (3.23) once $T/|W|$ and $\hat{W}$ are known. Note that both $\hat{W}$ and $\hat{R}$ have been normalized in such a way that they tend to unity as $e \to 0$. Although the definitions (3.27) are general and will be used for other configurations, they can be written explicitly as simple functions of e (or λ) for Maclaurin spheroids. Using the results of § 3.1 we find

$$\hat{\Omega}^2 = 2\left[\frac{(1-e^2)^{1/2}}{e^3}(3-2e^2)\sin^{-1}e - \frac{3(1-e^2)}{e^2}\right],$$

$$\hat{J}^2 = \frac{3}{25}(1-e^2)^{-2/3}\hat{\Omega}^2, \qquad (3.28)$$

$$\hat{W} = g(\lambda),$$

$$\hat{R} = \left[g(\lambda)\left(1 - 2\frac{T}{|W|}\right)\right]^{-1},$$

with $g(\lambda)$ and $T/|W|$ given by expressions (3.8) and (3.21).

3.3. *The Mass-Shedding Limit*

Because of the limited number of degrees of freedom in our approximation, the equilibrium configurations constructed in § 3.2 are not guaranteed to satisfy the exact hydrostatic equilibrium condition locally at every point in the fluid. In particular, mass shedding can occur when a fluid element near the equator can no longer be held by gravity against the centrifugal effect of rotation.

We list in Table 3 the values of all equilibrium parameters at the mass-shedding limit of sequences with different polytropic indices. To construct this table we have used the values of $T/|W|$ at the mass-shedding limit as published in recent numerical studies of rotating polytropes by Hachisu & Eriguchi (1982), Hachisu, Eriguchi, & Sugimoto (1982), Hachisu (1986a), and Cook et al. (1992). For several values of n, we have confirmed the position of the mass-shedding limit by per-

TABLE 3

MASS-SHEDDING LIMITS FOR ROTATING POLYTROPES[a]

Ref.	n	a_2/a_1	a_3/a_1	$T/\|W\|$	$\bar{\Omega}^2$	$\bar{J}$	$\bar{E}$	R/R_o
Axisymmetric Configurations								
	0.	1.	0.	0.5	0.	∞	0.	1.
[2]	0.1	1.	0.2680	0.295	0.4072	0.5485	-0.3552	1.036
[3]	0.1	1.	0.2284	0.320	0.3779	0.5944	-0.3303	1.042
[3]	0.2	1.	0.2945	0.279	0.4040	0.5247	-0.3579	1.069
[3]	0.3	1.	0.3563	0.244	0.4191	0.4675	-0.3786	1.088
[3]	0.4	1.	0.4138	0.214	0.4270	0.4197	-0.3938	1.101
[1, 2]	0.5	1.	0.4846	0.180	0.4315	0.3657	-0.4122	1.103
[3]	0.5	1.	0.4631	0.190	0.4297	0.3818	-0.4030	1.111
[1]	1.0	1.	0.6716	0.103	0.4131	0.2423	-0.4139	1.130
[1, 2]	1.5	1.	0.7974	0.0595	0.3839	0.1660	-0.3742	1.140
[1]	2.0	1.	0.8801	0.0338	0.3478	0.1146	-0.2983	1.154
[1]	2.5	1.	0.9338	0.0182	0.2835	0.0785	-0.1778	1.206
Triaxial Configurations								
[4]	0.1	0.456	0.3589	0.1600	0.2974	0.3782	-0.4564	1.016
[4]	0.2	0.532	0.4002	0.1524	0.3297	0.3507	-0.4585	1.031
[4]	0.3	0.591	0.4295	0.1480	0.3526	0.3349	-0.4548	1.045
[4]	0.4	0.670	0.4654	0.1437	0.3773	0.3199	-0.4508	1.060
[4]	0.5	0.732	0.4912	0.1413	0.3942	0.3115	-0.4430	1.076

[a] $\bar{\Omega}$, $\bar{J}$, and $\bar{E}$ are defined in eq. (3.26).
REFERENCES: [1] Cook et al. 1992; [2] Hachisu 1986a; [3] Hachisu et al. 1982; [4] Hachisu & Eriguchi 1982.

forming *dynamical* simulations using our own smooth-particle-hydrodynamics (SPH) code (see Rasio & Shapiro 1992, 1993). With SPH we were able to locate the mass-shedding limit to within an accuracy of about 5% in $T/|W|$, comparable to the spread in other published values. The other equilibrium quantities listed in Table 3 were calculated using the results of § 3.1 and are therefore subject to our approximations. For large n, we see that the values of $T/|W|$ and J at mass shedding decrease sharply with increased compressibility. This is a well-known result: centrally condensed objects rotating uniformly cannot sustain much rotation (see, e.g., Tassoul 1978, chap. 10).

Note that it is possible to use the results of § 3.1 to calculate analytically the mass-shedding limit by setting the surface gravity at the equator (calculated using the results of Ch69, chap. 3) equal to the centrifugal force there. However, we find that, in the case of large n, the results are not in good agreement with those obtained from the more accurate, self-consistent numerical calculations (which we have used in constructing Table 3). This is because the location of the mass-shedding limit is extremely sensitive to the precise shape of the stellar surface, which our ellipsoidal approximation cannot determine accurately for very compressible, rapidly rotating stars. All the quantities calculated in § 3.2, however, are *global* quantities, which are not very sensitive to surface effects. This is even true of the eccentricity e, if we consider it to be the *mean* eccentricity of isodensity surfaces in the *interior* of the star, rather than a measure of surface distortion (see § 3.4 below for a demonstration of this point).

A related point concerns the applicability of our equilibrium sequences well past the true mass-shedding limit. While no equilibrium configuration in strictly uniform rotation can exist beyond this limit, very similar configurations with a slight amount of *differential* rotation probably do. Axisymmetric models of differentially rotating polytropes which resemble in all essential respects the Maclaurin spheroids have been constructed numerically by Bodenheimer & Ostriker (1973). Their models cover most of the range allowed by the virial theorem, having $0 \leq T/|W| \lesssim 0.5$, even though differential rotation always remains very moderate, with most models having $\Omega(center)/\Omega(equator) \gtrsim 1$. Therefore, we expect that the uniformly rotating equilibrium models constructed here beyond mass shedding are reasonable approximations for the interior of these more realistic, differentially rotating structures.

3.4. *Comparison with Other Work*

To check the validity of our assumptions and the accuracy of our method, we have compared in detail our results for axisymmetric rotating equilibria to recent numerical calculations by Hachisu (1986a) and Cook et al. (1992). These calculations for rotating polytropes are based on a mixed integral, finite-difference method using a Green's function to invert Poisson's equation for the potential. They improve on earlier work based on the self-consistent-field method of Ostriker & Mark (1968). The new schemes are capable of handling extreme configurations which rotate rapidly, are far from spherical, and approach mass shedding. We have also used the results of our own numerical calculations using the SPH method (Rasio & Shapiro 1992, 1993). This method has the advantage of being dynamical, so that it can be applied to study the stability of the solutions as well. Moreover, it is fully three-dimensional and can be used to construct numerically the triaxial equilibrium configurations considered later in this paper. All the SPH results reported in this paper were obtained with about 10^4 particles per star and using an initially uniform spatial distribution of particles (i.e., varying the individual particle masses). The relaxation technique described by Rasio & Shapiro (1992) was used to construct rotating equilibrium models.

In Figure 3 we show the behavior of $\bar{E}$ and $\bar{\Omega}^2$ as a function of $\bar{J}$ (cf. eq. [3.26]), as predicted by the different methods. The agreement with the results of § 3.2 is excellent, even for very compressible configurations. This is in part because the numerical solutions cannot extend beyond the mass-shedding limit. The rapidly rotating, very compressible structures, for which the ellipsoidal approximation should be poorest, do not exist. As seen in Figure 3, the disagreement is indeed largest near the mass-shedding limit of each sequence. The largest fractional deviation is about 3% for $\bar{\Omega}^2$, and occurs near the mass-shedding point of the $n = 1$ sequence. The fractional deviation of $\bar{E}$ never exceeds 1% for all sequences.

In Figure 4 we show our predicted profile for $T/|W|$ as a function of e (eq. [3.21]), compared to numerical results obtained with SPH. Note that, in contrast to J, which is a well-

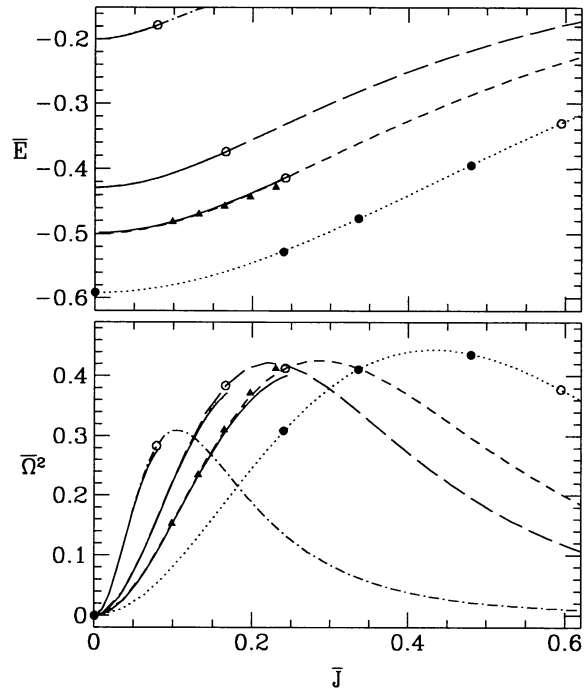

FIG. 3.—Comparison of our analytic results for compressible Maclaurin sequences with those of numerical calculations. Our curves for the equilibrium energy and angular frequency of rotation as a function of angular momentum are shown for $n = 0.1$ (*dotted lines*), $n = 1$ (*short-dashed lines*), $n = 1.5$ (*long-dashed lines*), and $n = 2.5$ (*dotted-dashed lines*). The open circles mark the position along the sequences of the mass-shedding limit as determined in Table 3. The solid lines show the numerical results obtained by Cook et al. (1992) for $n = 1$, 1.5, and 2.5 using a self-consistent-field method; these lines terminate at the mass-shedding limit. Also shown are the results of our own SPH calculations for $n = 0.1$ (*filled circles*) and $n = 1$ (*triangles*). Units are defined in eq. (3.26).

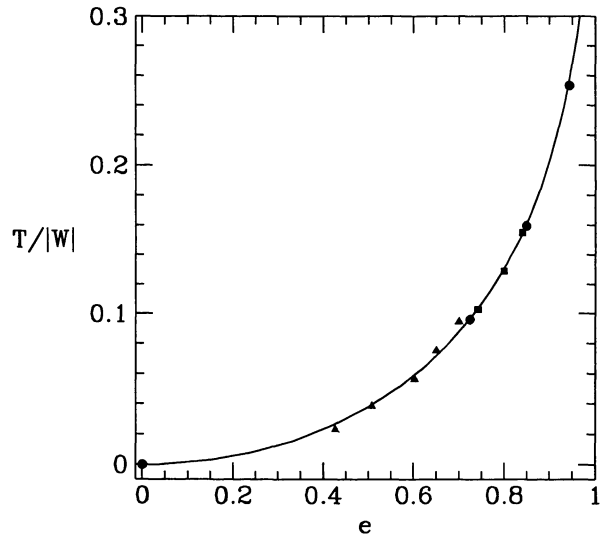

FIG. 4.—Comparison of our predicted equilibrium curve for $T/|W|$ as a function of e (cf. eq. [3.21]; recall that this curve is independent of n in our approximation) with the results of SPH calculations for $n = 0.1$ (*filled circles*), $n = 0.5$ (*filled squares*), and $n = 1$ (*triangles*). Equation (3.29) was used to define e for the SPH models.

defined global quantity, there is no unique way to define e for a numerical solution. In Figure 4, the value of e for the SPH solution was calculated as an *average* over the interior of the star, as

$$\langle e \rangle = \frac{1}{M} \int e(m) dm \,, \tag{3.29}$$

where $e(m)$ is the eccentricity of the isodensity surface containing an interior mass m. Clearly, the agreement is excellent. However, had we instead determined e by looking at the shape of the outer surface in the numerical solution, the agreement would not have been nearly as good. Indeed, as illustrated in Figure 5, the distribution $e(m)$ remains nearly constant in the interior of the star, but varies more rapidly near the surface. This result confirms our assumption (§ 2.2) that the isodensity surfaces in the interior of a rotating polytrope can be well approximated as self-similar ellipsoids. Figure 5 also shows that the density profile $\rho(m)$ is nearly independent of rotation, confirming the other key assumption in our model.

4. COMPRESSIBLE JACOBI ELLIPSOIDS

In this section we consider uniformly rotating *triaxial* structures, the compressible analogues of the classical Jacobi ellipsoids (see Ch69, chap. 6). Many of the results derived in this section can be generalized to all triaxial configurations and will be reused many times throughout our paper. To our knowledge this is the first time that the energy variational method has been applied to the calculation of nonaxisymmetric rotating configurations.

4.1. *Equilibrium Conditions*

Consider as in § 3 a polytropic star, rotating rigidly with angular velocity $\Omega = \Omega e_3$. In this section we construct approximate, nonaxisymmetric equilibrium configurations with principal axes $a_1 > a_2 > a_3$.

We begin by writing the general expression for the total energy of a rigidly rotating triaxial structure in the ellipsoidal approximation. The expression for the internal energy U, a function of the central density ρ_c alone, is identical to that used for Maclaurin spheroids, equation (3.1). We use the same argument as in § 3.1 to find the expression for the gravitational potential energy W. For a homogeneous ellipsoid of density ρ, we have (cf. Ch69, eq. [3.128])

$$W(\text{Ellipsoid}) = -\frac{3}{10} GM^2 \frac{\mathcal{I}}{a_1 a_2 a_3} = -\frac{3}{5} \frac{GM^2}{R} f \,, \tag{4.1}$$

where we have defined the mean radius $R \equiv (a_1 a_2 a_3)^{1/3}$, the quantity

$$\mathcal{I} \equiv A_1 a_1^2 + A_2 a_2^2 + A_3 a_3^2 \tag{4.2}$$

(called I in Ch69, cf. his eqs. [3.15] and [3.22]), and the dimensionless ratio

$$f \equiv \frac{1}{2} \frac{\mathcal{I}}{(a_1 a_2 a_3)^{2/3}} \,. \tag{4.3}$$

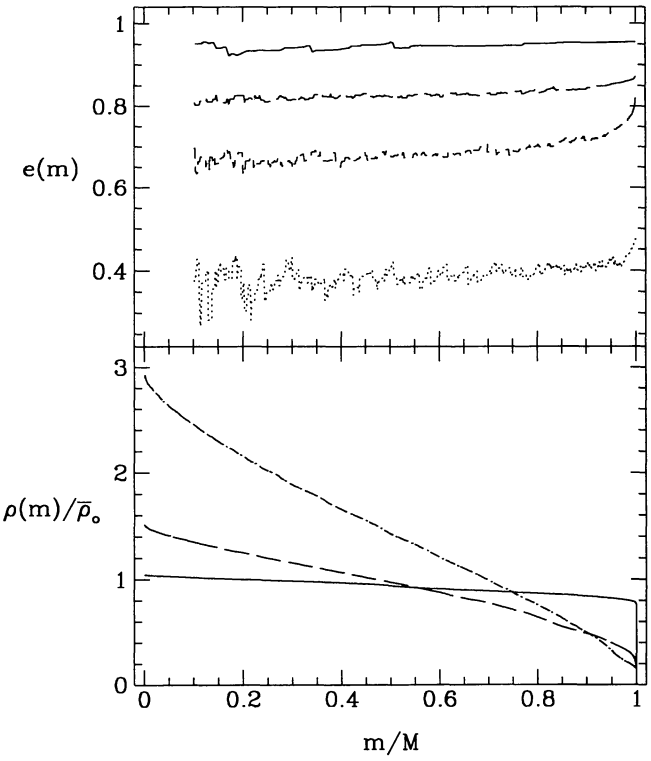

FIG. 5.—Interior eccentricity and density profiles of axisymmetric rotating polytropes constructed with SPH. Here m is the mass enclosed by a surface of constant density $\rho(m)$, and $e(m)$ is the eccentricity of that surface (defined by eq. [3.4]). We show three models near the mass-shedding limits of the Maclaurin sequences with $n = 0.1$ (*solid lines*; $T/|W| = 0.26$), $n = 0.5$ (*long-dashed lines*; $T/|W| = 0.16$), and $n = 1$ (*short-dashed lines*; $T/|W| = 0.10$), and one slowly rotating model with $n = 1$ (*dotted lines*; $T/|W| = 0.02$). The two $\rho(m)$ curves for $n = 1$ are practically indistinguishable. (Numerical values of $e(m)$ near the center, where $m/M \lesssim 0.1$, are not reliable because of poor spatial resolution.)

The dimensionless coefficients A_i can be calculated in terms of elliptic integrals involving only the axis ratios a_3/a_1 and a_3/a_2 (see Ch69, § 17). Here it is convenient to introduce two oblateness parameters,

$$\lambda_1 \equiv \left(\frac{a_3}{a_1}\right)^{2/3}, \quad \lambda_2 \equiv \left(\frac{a_3}{a_2}\right)^{2/3}. \tag{4.4}$$

In terms of these parameters we have

$$f = f(\lambda_1, \lambda_2) = \frac{1}{2}\left(\frac{A_1\lambda_2}{\lambda_1^2} + \frac{A_2\lambda_1}{\lambda_2^2} + A_3\lambda_1\lambda_2\right), \tag{4.5}$$

with $A_i = A_i(\lambda_1, \lambda_2)$. As before, when compared to that of the spherical polytrope of radius R, the potential energy of the rotating compressible configuration is modified by rotation in the same way that it is for a homogeneous object. Comparing equations (4.1) and (3.2), it follows that, for our compressible ellipsoid,

$$\begin{aligned} W &= -\frac{3}{5-n}\frac{GM^2}{R} f(\lambda_1, \lambda_2) \\ &= -k_2 G M^{5/3} \rho_c^{1/3} f(\lambda_1, \lambda_2), \end{aligned} \tag{4.6}$$

where the polytropic structure constant k_2 is given by equation (2.10).

For an ellipsoid, the moment of inertia $I \propto M(a_1^2 + a_2^2)$, so that

$$\frac{I}{I_s} = \frac{(a_1^2 + a_2^2)/2}{R^2} = \frac{1}{2}\frac{a_1^2 + a_2^2}{(a_1 a_2 a_3)^{2/3}} \equiv \frac{1}{h} \tag{4.7}$$

where I_s is the moment of inertia of a sphere of same volume, equation (3.13). Therefore we have

$$I = \frac{I_s}{h(\lambda_1, \lambda_2)} = \frac{1}{5}\kappa_n(a_1^2 + a_2^2)M, \tag{4.8}$$

and the kinetic energy of rotation can then be written as

$$T = \frac{J^2}{2I} = k_3 h(\lambda_1, \lambda_2) J^2 M^{-5/3} \rho_c^{2/3}, \tag{4.9}$$

with

$$h(\lambda_1, \lambda_2) = \frac{2\lambda_1^2\lambda_2^2}{\lambda_1^3 + \lambda_2^3}. \tag{4.10}$$

The structure constants κ_n and k_3 are given by equations (3.14) and (3.17). Note that when $a_1 = a_2$, $\lambda_1 = \lambda_2 = \lambda$ (eq. [3.6]), and $f(\lambda_1, \lambda_2)$ and $h(\lambda_1, \lambda_2)$ reduce to $g(\lambda)$ and λ, respectively (cf. eqs. [3.7] and [3.16]).

For a configuration with given mass M and angular momentum J, the equilibrium conditions are

$$\frac{\partial E}{\partial \rho_c} = \frac{\partial E}{\partial \lambda_1} = \frac{\partial E}{\partial \lambda_2} = 0, \tag{4.11}$$

where $E(\rho_c, \lambda_1, \lambda_2; M, J) = U + W + T$ is the total energy. The first condition leads to the same virial relation as in the axisymmetric case, equation (3.20). The equilibrium relations (3.22) and (3.23) also retain the same form, except that $f(\lambda_1, \lambda_2)$ replaces $g(\lambda)$ in relation (3.22). For the second and third conditions we need to evaluate the partial derivatives $\partial f/\partial\lambda_1$ and $\partial f/\partial\lambda_2$. This can be done easily with the help of the relation (cf. Ch69, eq. [3.23])

$$\frac{\partial \mathcal{I}}{\partial a_i} = a_i\left(\frac{\mathcal{I}}{a_i^2} - A_i\right). \tag{4.12}$$

After some algebra we find

$$\begin{aligned} 0 &= \frac{W}{f}\frac{1}{2R^2}\left(A_1 a_1^2 - \frac{1}{2}A_2 a_2^2 - \frac{1}{2}A_3 a_3^2\right) \\ &\quad + T\left(\frac{2a_1^2 - a_2^2}{a_1^2 + a_2^2}\right) \\ 0 &= (1 \leftrightarrow 2). \end{aligned} \tag{4.13}$$

Adding these two conditions, we obtain a simple expression giving the ratio $T/|W|$ in terms of the principal axes,

$$\frac{T}{|W|} = \frac{A_1 a_1^2 + A_2 a_2^2 - 2A_3 a_3^2}{2\mathcal{I}}. \tag{4.14}$$

One can easily verify that this expression reduces to equation (3.21) when $a_1 = a_2$. The total equilibrium energy is still given by expression (3.23), which results directly from the virial relation (3.20), but with $T/|W|$ calculated from equation (4.14) and W from equation (4.6).

Using equation (4.6) for W and $T = (1/2)I\Omega^2$, with I given by expression (4.8), the two equilibrium conditions (4.13) can be rewritten as

$$\begin{aligned} 0 &= -\frac{20\pi G\bar{\rho}}{5-n}\left(A_1 a_1^2 - \frac{1}{2}A_2 a_2^2 - \frac{1}{2}A_3 a_3^2\right) \\ &\quad + \kappa_n(2a_1^2 - a_2^2)\Omega^2 \\ 0 &= (1 \leftrightarrow 2), \end{aligned} \tag{4.15}$$

where $\bar{\rho} \equiv 3M/(4\pi R^3)$. We now combine these two conditions by adding each one to $\frac{1}{2}$ times the other and get

$$\tilde{\Omega}^2 a_1^2 q_n - 2A_1 a_1^2 = \tilde{\Omega}^2 a_2^2 q_n - 2A_2 a_2^2 = -2A_3 a_3^2, \tag{4.16}$$

where we have defined

$$\tilde{\Omega} \equiv \frac{\Omega}{(\pi G\bar{\rho})^{1/2}}, \tag{4.17}$$

(not to be confused with $\bar{\Omega}$; cf. eq. [3.26]) and

$$q_n \equiv \kappa_n\left(1 - \frac{n}{5}\right). \tag{4.18}$$

Expression (4.16) reduces to expression (6.2) of Ch69 when $n = 0$ ($q_n = 1$). Following Ch69, we now introduce the quantities ("index symbols"; see Ch69, § 21)

$$A_{12} = A_{21} = \frac{A_1 - A_2}{a_2^2 - a_1^2}, \tag{4.19}$$

$$B_{12} = B_{21} = A_2 - a_1^2 A_{12}, \tag{4.20}$$

and we add a term $2a_1^2 a_2^2 A_{12}$ to each of the three sides of expression (4.16). This gives

$$a_1^2(\tilde{\Omega}^2 q_n - 2B_{12}) = a_2^2(\tilde{\Omega}^2 q_n - 2B_{12}) = 2(A_{12}a_1^2 a_2^2 - A_3 a_3^2), \tag{4.21}$$

which reduces to equation (6.3) of Ch69 when $n = 0$. Clearly, solutions with $a_1 \neq a_2$ exist if and only if

$$a_1^2 a_2^2 A_{12} = a_3^2 A_3, \tag{4.22}$$

and

$$\tilde{\Omega}^2 = \frac{2B_{12}}{q_n}. \tag{4.23}$$

Equation (4.22), which gives the relation between the axis ratios in equilibrium, is identical to that obtained in the incompressible case (cf. Ch69, eq. [6.4]). As a consequence, the ratio $T/|W|$, equation (4.14), is also identical for compressible and incompressible equilibrium configurations with the same axis ratios. The expression (4.23) for $\tilde{\Omega}^2$ is modified by the presence of the factor $1/q_n$ (cf. Ch69, eq. [6.5]).

Finally, given equation (4.23) for $\tilde{\Omega}$ and expression (4.8) for I, we can calculate the angular momentum as $J = I\Omega$, or

$$\tilde{J} \equiv \frac{J}{(GM^3R)^{1/2}} = \frac{\sqrt{3}}{10}\frac{a_1^2 + a_2^2}{R^2}\kappa_n \tilde{\Omega}. \tag{4.24}$$

4.2. *Constructing the Equilibrium Sequences*

As in § 3.2, we now proceed to construct sequences of equilibrium models corresponding to fixed M, K, and n. The procedure we use is as follows. Given the ratio a_2/a_1, we calculate a_3/a_1 from equation (4.22). The quantities A_i, $\mathscr{I}$, B_{ij}, and A_{ij} are obtained by performing numerically the quadratures appearing in their definitions (cf. Ch69, expressions [3.103] and [3.104]). We then calculate $T/|W|$ and f, which depend only on the axis ratios, from equations (4.3) and (4.14). As in § 3.2, we construct the dimensionless ratios defined in equations (3.26) by introducing the radius R_0 of the spherical equilibrium polytrope of same M, K, and n (eq. [3.24]). Using the virial relation (3.20), together with expressions (3.1) for U and (4.6) for W, we can relate the mean radius $R = (a_1 a_2 a_3)^{1/3}$ to R_0 by (cf. eq. [3.25])

$$R = R_0\left[f(\lambda_1, \lambda_2)\left(1 - 2\frac{T}{|W|}\right)\right]^{-n/(3-n)}. \tag{4.25}$$

We calculate the ratio R/R_0 using expression (4.25), and then the quantities $\bar{\Omega}$, $\bar{J}$, and $\bar{E}$ from equations (4.23), (4.24), and (3.23).

We illustrate some of our results in Figures 6 and 7. The compressible Jacobi sequences bifurcate from the compressible Maclaurin sequences at the point where $T/|W| = 0.1375$, independent of n in our approximation. For all polytropic indices, the compressible Jacobi ellipsoid has always lower equilibrium energy than the Maclaurin spheroid of same J and n, although for large n the fractional energy difference is very small. Also note that $d\Omega/dJ < 0$ along all compressible Jacobi sequences, indicating that the secular loss of angular momentum (e.g., via gravitational or electromagnetic radiation) will cause the configuration to spin-*up* (see Chau et al. 1992). For $n < 1$ spin-down occurs once the configuration becomes axisymmetric.

In Table 4 we give the variation along the compressible Jacobi sequences of the universal variables defined in equation (3.27), as well as $T/|W|$ and the two axis ratios. This table allows one to calculate very easily the equilibrium properties of a Jacobi ellipsoid for any polytropic index n. The total equilibrium energy can be calculated from expression (3.23) once $T/|W|$ and $\hat{W}$ are known.

4.3. *The Mass-Shedding Limit*

It is well known that for $n > 0.808$ the mass-shedding limit along the Maclaurin sequence occurs before the point of bifurcation into the Jacobi sequence (James 1964; see Tassoul 1978, § 10.3, for a summary). Thus, strictly speaking, Jacobi ellipsoids can exist only when $n < 0.808$ (but see the discussion in § 3.3).

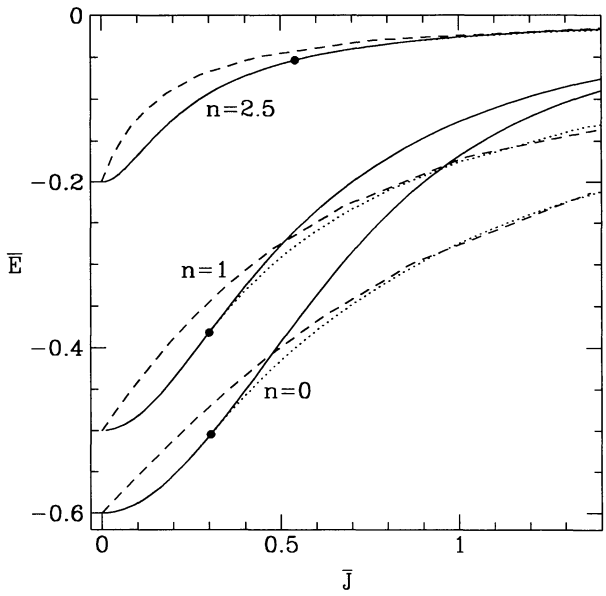

FIG. 6.—Equilibrium curves of total energy as a function of angular momentum along compressible Maclaurin (*solid lines*), Jacobi (*dotted lines*), and irrotational Riemann-S (*dashed lines*) sequences with $n = 0$, 1, and 2.5. The filled circles show the position of the secular instability limit along each Maclaurin sequence (cf. § 6.2). Units are defined in eq. (3.26).

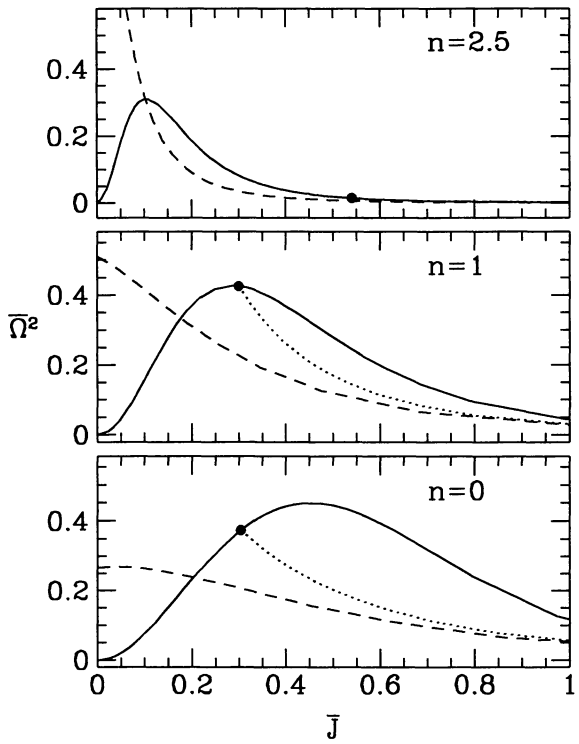

FIG. 7.—Equilibrium curves of Ω^2 as a function of J for the same sequences as shown in Fig. 6. Conventions are as in Fig. 6.

We are aware of only one numerical study of the mass-shedding limit along the compressible Jacobi sequence itself, done by Hachisu & Eriguchi (1982). These authors find that, even for very small $n \neq 0$, the mass-shedding limit along the Jacobi sequence never extends much past the bifurcation point: for $0.1 \leq n \leq 0.5$, the mass-shedding limit corresponds to $0.14 \leq T/|W| \leq 0.16$, whereas $T/|W| = 0.1375$ at the bifurcation point (see Table 3). This important result implies that uniformly rotating, triaxial equilibria may in fact be of little astrophysical interest. It is possible that, as in the case of axisymmetric configurations (cf. § 3.3), a small amount of differential rotation may stabilize triaxial ellipsoids against mass shedding, but we are unaware of any numerical study of this particular question.

4.4. *Comparison with Other Work*

In Figure 8 we compare our solution to the numerical results of Hachisu (1986a) and Hachisu & Eriguchi (1982) for $n = 0.5$. The variation of Ω^2 as a function of angular momentum J is shown near the bifurcation point. Note that, to make this comparison possible given their published data, we had to express Ω^2 and J in units based on the mean radius R, rather than R_0. Thus the quantities $\tilde{\Omega}^2$ and $\tilde{J}$ are shown (eqs. [4.17] and [4.24]). Clearly, the agreement is excellent. The Jacobi sequence for $n = 0.5$ terminates at the point where $\tilde{\Omega}^2 = 0.492$ and $\tilde{J} = 0.297$, which is the last point shown in Figure 8.

In our approximation the bifurcation of the Maclaurin sequence into the Jacobi sequence always occurs at the point where $T/|W| = 0.1375$, independent of the polytropic index.

TABLE 4

COMPRESSIBLE JACOBI SEQUENCE[a]

a_2/a_1	a_3/a_1	$T/\|W\|$	$\hat{\Omega}^2$	$\hat{J}$	$\hat{W}$	$\hat{R}$
1.00	0.5827	0.1375	0.3742	0.3038	0.9751	1.415
0.95	0.5677	0.1376	0.3738	0.3041	0.9749	1.415
0.90	0.5519	0.1380	0.3726	0.3051	0.9742	1.418
0.85	0.5351	0.1386	0.3703	0.3070	0.9730	1.422
0.80	0.5172	0.1395	0.3668	0.3098	0.9711	1.428
0.75	0.4983	0.1407	0.3620	0.3139	0.9684	1.437
0.70	0.4781	0.1424	0.3557	0.3193	0.9649	1.449
0.65	0.4567	0.1446	0.3475	0.3264	0.9602	1.465
0.60	0.4338	0.1474	0.3373	0.3356	0.9542	1.486
0.55	0.4094	0.1509	0.3248	0.3474	0.9467	1.513
0.50	0.3833	0.1553	0.3096	0.3624	0.9371	1.548
0.45	0.3554	0.1606	0.2913	0.3815	0.9251	1.593
0.40	0.3256	0.1673	0.2697	0.4061	0.9099	1.651
0.35	0.2937	0.1754	0.2443	0.4380	0.8906	1.730
0.30	0.2594	0.1855	0.2149	0.4801	0.8659	1.836
0.25	0.2228	0.1980	0.1813	0.5372	0.8337	1.986
0.20	0.1835	0.2138	0.1436	0.6181	0.7908	2.209
0.15	0.1416	0.2339	0.1027	0.7401	0.7315	2.569
0.10	0.9682(-1)	0.2608	0.6047(-1)	0.9470	0.6445	3.243
0.08	0.7817(-1)	0.2743	0.4417(-1)	0.1079(+1)	0.5967	3.713
0.05	0.4944(-1)	0.2997	0.2187(-1)	0.1404(+1)	0.5001	4.991
0.	0.	0.5	0.	∞	0.	∞

[a] $\hat{\Omega}$, $\hat{J}$, $\hat{W}$, and $\hat{R}$ are defined in eq. (3.27).

Although this is probably not an exact result (for a discussion, see Tassoul 1978, chap. 10), the numerical data of Hachisu & Eriguchi (1982) indicate that, for $0 \leq n \leq 0.5$, the value of $T/|W|$ at the bifurcation point is constant to within about 2% (see Table 3).

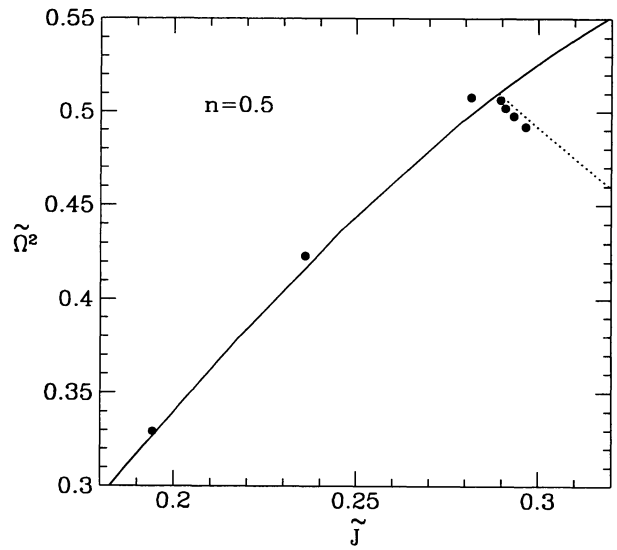

FIG. 8.—Comparison of our analytic results for the bifurcation of the $n = 0.5$ Maclaurin sequence (*solid line*) into the $n = 0.5$ Jacobi sequence (*dotted line*) with the numerical results (*filled circles*) of Hachisu (1986a) for axisymmetric configurations and Hachisu & Eriguchi (1982) for triaxial configurations. The last circle along the Jacobi branch corresponds to the mass-shedding limit for triaxial configurations (cf. Table 3). The units are defined in eqs. (4.17) and (4.24) (note that they differ from the units used in previous figures).

5. COMPRESSIBLE RIEMANN-S ELLIPSOIDS

We now generalize the treatment of § 4 to allow for the presence of *nonuniform* rotation. We restrict our discussion to the case where internal fluid motions have uniform vorticity parallel to the rotation axis, as in the classical Riemann-S ellipsoids (Ch69, chap. 7). The notations and definitions of § 4 are used except when noted.

5.1. *Equilibrium Conditions*

Consider first an ellipsoidal equilibrium configuration rotating rigidly with angular velocity $\boldsymbol{\Omega} = \Omega \boldsymbol{e}_3$, as in § 4. Now superpose on this background rigid rotation an internal velocity field specified by two requirements: (1) it must have a uniform vorticity parallel to $\boldsymbol{\Omega}$; (2) it must leave the ellipsoidal figure unchanged, that is, the velocity vector at any point in the fluid must be tangent to the isodensity surface passing through that point. Following Ch69 (chaps. 4 and 7) we write the fluid velocity *in the frame corotating with the equilibrium figure as*

$$\boldsymbol{u} = Q_1 x_2 \boldsymbol{e}_1 + Q_2 x_1 \boldsymbol{e}_2 , \tag{5.1}$$

where Q_1 and Q_2 are constants. This form ensures that our first requirement is satisfied. The second requirement can be used to calculate the values of Q_1 and Q_2 for a given vorticity. We find

$$\begin{aligned} Q_1 &= -\frac{a_1^2}{a_1^2 + a_2^2}\,\zeta = +\frac{a_1}{a_2}\,\Lambda , \\ Q_2 &= +\frac{a_2^2}{a_1^2 + a_2^2}\,\zeta = -\frac{a_2}{a_1}\,\Lambda , \end{aligned} \tag{5.2}$$

where ζ is the vorticity in the corotating frame,

$$\zeta \equiv (\nabla \times \boldsymbol{u}) \cdot \boldsymbol{e}_3 = -\frac{a_1^2 + a_2^2}{a_1 a_2}\,\Lambda , \tag{5.3}$$

and Λ is the angular frequency of the internal fluid motions.

The fluid velocity in the *inertial* frame is given by

$$\boldsymbol{u}^{(0)} = \boldsymbol{u} + \boldsymbol{\Omega} \times \boldsymbol{x} . \tag{5.4}$$

Using equations (5.1)–(5.4) one can easily calculate the total angular momentum $\boldsymbol{J}$ and rotational kinetic energy T. We find

$$\boldsymbol{J} \equiv \int \boldsymbol{x} \times \boldsymbol{u}^{(0)} \rho d^3x = (I\Omega - \tfrac{2}{5}\kappa_n M a_1 a_2 \Lambda)\boldsymbol{e}_3 , \tag{5.5}$$

and

$$\begin{aligned} T &\equiv \frac{1}{2}\int \boldsymbol{u}^{(0)} \cdot \boldsymbol{u}^{(0)} \rho d^3x \\ &= \tfrac{1}{2} I(\Lambda^2 + \Omega^2) - \tfrac{2}{5}\kappa_n M a_1 a_2 \Lambda\Omega \\ &= \tfrac{1}{20}\kappa_n M (a_1 - a_2)^2 (\Omega + \Lambda)^2 \\ &\quad + \tfrac{1}{20}\kappa_n M (a_1 + a_2)^2 (\Omega - \Lambda)^2 , \end{aligned} \tag{5.6}$$

where I is the moment of inertia, given by equation (4.8), and κ_n is given by expression (3.14). Also of interest are the fluid circulation along the equator,

$$C \equiv \oint_{\text{equator}} \boldsymbol{u}^{(0)} \cdot \boldsymbol{dl} = \pi(2 + f_{\mathrm{R}}) a_1 a_2 \Omega , \tag{5.7}$$

and the vorticity in the inertial frame,

$$\zeta^{(0)} \equiv (\nabla \times \boldsymbol{u}^{(0)}) \cdot \boldsymbol{e}_3 = (2 + f_{\mathrm{R}})\Omega , \tag{5.8}$$

where we have defined the ratio

$$f_{\mathrm{R}} \equiv \frac{\zeta}{\Omega} . \tag{5.9}$$

Conventionally Riemann-S equilibrium sequences have $f_{\mathrm{R}} =$ constant along the sequence. The Riemann-S sequence corresponding to $f_{\mathrm{R}} = \zeta = 0$ is the Jacobi sequence (§ 4), while that corresponding to $f_{\mathrm{R}} = \infty$ is the Dedekind sequence (Ch69, chap. 6). Dedekind ellipsoids have $\Omega = 0$, that is, they are stationary in the inertial frame, their triaxial ellipsoidal shape being supported entirely by internal fluid motions. Also of astrophysical interest is the *irrotational* Riemann-S sequence, which has $f_{\mathrm{R}} = -2$ and therefore $\zeta^{(0)} = C = 0$. Since C is a conserved quantity in the absence of viscosity, it may be more interesting to consider in general sequences of constant $C \neq 0$, rather than sequences of constant f_{R} (see, e.g., Kochanek 1992b).

Before we proceed to derive the equilibrium conditions, it is useful to rewrite the kinetic energy in a more convenient form, similar to those obtained in previous sections. We first introduce a conserved quantity $\mathscr{C}$, proportional to the circulation C, but with dimensions of an angular momentum,

$$\mathscr{C} \equiv -\frac{1}{5\pi}\kappa_n M C = I\Lambda - \frac{2}{5}\kappa_n M a_1 a_2 \Omega . \tag{5.10}$$

Since the quantity C as defined by equation (5.7) rarely appears explicitly in our results, we often refer to $\mathscr{C}$ itself as the circulation. In terms of the two conserved quantities J and $\mathscr{C}$, the kinetic energy, equation (5.6), can be rewritten in a form similar to that of equation (4.9) as

$$\begin{aligned} T &\equiv T_+ + T_- \\ &= \tfrac{1}{2} k_3 (J + \mathscr{C})^2 M^{-5/3} \rho_c^{2/3} h_+ \\ &\quad + \tfrac{1}{2} k_3 (J - \mathscr{C})^2 M^{-5/3} \rho_c^{2/3} h_- , \end{aligned} \tag{5.11}$$

where we have defined (cf. eqs. [4.4], [4.7], and [4.10])

$$h_\pm \equiv \frac{2(a_1 a_2 a_3)^{2/3}}{(a_1 \mp a_2)^2} = \frac{2\lambda_1^2 \lambda_2^2}{(\lambda_1^{3/2} \mp \lambda_2^{3/2})^2} . \tag{5.12}$$

When $\Lambda = 0$, that is, for Jacobi ellipsoids, we see from equations (5.10), (5.5), and (4.8) that $\mathscr{C} = -2a_1 a_2 J/(a_1^2 + a_2^2)$, and expression (5.11) reduces to (4.9), as expected.

The equilibrium conditions are the same as in § 4, but now $E = E(\rho_c, \lambda_1, \lambda_2; M, J, \mathscr{C}) = U + T + W$ and the partial derivatives must be calculated at constant M, J, *and* $\mathscr{C}$. The

expressions for U and W are the same as in § 4, while T is given by equation (5.11). The condition $\partial E/\partial\rho_c = 0$ provides the same virial relation as before, equation (3.20). The two conditions $\partial E/\partial\lambda_1 = \partial E/\partial\lambda_2 = 0$ give

$$\begin{aligned} 0 = &-\frac{20\pi G\bar{\rho}}{5-n}\left(A_1a_1^2 - \frac{1}{2}A_2a_2^2 - \frac{1}{2}A_3a_3^2\right) \\ &+\frac{1}{2}\kappa_n(a_1-a_2)(2a_1+a_2)(\Omega+\Lambda)^2 \\ &+\frac{1}{2}\kappa_n(a_1+a_2)(2a_1-a_2)(\Omega-\Lambda)^2 , \\ 0 = &\ (1\leftrightarrow 2) , \end{aligned} \tag{5.13}$$

analogous to the two conditions (4.15). Following manipulations similar to those described in § 4.1, these two conditions can be rewritten in terms of $\tilde{\Omega}$ (eq. [4.17]) and f_R as

$$\left[1+\frac{a_1^2a_2^2}{(a_1^2+a_2^2)^2}f_R^2\right]\tilde{\Omega}^2 = \frac{2B_{12}}{q_n} , \tag{5.14}$$

and

$$q_n\frac{a_1^2a_2^2}{a_1^2+a_2^2}f_R\tilde{\Omega}^2 = a_1^2a_2^2A_{12} - a_3^2A_3 . \tag{5.15}$$

These two conditions agree with equations (7.33) and (7.34) of Ch69 when $n = 0$ ($q_n = 1$). If we eliminate $\tilde{\Omega}^2$ between expressions (5.14) and (5.15), we obtain an equation relating the axis ratios along a given sequence (with fixed f_R),

$$\frac{a_1^2a_2^2}{(a_1^2+a_2^2)^2}f_R^2 + \frac{2a_1^2a_2^2B_{12}}{a_3^2A_3 - a_1^2a_2^2A_{12}}\frac{f_R}{a_1^2+a_2^2} + 1 = 0 . \tag{5.16}$$

Once the axis ratios are known, equation (5.14) can be solved for $\tilde{\Omega}^2$.

Note that, as we found in §§ 3 and 4, the equilibrium relation (5.16) for the axis ratios is *independent of the polytropic index* n. All properties of the incompressible Riemann-S ellipsoids resulting from this relation (Ch69, § 48) apply equally to the compressible analogues. In particular, to any compressible Riemann-S ellipsoid there corresponds another *adjoint ellipsoid* with the same axis ratios. If (f_R, Ω) and $(f_R^\dagger, \Omega^\dagger)$ define ellipsoids adjoints of one another, then

$$f_R^\dagger = \frac{(a_1^2+a_2^2)^2}{a_1^2a_2^2}\frac{1}{f_R} , \tag{5.17}$$

and

$$\Omega^\dagger = \frac{a_1a_2}{a_1^2+a_2^2}f_R\Omega . \tag{5.18}$$

This result is known as Dedekind's theorem (Ch69, §§ 28 and 48). Using equations (5.17) and (5.18) together with the definition (5.3) for Λ, we see that the adjoint ellipsoids have

$$\Omega^\dagger = -\Lambda, \quad \Lambda^\dagger = -\Omega . \tag{5.19}$$

Similarly, from equations (5.5) and (5.10) we see that

$$J^\dagger = -\mathscr{C}, \quad \mathscr{C}^\dagger = -J . \tag{5.20}$$

The Jacobi ($f_R = 0$) and Dedekind ($f_R = \infty$) sequences are adjoints of one another. In general, however, the configurations adjoint to the members of a Riemann-S sequence do not, strictly speaking, form another Riemann-S sequence, since they do not have f_R = constant. An important example is the sequence of configurations adjoint to the irrotational ($\mathscr{C} = 0$, $f_R = -2$) Riemann-S ellipsoids. These configurations have *zero angular momentum* in the inertial frame ($J = 0$, cf. eq. [5.20]), although both Ω and Λ are nonzero.

5.2. *Constructing the Equilibrium Sequences*

The procedure we use for constructing compressible Riemann-S sequences is similar to that described in § 4.2 for Jacobi ellipsoids. For given f_R and a_2/a_1, we determine a_3/a_1 by solving equation (5.16). We then calculate $\tilde{\Omega}$ from equation (5.14) and $\tilde{\Lambda} \equiv \Lambda/(\pi G\bar{\rho})^{1/2} = -a_1a_2f_R\tilde{\Omega}/(a_1^2+a_2^2)$. We calculate the ratio $T/|W|$ by using expressions (5.6) for T and expression (4.6) for W. The ratio R/R_0 is obtained from equation (4.25), and, finally, $\bar{J}$ and $\bar{E}$ from equations (5.5) and (3.23).

Figures 6 and 7 illustrate our results for the irrotational case ($f_R = -2$ and $\mathscr{C} = 0$). The variation of E and Ω^2 is shown along sequences with different values of n. Also shown are the corresponding Jacobi and Maclaurin sequences. The first member of each irrotational Riemann-S sequence is actually a nonrotating ($J = 0$) sphere, in which the rigid rotation (with $\Omega \neq 0$) and internal fluid motions cancel each other exactly. This can be seen from equations (5.5) and (4.8) with $a_1 = a_2 = R$. Thus the compressible Riemann-S sequences with $\mathscr{C} = 0$ bifurcate from a spherical polytrope.

In Table 5 we give the universal irrotational sequence, in terms of the variables introduced in § 3.2 (eq. [3.27]). Note that the irrotational Riemann-S ellipsoids all have $a_1 \geq a_3 \geq a_2$, in contrast to the Jacobi ellipsoids which have $a_1 \geq a_2 \geq a_3$ (cf. Table 4). With the help of the results (5.19) and (5.20), as well as the relation $\Lambda = 2a_1a_2\Omega/(a_1^2+a_2^2)$ for irrotational Riemann-S ellipsoids (cf. eqs. [5.3] and [5.9] with $f_R = -2$), Table 5 can also be used to calculate the properties of the adjoint configurations, the zero-angular-momentum ellipsoids. Similarly, with the relation $\mathscr{C} = -2a_1a_2J/(a_1^2+a_2^2)$ for Jacobi ellipsoids, Table 4 can be used to calculate the properties of the Dedekind sequence.

In the limit where $J \to 0$, the value of the angular frequency Ω for an irrotational Riemann-S ellipsoid is equal to half the eigenfrequency of the $l = 2$ f-mode of oscillation of a spherical polytrope (see, e.g., Cox 1980, chap. 17). Using the definition (3.27) of $\tilde{\Omega}^2$ and the result $\tilde{\Omega}^2 = \frac{4}{15}$ for $J = 0$ (cf. Table 5), we obtain a very simple approximate expression for this eigenfrequency as a function of polytropic index,

$$\frac{\Omega_{f,l=2}^2}{GM/R_0^3} = \frac{4}{\kappa_n(5-n)} . \tag{5.21}$$

For $n = 0$, this gives $\Omega_{f,l=2}/(GM/R_0^3)^{1/2} = 2/\sqrt{5}$, an exact result (cf. Cox 1980, eq. [17.80]). For $n = \frac{3}{2}$, expression (5.21) together with Table 1 gives $\Omega_{f,l=2}/(GM/R_0^3)^{1/2} = 1.495$,

TABLE 5

COMPRESSIBLE RIEMANN-S SEQUENCE WITH $\mathscr{C} = 0$[a]

a_2/a_1	a_3/a_1	$T/\|W\|$	$\hat{\Omega}^2$	$\hat{J}$	$\hat{W}$	$\hat{R}$
1.00	1.	0.	0.2667	0.	1.	1.
0.95	0.9741	0.1755(-3)	0.2667	0.4707(-3)	0.9998	1.001
0.90	0.9464	0.7412(-3)	0.2669	0.1986(-2)	0.9993	1.002
0.85	0.9167	0.1767(-2)	0.2673	0.4728(-2)	0.9982	1.005
0.80	0.8848	0.3341(-2)	0.2677	0.8917(-2)	0.9967	1.010
0.75	0.8505	0.5575(-2)	0.2683	0.1483(-1)	0.9945	1.017
0.70	0.8136	0.8611(-2)	0.2688	0.2282(-1)	0.9915	1.026
0.65	0.7736	0.1263(-1)	0.2692	0.3332(-1)	0.9876	1.039
0.60	0.7304	0.1788(-1)	0.2691	0.4691(-1)	0.9825	1.056
0.55	0.6835	0.2464(-1)	0.2683	0.6433(-1)	0.9759	1.078
0.50	0.6325	0.3331(-1)	0.2660	0.8660(-1)	0.9675	1.107
0.45	0.5772	0.4438(-1)	0.2614	0.1151	0.9566	1.147
0.40	0.5174	0.5842(-1)	0.2534	0.1516	0.9425	1.201
0.35	0.4531	0.7613(-1)	0.2403	0.1988	0.9239	1.277
0.30	0.3850	0.9826(-1)	0.2206	0.2606	0.8990	1.384
0.25	0.3143	0.1255	0.1927	0.3428	0.8653	1.543
0.20	0.2430	0.1584	0.1559	0.4551	0.8189	1.787
0.15	0.1737	0.1970	0.1117	0.6154	0.7534	2.190
0.10	0.1094	0.2415	0.6454(-1)	0.8666	0.6578	2.941
0.08	0.8546(-1)	0.2612	0.4653(-1)	0.1017(+1)	0.6063	3.454
0.05	0.5167(-1)	0.2941	0.2252(-1)	0.1370(+1)	0.5045	4.814
0.	0.	0.5	0.	∞	0.	∞

[a] $\hat{\Omega}$, $\hat{J}$, $\hat{W}$, and $\hat{R}$ are defined in eq. (3.27).

which agrees to better than 3% with the value 1.456 from Table 17.2 of Cox (1980). As expected from our use of a variational principle, expression (5.21) slightly *overestimates* the eigenfrequency. For an $n = 3$ polytrope with adiabatic index $\Gamma_1 = \frac{5}{3}$, Cox (1980) gives $\Omega_{f,l=2}/(GM/R_0^3)^{1/2} = 2.86$, still in reasonable agreement (to within about 15%) with the value 3.26 predicted by equation (5.21) for $n = 3$ (and $\Gamma = \Gamma_1 = \frac{4}{3}$; note that, f-modes being nearly incompressible, their eigenfrequencies should depend mostly on n, and very little on Γ_1).

6. STABILITY PROPERTIES OF SINGLE ROTATING STARS

As discussed in § 2.3, the energy variational method can be used to assess the stability of equilibrium configurations. As an illustration we study here the stability properties of compressible Maclaurin spheroids. Specifically, we identify the onset of instability to axisymmetric perturbations (§ 6.1), secular instability to nonaxisymmetric perturbations (§ 6.2), and dynamical instability (§ 6.3). We adopt the notations and definitions of §§ 3–5.

6.1. *Instability to Axisymmetric Perturbations*

The energy function $E(\rho_c, \lambda; M, J)$ of a compressible Maclaurin spheroid was given in § 3.1. Using the equilibrium conditions (3.20) and (3.21) we can calculate the second derivatives appearing in the condition (2.15). We find

$$\left(\frac{\partial^2 E}{\partial \rho_c^2}\right)_{\rm eq} = -\frac{W}{3\rho_c^2}\left[\left(\Gamma - \frac{4}{3}\right) - 2\left(\Gamma - \frac{5}{3}\right)\frac{T}{|W|}\right],$$

$$\left(\frac{\partial^2 E}{\partial \rho_c \partial \lambda}\right)_{\rm eq} = -\frac{W}{3\rho_c}\frac{g'}{g} = \frac{1}{3\rho_c \lambda}T, \qquad (6.1)$$

$$\left(\frac{\partial^2 E}{\partial \lambda^2}\right)_{\rm eq} = W\frac{g''}{g},$$

where the primes indicate a derivative with respect to λ and we have used the relation $g' = (g/\lambda)(T/|W|)$ (cf. ST, eq. [7.4.36]). The onset of instability is then determined by condition (2.15),

$$\left(\frac{\partial^2 E}{\partial \rho_c^2}\right)_{\rm eq}\left(\frac{\partial^2 E}{\partial \lambda^2}\right)_{\rm eq} - \left(\frac{\partial^2 E}{\partial \rho_c \partial \lambda}\right)_{\rm eq}^2 = 0\,. \qquad (6.2)$$

Substituting expressions (6.1) yields

$$\Gamma - \frac{4}{3} = -2\left(\frac{5}{3} - \Gamma\right)\frac{T}{|W|} - \frac{g}{3\lambda^2 g''}\left(\frac{T}{|W|}\right)^2. \qquad (6.3)$$

This condition becomes realized when Γ falls below a critical value $\Gamma_{\rm crit}$. Although $g'' < 0$, the first term in the righthand side of equation (6.3) is always dominant, so that $\Gamma_{\rm crit} \leq \frac{4}{3}$. Thus we recover the well-known result that rotation always tends to stabilize a star against collapse (see ST, § 9.6 and references therein[9]). In Figure 9 we plot the critical value $\Gamma_{\rm crit}$ for instability, determined from equation (6.3), as a function of the ratio $T/|W|$. We see that for rapidly rotating stars, the deviation from $\Gamma_{\rm crit} = \frac{4}{3}$ can be very large.

According to our discussion in § 2.4, the instability discussed above can be triggered only in the presence of viscosity, since uniform rotation was assumed in constructing the equilibrium model and maintained in the variation (i.e., M and J, but not $\mathscr{C}$, were held fixed). Therefore, we can only conclude here that the condition (6.3) signals the onset of *secular* instability to

[9] Note that the condition $(\partial^2 E/\partial \rho_c^2)_{\rm eq} = 0$ used in both ZN (§ 11.15) and ST (§ 9.6) is too restrictive, being limited to perturbations which do not change λ (see Colpi, Shapiro & Teukolsky 1991). Note also that our result is valid only for infinitesimal perturbations. It has been shown that for $\Gamma_{\rm crit} < \Gamma < \frac{4}{3}$, the rotating polytrope is metastable, i.e., it is unstable to finite-amplitude perturbations (Tassoul 1970; Tassoul & Tassoul 1971).

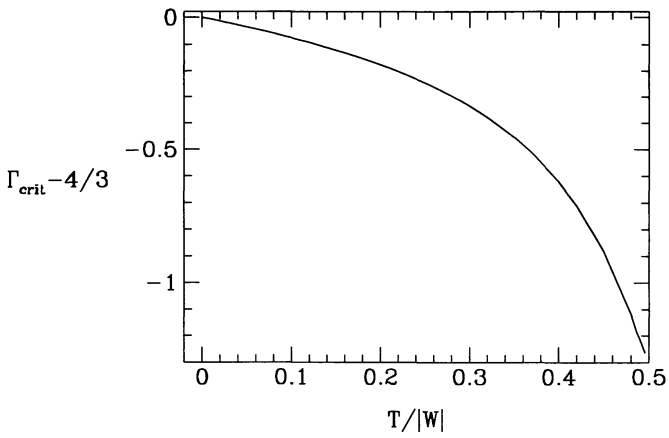

FIG. 9.—Critical adiabatic exponent for the onset of radial instability in a compressible Maclaurin spheroid.

axisymmetric perturbations. However, we will show in § 6.3 that the same condition applies in fact at the onset of *dynamical* instability to "radial" collapse.

6.2. *Secular Instability to Nonaxisymmetric Perturbations*

We now allow for more general, nonaxisymmetric perturbations, but still maintaining uniform rigid rotation. This is done by using the energy function $E = E(\rho_c, \lambda_1, \lambda_2; M, J)$ of a compressible *Jacobi ellipsoid* (§ 4.1) in condition (2.15), but evaluating the determinant along the equilibrium *Maclaurin* sequence (for which $\lambda_1 = \lambda_2$). Using the results of §§ 3.1 and 4.1 we find

$$\rho_c^2\left(\frac{\partial^2 E}{\partial \rho_c^2}\right)_{eq} = \frac{W}{3}\left[\left(\frac{1}{3}-\frac{1}{n}\right) - 2\left(\frac{2}{3}-\frac{1}{n}\right)\frac{T}{|W|}\right],$$

$$\rho_c\lambda_1\left(\frac{\partial^2 E}{\partial \rho_c \partial \lambda_1}\right)_{eq} = \frac{2h_{(1)}}{3}T + \frac{\mathcal{I}_{(1)}}{3}W = \frac{h_{(1)}}{3}T = \frac{1}{6}T,$$

$$\lambda_1^2\left(\frac{\partial^2 E}{\partial \lambda_1^2}\right)_{eq} = h_{(11)}T + \mathcal{I}_{(11)}W = -\frac{5}{2}T + \mathcal{I}_{(11)}W, \tag{6.4}$$

$$\lambda_1\lambda_2\left(\frac{\partial^2 E}{\partial \lambda_1 \partial \lambda_2}\right)_{eq} = h_{(12)}T + \mathcal{I}_{(12)}W = \frac{5}{2}T + \mathcal{I}_{(12)}W,$$

where the quantities $h_{(i)}$, $h_{(ij)}$, $\mathcal{I}_{(i)}$, and $\mathcal{I}_{(ij)}$ are defined in Appendix A and have been evaluated here for $\lambda_1 = \lambda_2$. When $\lambda_1 = \lambda_2$, the determinant appearing in condition (2.15) can be factored explicitly into a product of two expressions, corresponding to the two eigenmodes of perturbation (cf. § 2.3). Two stability conditions are obtained by setting either expression equal to zero.

The first condition is

$$\left(\frac{\partial^2 E}{\partial \rho_c^2}\right)_{eq}\left[\left(\frac{\partial^2 E}{\partial \lambda_1 \partial \lambda_2}\right)_{eq} + \left(\frac{\partial^2 E}{\partial \lambda_1^2}\right)_{eq}\right] = 2\left(\frac{\partial^2 E}{\partial \rho_c \lambda_1}\right)_{eq}^2. \tag{6.5}$$

Substituting expressions (6.4) gives

$$\Gamma - \frac{4}{3} = -2\left(\frac{5}{3}-\Gamma\right)\frac{T}{|W|} - \frac{1}{6(\mathcal{I}_{(11)}+\mathcal{I}_{(12)})}\left(\frac{T}{|W|}\right)^2. \tag{6.6}$$

Using the results of Appendix A and chapter 3 of Ch69 for $a_1 = a_2$, we find that

$$\mathcal{I}_{(11)} + \mathcal{I}_{(12)} = \frac{1}{\mathcal{I}}(-9a_1^2B_{11} + 2a_1^2A_1 + a_3^2A_3) = \frac{\lambda^2 g''}{2g}, \tag{6.7}$$

and we recover with equation (6.6) the condition (6.3) for the onset of secular instability to axisymmetric perturbations already derived in § 6.1.

The second condition is

$$\left(\frac{\partial^2 E}{\partial \lambda_1^2}\right)_{eq} = \left(\frac{\partial^2 E}{\partial \lambda_1 \partial \lambda_2}\right)_{eq}. \tag{6.8}$$

Substituting expressions (6.4) we get

$$\frac{T}{|W|} = \frac{1}{5}(\mathcal{I}_{(12)} - \mathcal{I}_{(11)}). \tag{6.9}$$

With the help of the results of Appendix A and chapter 3 of Ch69 for $a_1 = a_2$, one can see that

$$\mathcal{I}_{(12)} - \mathcal{I}_{(11)} = \frac{1}{2\mathcal{I}}(9a_1^2B_{11} + a_1^2A_1 - a_3^2A_3) = \frac{5a_1^2B_{11}}{\mathcal{I}}, \tag{6.10}$$

where we have used equation (6.9) and the equilibrium relation (4.14) for $a_1 = a_2$ to obtain the last expression. On the other hand, the equilibrium relations (4.14) and (4.16) give

$$\frac{T}{|W|} = \frac{1}{2}q_n\tilde{\Omega}^2\frac{a_1^2}{\mathcal{I}}, \tag{6.11}$$

so that the condition (6.9) is equivalent to

$$\tilde{\Omega}^2 = \frac{2B_{11}}{q_n} \quad \text{(secular instability)}. \tag{6.12}$$

Comparing this to equation (4.23), and noting that $B_{11} = B_{12}$ when $a_1 = a_2$, we see that the condition becomes realized precisely at the point where the Jacobi and Dedekind sequences

bifurcate from the Maclaurin sequence. Thus we have shown that, just as in the incompressible case (Ch69, § 37), compressible Maclaurin spheroids become secularly unstable to triaxial deformations at the bifurcation point, where $T/|W| = 0.1375$.

In our approximation, the value of $T/|W| \equiv (T/|W|)_{sec}$ at the secular instability limit is therefore independent of the polytropic index n. This prediction is in agreement with the results of extensive numerical studies of the oscillations of axisymmetric polytropes in rapid rotation. In the most recent of these studies, Ipser & Lindblom (1990) give a value of $(T/|W|)_{sec} = 0.1298$ for $n = 0.75$, very close to the value $(T/|W|)_{sec} = 0.1375$ obtained for $n = 0$. These values correspond to the point where a uniformly rotating polytrope becomes secularly unstable to the $l = m = 2$ f-mode of oscillation. This is the only mode of oscillation compatible with our ellipsoidal approximation. However, it should be noted that higher modes of oscillations, with $m > 2$, can become unstable at values of $T/|W|$ that are somewhat smaller and depend more sensitively on the compressibility (see Ipser & Lindblom 1990 and references therein). This reflects our expectation that the conditions given in § 2.3 are only sufficient—but not necessary—conditions for instability.

The analysis presented above is based on an equilibrium model for which we specify the angular momentum J. As noted in § 2.4, the secular instability identified here can therefore be triggered only by a dissipation mechanism which conserves J, such as viscosity. We can also use our method to study secular stability against a dissipation mechanism which conserves the circulation $\mathscr{C}$, rather than J, such as the emission of gravitational radiation. The energy function of a *Dedekind* ellipsoid (§ 5.1) should then be used in condition (2.15), before evaluating it along the equilibrium Maclaurin sequence. Because the energy function of a general Riemann-S ellipsoid (§ 5.1) is symmetric under interchange of J and $\mathscr{C}$ (cf. eq. [5.11]), the analysis is virtually identical to the one presented above, with $\mathscr{C}$ appearing in place of J in all results. In particular, the onset of secular instability is again given by equation (6.12), and occurs at the bifurcation point. Physically, viscous forces (which conserve J but not $\mathscr{C}$) can drive a perturbed Maclaurin spheroid past the point of bifurcation to a (lower energy) Jacobi ellipsoid, while gravitational radiation reaction forces (which conserve $\mathscr{C}$ but not J) can drive it to a Dedekind ellipsoid. These results are well established for the incompressible case (see ST, § 7.3 and references therein).

6.3. *Dynamical Instability*

We now consider the stability of compressible Maclaurin spheroids to perturbations which conserve M, J, *and* $\mathscr{C}$. According to our discussion of § 2.4, we refer to this as dynamical stability. We use the energy function $E = E(\rho_c, \lambda_1, \lambda_2; M, J, \mathscr{C})$ of a general Riemann-S ellipsoid (§ 5.1) to evaluate the determinant of condition (2.15) for $a_1 = a_2$.

The only difference between the energy functions of Jacobi and Riemann-S ellipsoids lies in the kinetic energy term. For Riemann-S ellipsoids we can write T in the form (cf. eqs. [4.7]–[4.9] and [5.11])

$$T = T_+ + T_- = \frac{(J + \mathscr{C})^2}{4I_s} h_+ + \frac{(J - \mathscr{C})^2}{4I_s} h_- . \quad (6.13)$$

However, since

$$J + \mathscr{C} = \tfrac{1}{5}\kappa_n M(a_1 - a_2)^2(\Omega + \Lambda) , \quad (6.14)$$

(cf. eqs. [5.6] and [5.11]), while for Maclaurin spheroids $a_1 = a_2$, the perturbed configurations must have $J + \mathscr{C} = 0$ if J and $\mathscr{C}$ are both conserved. Thus we can write here

$$T = T_- = \frac{J^2}{I_s} h_- , \quad (6.15)$$

whereas $T = (J^2/2I_s)h$ for Jacobi ellipsoids (cf. eq. [4.9]), so that the stability analysis proceeds exactly as in § 6.2 but with $2h_-$ replacing h in all expressions. In particular we find that the second derivatives are given by expressions similar to expression (6.4), but we now have to use the values $h_{-(1)} = \frac{1}{2}$, $h_{-(11)} = -\frac{11}{8}$ and $h_{-(12)} = \frac{11}{8}$.

Once again the determinant can be factored into a product of two expressions, leading to the two conditions (6.5) and (6.8). As in § 6.2, with the first one, we recover the condition (6.3) obtained in § 6.1 for the onset of secular instability to axisymmetric perturbations. Therefore, this condition does in fact give the onset of *dynamical* instability to "radial" collapse as well.

Using the results of Appendix A and chapter 3 of Ch69 for $a_1 = a_2$, we find that the second condition (eq. [6.8]) leads to

$$\frac{T}{|W|} = \frac{4}{11}(\mathscr{I}_{(12)} - \mathscr{I}_{(11)}) = \frac{2}{11\mathscr{I}}(9a_1^2 B_{11} + a_1^2 A_1 - a_3^2 A_3) = \frac{2a_1^2 B_{11}}{\mathscr{I}} . \quad (6.16)$$

With equation (6.11), this is equivalent to

$$\tilde{\Omega}^2 = \frac{4B_{11}}{q_n} \quad \text{(dynamical instability)} . \quad (6.17)$$

This is the compressible analog of a well-known result for the dynamical instability of classical Maclaurin spheroids (Ch69, § 33). When $n = 0$ ($q_n = 1$), expression (6.17) reduces to equation (5.58) of Ch69. This result confirms our interpretation of condition (2.15) in terms of a dynamical instability when nonuniform rotation of the equilibrium model is allowed (§ 2.4). The onset of instability occurs at the point where $e = 0.9529$ and $T/|W| = 0.2738$, independent of n in our approximation. This point was in fact identified by Riemann (1860) for incompressible spheroids, using a variational method very similar to ours (see Ch69, § 53, for a summary).

7. COMPRESSIBLE ROCHE ELLIPSOIDS

In this section we apply our energy variational method to the classical Roche problem for a polytrope in circular orbit about a point-mass companion. So far as we know, this is the first time that the energy variational method has been applied to determine the equilibrium and stability properties of a binary stellar configuration. Except when noted, we adopt the notations and definitions of § 4.

7.1. *Equilibrium Conditions*

Consider a binary system consisting of a polytrope of mass M and central density ρ_c, in circular orbit around a pointlike companion of mass M'. The binary is assumed to be in a state of synchronized rotation, with the spin of the polytrope aligned and equal in magnitude to the orbital angular frequency Ω. We denote the mass ratio by $p \equiv M/M'$ and the distances from the centers of mass of M and M' to that of the binary by $r_{\rm cm}$ and $r'_{\rm cm}$. The binary separation can then be written as $r = r_{\rm cm} + r'_{\rm cm} = (1+p)r_{\rm cm}$. We denote by J the total angular momentum of the binary. Under the combined effects of centrifugal and tidal forces, the polytrope assumes a nonspherical equilibrium configuration which we approximate by a triaxial ellipsoid as described in § 2.2. We denote the principal axes of the outer surface by a_1, a_2, and a_3, with a_1 measured along the axis of the binary, a_2 in the direction of the orbital motion, and a_3 along the rotation axis.

The total energy of the system (not necessarily in equilibrium) can be written

$$E(\rho_c, \lambda_1, \lambda_2, r; M, M', J) = U + T + W + W_i \,. \quad (7.1)$$

Here W is the gravitational potential self-energy of the star, whereas W_i is the gravitational interaction energy of the binary. The expressions for the internal energy U and the potential energy W retain the same form they had for an isolated rotating star (eqs. [3.1] and [4.6]). The kinetic energy T is modified by the orbital motion,

$$T = \frac{J^2}{2I_{\rm cm}} = \frac{1}{2} I_{\rm cm}\Omega^2 \,, \quad (7.2)$$

with

$$I_{\rm cm} = Mr_{\rm cm}^2 + M'r_{\rm cm}'^2 + I = \frac{Mr^2}{1+p} + \frac{M^{5/3}\rho_c^{-2/3}}{2k_3 h(\lambda_1, \lambda_2)} \,, \quad (7.3)$$

where I is the moment of inertia of M about the polar axis a_3 (cf. eqs. [4.8]–[4.10]). The general form of the gravitational interaction energy W_i for two ellipsoidal configurations in a binary system is given in Appendix B. Here, since M' is a point mass, we have $I'_{jj} = 0$, and equation (B7) gives

$$W_i = -\frac{GMM'}{r} - \frac{1}{2}\frac{GM'}{r^3}(2I_{11} - I_{22} - I_{33}) \,, \quad (7.4)$$

where the I_{jj} are given by equation (B8). There are now four equilibrium conditions,

$$\frac{\partial E}{\partial r} = \frac{\partial E}{\partial \rho_c} = \frac{\partial E}{\partial \lambda_1} = \frac{\partial E}{\partial \lambda_2} = 0 \,, \quad (7.5)$$

where the derivatives are evaluated at constant M, M', and J.

The first condition, $\partial E/\partial r = \partial T/\partial r + \partial W_i/\partial r = 0$, provides us with an equilibrium relation between Ω^2 and r, that is, the *modified Kepler's law* for the binary. Using equations (7.2)–(7.4) we find

$$\Omega^2 = \frac{(1+p)}{Mr}\frac{\partial W_i}{\partial r} = \frac{G(M+M')}{r^3}(1+\delta) \,, \quad (7.6)$$

where we have defined

$$\delta \equiv \frac{3}{2}\frac{(2I_{11} - I_{22} - I_{33})}{Mr^2} = \frac{3}{10}\kappa_n(2a_1^2 - a_2^2 - a_3^2)\frac{1}{r^2} \,, \quad (7.7)$$

with κ_n given by equation (3.14). Note that the conventional TV treatment of the Roche problem uses instead the *unmodified* Kepler's law, $\Omega^2 = \Omega_{\rm K}^2 \equiv G(M+M')/r^3$ (cf. Ch69, eq. [8.5]). This is because Ω^2 is determined by the requirement that certain terms linear in the coordinates disappear from the fluid equation of motion, to lowest order (Ch69, § 65). We refer the reader to Appendix C, however, for a discussion of how the more accurate equation (7.6) can actually be obtained within the TV approach.

As before, the equilibrium condition $\partial E/\partial \rho_c = 0$ leads to the virial relation. Using equations (7.1)–(7.4) we get

$$\frac{3}{n}U + W + 2T_s = 2W_t \,, \quad (7.8)$$

where we have defined the spin kinetic energy,

$$T_s \equiv \tfrac{1}{2} I\Omega^2 \,, \quad (7.9)$$

and the tidal interaction energy,

$$W_t \equiv W_i + \frac{GMM'}{r} \,. \quad (7.10)$$

Combining this with equations (7.1)–(7.4) we can calculate the total *equilibrium* energy. We find

$$E_{\rm eq} = \frac{3-n}{3}W\left[1 - \left(\frac{3-2n}{3-n}\right)\frac{T_s}{|W|}\right] + \frac{Mr^2\Omega^2}{2(1+p)} - \frac{GMM'}{r} - \left(\frac{2n+3}{6}\right)\frac{GM'}{r^3}(2I_{11} - I_{22} - I_{33}) \,. \quad (7.11)$$

The first term in this expression represents the "intrinsic" energy of the polytrope (cf. eq. [3.23]), the second term the orbital kinetic energy, and the last two terms the gravitational interaction energy. The total angular momentum of the system in equilibrium is

$$J = I_{\rm cm}\Omega = \left[\frac{Mr^2}{(1+p)} + I\right]\Omega \,, \quad (7.12)$$

with Ω calculated from equation (7.6). Note that $I = I_{11} + I_{12}$ (cf. eqs. [4.8] and [B4]).

Following manipulations similar to those described in § 4, the two equilibrium conditions $\partial E/\partial\lambda_1 = \partial T/\partial\lambda_1 + \partial W/\partial\lambda_1 + \partial W_i/\partial\lambda_1 = 0 = \partial E/\partial\lambda_2$ can be written

$$0 = \left(\mathcal{M}_{11} - \frac{1}{2}\mathcal{M}_{22} - \frac{1}{2}\mathcal{M}_{33}\right) + I_{11}(2\mu + \Omega^2) + I_{22}\left(\frac{\mu}{2} - \frac{1}{2}\Omega^2\right) + I_{33}\frac{\mu}{2}, \\ = (1 \leftrightarrow 2), \tag{7.13}$$

where, following Ch69, we have introduced the components of the *potential-energy tensor* (Ch69, § 10),

$$\mathcal{M}_{ij} \equiv -2\pi G\bar{\rho}A_i\left(\frac{Ma_i^2\delta_{ij}}{5-n}\right) \quad \text{(no summation)}, \tag{7.14}$$

such that $W = \mathcal{M}_{ii}$, and the quantity

$$\mu \equiv \frac{GM'}{r^3}, \tag{7.15}$$

which measures the strength of the tidal forces. Note that the quantity in parentheses in expression (7.14) is equal to I_{ij} (eq. [B4]) only in the incompressible limit, so that the result (3.128) of Ch69 applies only when $n = 0$. Together with the virial relation, equation (7.8), the two conditions (7.13) can be rewritten in the symmetric form

$$\mathcal{M}_{11} + I_{11}(\Omega^2 + 2\mu) = \mathcal{M}_{22} + I_{22}(\Omega^2 - \mu) \\ = \mathcal{M}_{33} - \mu I_{33} = -\frac{U}{n}. \tag{7.16}$$

These are the compressible generalizations of equations (8.9) of Ch69, but now, according to equation (7.6), we have

$$\Omega^2 = (1+p)\mu(1+\delta), \tag{7.17}$$

instead of $\Omega^2 = \Omega_K^2 = (1+p)\mu$(Ch69, eq. [8.12]). The first two conditions in equation (7.16) can also be written as

$$q_n\{[2 + (1+p)(1+\delta)]a_1^2 + a_3^2\}\tilde{\mu} \\ = 2(A_1a_1^2 - A_3a_3^2) \equiv 2(a_1^2 - a_3^2)B_{13}, \tag{7.18}$$

and

$$q_n\{[(1+p)(1+\delta) - 1]a_2^2 + a_3^2\}\tilde{\mu} \\ = 2(A_2a_2^2 - A_3a_3^2) \equiv 2(a_2^2 - a_3^2)B_{23}, \tag{7.19}$$

where we have defined $\tilde{\mu} \equiv \mu/(\pi G\bar{\rho})$ and introduced the index symbols B_{13} and B_{23} (Ch69, § 21). Taking the ratio of these two conditions, we get

$$\frac{[2 + (1+p)(1+\delta)]a_1^2 + a_3^2}{[(1+p)(1+\delta) - 1]a_2^2 + a_3^2} = \frac{(a_1^2 - a_3^2)B_{13}}{(a_2^2 - a_3^2)B_{23}}. \tag{7.20}$$

If we set $\delta = 0$, that is, neglect the correction to Kepler's law, this equation reduces to the same relation between the axis ratios of incompressible Roche ellipsoids given by Ch69 (cf. his eq. [8.16]). But since $\delta \neq 0$ in our treatment, simply taking the ratio of equations (7.18) and (7.19) does not yield a relation between the axis ratios, since δ has an explicit dependence on r (cf. eq. [7.7]). Instead, we have to properly eliminate r between equations (7.18) and (7.19), after replacing δ and $\tilde{\mu}$ by their definitions. Since the result is very cumbersome, and not useful in practice (cf. § 7.2), we do not give it explicitly. It is worth noting, however, that the relation between the axis ratios for compressible Roche ellipsoids is *not* independent of n (in contrast to the result obtained for all isolated configurations). But the explicit dependence on compressibility is very weak. This can be seen as follows. From equation (7.20) we see that δ is uniquely specified once the two axis ratios are known. Therefore the dependence on compressibility in equations (7.18) and (7.19) is through the product $q_n\tilde{\mu}$ only. But since $\delta \propto \kappa_n/r^2$, we have $q_n\tilde{\mu} \propto \kappa_n(1 - n/5)/r^3 \propto (1 - n/5)/\kappa_n^{1/2}$, where all constants of proportionality are functions of the axis ratios only. Using the values listed in Table 1, we find that the quantity $(1 - n/5)/\kappa_n^{1/2}$ varies only between 0.9 and 1.0 for $0 \leq n \leq 3$.

7.2. *Constructing Equilibrium Sequences*

For given masses M and M', we construct a one-parameter sequence of equilibrium configurations, parameterized by the binary separation r or the angular momentum J, as follows. We choose a value for the ratio r/a_1 and solve equations (7.18) and (7.19) for the two axis ratios a_2/a_1 and a_3/a_1. This is done by iteration, starting with the values given in Ch69 (for $n = 0$ and $\delta = 0$) as initial guesses, and using a multidimensional Newton-Raphson scheme. The quantities $\tilde{\Omega}$, $f(\lambda_1, \lambda_2)$, and $T_s/|W|$ are then determined using equations (7.17), (4.3), (7.9) and (4.6). The angular momentum J and total energy E_{eq} are obtained from equations (7.12) and (7.11). As before, we will give numerical values in units scaled to the spherical polytrope of radius R_0 (eq. [3.24]). One can convert from units based on R_0 to units based on the mean radius $R = (a_1a_2a_3)^{1/3}$ by using the relation

$$R = R_0\left[f(\lambda_1, \lambda_2)\left(1 - 2\frac{T_s}{|W|}\right) - \left(\frac{5-n}{3p}\right)g_t\right]^{-n/(3-n)}, \tag{7.21}$$

which can be derived easily from the results of § 7.1. Here we have defined

$$g_t \equiv \frac{R}{Mr^3}(2I_{11} - I_{22} - I_{33}) = \frac{2}{3}\frac{R}{r}\delta. \tag{7.22}$$

Universal variables (cf. § 3.2) cannot be defined here because of the explicit dependence of δ on the polytropic index (The limiting case $p = 0$ is an exception and is discussed in § 8.3). Therefore, equilibrium sequences must be calculated separately and explicitly for each n. Representative results are given in Table 6 for $p = 1$ and 0.1, and $n = 0$, 1, 1.5, and 2.5.

TABLE 6

COMPRESSIBLE ROCHE SEQUENCES[a]

$rp^{1/3}/a_1$ [b]	$rp^{1/3}/R_o$	a_2/a_1	a_3/a_1	$T_s/\|W\|$	$\tilde{\Omega}$	$\tilde{J}$	$\tilde{E}$	R/R_o
			$p = 1, \quad n = 0$					
5.0	5.131	0.9707	0.9533	0.506(-2)	0.1406	1.653	-0.6943	1.
4.0	4.202	0.9441	0.9139	0.943(-2)	0.1901	1.522	-0.7128	1.
3.0	3.348	0.8750	0.8222	0.199(-1)	0.2690	1.408	-0.7349	1.
2.7	3.124	0.8345	0.7738	0.257(-1)	0.3000	1.386	-0.7404	1.
2.5	2.989	0.7981	0.7330	0.306(-1)	0.3222	1.377	-0.7427	1.
2.380*	2.916	0.7715	0.7044	0.341(-1)	0.3358	1.375	-0.7432	1.
2.2	2.821	0.7236	0.6553	0.401(-1)	0.3556	1.380	-0.7418	1.
2.112**	2.783	0.6960	0.6281	0.436(-1)	0.3648	1.386	-0.7399	1.
2.0	2.744	0.6561	0.5901	0.484(-1)	0.3753	1.399	-0.7358	1.
1.801***	2.713	0.5708	0.5123	0.588(-1)	0.3886	1.441	-0.7218	1.
1.697	2.724	0.5184	0.4664	0.653(-1)	0.3908	1.477	-0.7097	1.
1.6	2.759	0.4644	0.4198	0.724(-1)	0.3884	1.524	-0.6939	1.
1.5	2.831	0.4040	0.3682	0.810(-1)	0.3798	1.590	-0.6717	1.
1.0	5.312	0.0823	0.0811	0.167	0.1685	2.888	-0.3772	1.
			$p = 1, \quad n = 1$					
5.0	5.083	0.9845	0.9748	0.271(-2)	0.1425	1.628	-0.5963	1.0028
4.0	4.129	0.9701	0.9524	0.516(-2)	0.1948	1.484	-0.6170	1.0055
3.0	3.228	0.9314	0.8960	0.114(-1)	0.2826	1.344	-0.6453	1.0131
2.5	2.826	0.8860	0.8359	0.183(-1)	0.3465	1.288	-0.6605	1.0228
2.2	2.619	0.8393	0.7794	0.250(-1)	0.3905	1.267	-0.6671	1.0336
2.047*	2.531	0.8063	0.7420	0.295(-1)	0.4131	1.264	-0.6683	1.0418
1.9	2.462	0.7664	0.6991	0.347(-1)	0.4332	1.268	-0.6668	1.0524
1.760**	2.417	0.7189	0.6506	0.407(-1)	0.4490	1.281	-0.6617	1.0661
1.7	2.406	0.6954	0.6275	0.436(-1)	0.4540	1.290	-0.6580	1.0734
1.632***	2.401	0.6656	0.5990	0.473(-1)	0.4579	1.305	-0.6522	1.0831
1.3	2.587	0.4723	0.4265	0.714(-1)	0.4272	1.472	-0.5873	1.1665
1.0	3.750	0.2327	0.2200	0.113	0.2634	2.046	-0.4185	1.3925
			$p = 1, \quad n = 1.5$					
5.0	5.067	0.9894	0.9825	0.187(-2)	0.1432	1.618	-0.5256	1.0038
4.0	4.104	0.9794	0.9667	0.359(-2)	0.1965	1.469	-0.5472	1.0075
3.0	3.185	0.9522	0.9256	0.812(-2)	0.2879	1.319	-0.5780	1.0180
2.5	2.767	0.9197	0.8799	0.133(-1)	0.3565	1.253	-0.5964	1.0313
2.2	2.545	0.8855	0.8353	0.184(-1)	0.4054	1.223	-0.6062	1.0463
2.0	2.420	0.8519	0.7942	0.232(-1)	0.4392	1.212	-0.6104	1.0621
1.902*	2.367	0.8309	0.7697	0.262(-1)	0.4551	1.210	-0.6110	1.0725
1.7	2.290	0.7749	0.7080	0.336(-1)	0.4824	1.219	-0.6072	1.1027
1.592**	2.272	0.7357	0.6674	0.386(-1)	0.4913	1.235	-0.6007	1.1260
1.564***	2.271	0.7243	0.6559	0.401(-1)	0.4926	1.240	-0.5983	1.1331
1.3	2.388	0.5848	0.5248	0.571(-1)	0.4696	1.347	-0.5533	1.2388
1.0	3.303	0.3447	0.3175	0.906(-1)	0.3069	1.782	-0.4086	1.5798
			$p = 1, \quad n = 2.5$					
5.0	5.056	0.9958	0.9931	0.740(-3)	0.1436	1.604	-0.2980	1.0075
4.0	4.088	0.9919	0.9866	0.143(-2)	0.1976	1.450	-0.3206	1.0147
3.0	3.159	0.9809	0.9691	0.333(-2)	0.2910	1.288	-0.3542	1.0352
2.5	2.732	0.9674	0.9481	0.562(-2)	0.3620	1.211	-0.3759	1.0617
2.0	2.375	0.9378	0.9050	0.104(-1)	0.4474	1.151	-0.3967	1.1245
1.9	2.321	0.9281	0.8914	0.120(-1)	0.4636	1.144	-0.3993	1.1468
1.763*	2.263	0.9112	0.8685	0.146(-1)	0.4825	1.140	-0.4009	1.1873
1.7	2.244	0.9018	0.8561	0.160(-1)	0.4889	1.141	-0.4005	1.2110
1.582***	2.229	0.8804	0.8289	0.192(-1)	0.4951	1.150	-0.3969	1.2681
1.294**	2.390	0.7966	0.7312	0.308(-1)	0.4510	1.238	-0.3605	1.5433
1.0	3.567	0.6268	0.5627	0.521(-1)	0.2552	1.625	-0.2455	2.5203

TABLE 6—*Continued*

$rp^{1/3}/a_1$ [b]	$rp^{1/3}/R_o$	a_2/a_1	a_3/a_1	$T_s/\|W\|$	$\bar{\Omega}$	$\bar{J}$	$\bar{E}$	R/R_o
			$p = 0.1, \quad n = 0$					
5.0	5.116	0.9711	0.9615	0.279(-2)	0.1047	10.048	-1.0519	1.
4.0	4.177	0.9454	0.9286	0.520(-2)	0.1419	9.100	-1.1520	1.
3.0	3.302	0.8812	0.8514	0.110(-1)	0.2022	8.131	-1.2943	1.
2.5	2.916	0.8129	0.7751	0.169(-1)	0.2441	7.682	-1.3808	1.
2.0	2.609	0.6923	0.6510	0.268(-1)	0.2900	7.337	-1.4599	1.
1.8	2.527	0.6211	0.5821	0.326(-1)	0.3053	7.268	-1.4777	1.
1.714*	2.503	0.5855	0.5484	0.355(-1)	0.3103	7.260	-1.4799	1.
1.670**	2.495	0.5661	0.5302	0.371(-1)	0.3122	7.262	-1.4793	1.
1.6	2.488	0.5328	0.4993	0.399(-1)	0.3143	7.277	-1.4752	1.
1.576***	2.487	0.5209	0.4883	0.409(-1)	0.3147	7.286	-1.4727	1.
1.3	2.591	0.3651	0.3461	0.557(-1)	0.3000	7.591	-1.3911	1.
1.0	3.315	0.1677	0.1637	0.843(-1)	0.2129	8.965	-1.0883	1.
			$p = 0.1, \quad n = 1$					
5.0	5.069	0.9846	0.9793	0.149(-2)	0.1061	9.989	-0.9567	1.0016
4.0	4.107	0.9705	0.9607	0.284(-2)	0.1455	9.004	-1.0628	1.0031
3.0	3.187	0.9335	0.9137	0.631(-2)	0.2130	7.957	-1.2226	1.0076
2.5	2.765	0.8913	0.8630	0.101(-1)	0.2637	7.437	-1.3295	1.0135
2.0	2.404	0.8098	0.7718	0.172(-1)	0.3262	6.977	-1.4461	1.0277
1.8	2.292	0.7575	0.7167	0.215(-1)	0.3510	6.842	-1.4859	1.0389
1.6	2.215	0.6879	0.6466	0.272(-1)	0.3708	6.765	-1.5098	1.0567
1.539*	2.201	0.6625	0.6218	0.292(-1)	0.3747	6.759	-1.5115	1.0641
1.460**	2.193	0.6262	0.5869	0.322(-1)	0.3775	6.770	-1.5081	1.0758
1.451***	2.193	0.6215	0.5824	0.326(-1)	0.3776	6.773	-1.5071	1.0774
1.3	2.224	0.5395	0.5054	0.393(-1)	0.3716	6.878	-1.4728	1.1096
1.0	2.676	0.3277	0.3121	0.599(-1)	0.2869	7.767	-1.2201	1.2515
			$p = 0.1, \quad n = 1.5$					
5.0	5.053	0.9894	0.9857	0.103(-2)	0.1066	9.967	-0.8870	1.0021
4.0	4.082	0.9796	0.9726	0.198(-2)	0.1468	8.969	-0.9953	1.0042
3.0	3.145	0.9532	0.9385	0.448(-2)	0.2172	7.892	-1.1621	1.0102
2.5	2.708	0.9224	0.9002	0.733(-2)	0.2720	7.342	-1.2780	1.0182
2.0	2.323	0.8604	0.8276	0.128(-1)	0.3428	6.833	-1.4126	1.0373
1.8	2.198	0.8190	0.7818	0.164(-1)	0.3730	6.668	-1.4638	1.0525
1.6	2.104	0.7620	0.7214	0.212(-1)	0.3992	6.553	-1.5020	1.0771
1.464*	2.068	0.7112	0.6697	0.253(-1)	0.4105	6.524	-1.5120	1.1032
1.397***	2.063	0.6817	0.6405	0.277(-1)	0.4127	6.533	-1.5089	1.1203
1.358**	2.065	0.6633	0.6226	0.292(-1)	0.4125	6.547	-1.5039	1.1319
1.2	2.126	0.5748	0.5383	0.364(-1)	0.3968	6.701	-1.4498	1.1984
1.0	2.443	0.4303	0.4054	0.491(-1)	0.3257	7.308	-1.2604	1.3652
			$p = 0.1, \quad n = 2.5$					
5.0	5.037	0.9958	0.9943	0.407(-3)	0.1071	9.943	-0.6602	1.0041
4.0	4.058	0.9919	0.9890	0.789(-3)	0.1481	8.930	-0.7709	1.0081
3.0	3.105	0.9811	0.9745	0.183(-2)	0.2214	7.821	-0.9452	1.0196
2.5	2.653	0.9678	0.9572	0.310(-2)	0.2803	7.239	-1.0708	1.0345
2.0	2.246	0.9395	0.9212	0.576(-2)	0.3600	6.678	-1.2253	1.0703
1.8	2.111	0.9192	0.8963	0.762(-2)	0.3954	6.484	-1.2886	1.0992
1.6	2.006	0.8894	0.8608	0.103(-1)	0.4268	6.337	-1.3409	1.1472
1.428*	1.961	0.8519	0.8180	0.136(-1)	0.4420	6.284	-1.3607	1.2182
1.398***	1.960	0.8440	0.8092	0.143(-1)	0.4426	6.286	-1.3600	1.2347
1.194**	2.043	0.7731	0.7329	0.203(-1)	0.4170	6.455	-1.2972	1.4156
1.0	2.449	0.6681	0.6273	0.288(-1)	0.3193	7.132	-1.0828	1.8326

[a] $p = M/M'$; $\bar{\Omega}$, $\bar{J}$, and $\bar{E}$ are defined in eq. (3.26); R_0 is given by eq. (3.24); T_s and W are the spin kinetic energy and the self-gravitational energy of the ellipsoid.

[b] One asterisk marks the secular instability limit, two the dynamical instability limit, and three the Roche limit.

Each line in the table corresponds to a given value of the quantity $rp^{1/3}/a_1$. This quantity varies monotonically along each sequence, and remains well behaved as $p \to 0$ (see § 8.3). The tabulations are terminated when $rp^{1/3}/a_1 = 1$.

Note that, because we use a more accurate rotation law, equation (7.17), our numerical results for $n = 0$ differ from those given in Ch69 (see his Table XVI). The differences are largest when the separation r is smallest. For the sequence with $n = 0$ and $p = 1$, the maximum difference along the sequence is about 10% for both the axis ratios and Ω. Thus the improvement resulting from our use of equation (7.17) can be quite significant. As a check on our numerical procedure, we have also calculated the results for $n = 0$ when setting $\delta = 0$ everywhere and have verified that the numbers listed in Table XVI of Ch69 are then recovered.

Several important features of the results are immediately apparent in Table 6. For a given separation r/R_0, the more incompressible stars (with smaller n) have a larger deformation. Clearly, this is because a more compressible star is also more centrally concentrated, and therefore less affected by tidal forces. Rotation always remains a small perturbation here, as can be seen from the small values of the ratio $T_s/|W|$. Along all equilibrium sequences, there exists a point (marked by a triple asterisk in Table 6) where the binary separation r reaches a minimum.[10] We identify this point with the *Roche limit* of the system, and we denote the minimum value of r by $r_{\rm lim}$. No equilibrium configuration can exist with $r < r_{\rm lim}$. Moreover, we will show in § 9 that all configurations located beyond the Roche limit (along the branch where r increases as the deformation increases) are unstable. In Ch69 (§ 56), it is stated that the Roche limit corresponds precisely to the point along the sequence where Ω^2 reaches a maximum. This is only because the TV treatment of Ch69 uses the *Keplerian* value $\Omega^2 = \Omega_K^2 = G(M + M')/r^3$, which obviously is maximum when r is minimum. However, because of the deviations from Kepler's law in close binaries, the true Ω^2 reaches its maximum *slightly beyond* the Roche limit (at a smaller value of r/a_1). For the sequence with $p = 1$ and $n = 0$ in Table 6, we have included enough entries near the Roche limit to make this result clearly apparent. The Roche limit is at $r_{\rm lim}/a_1 = 1.801$ and $r_{\rm lim}/R_0 = 2.713$, whereas $\bar{\Omega}^2$ reaches its maximum value, $\bar{\Omega}^2_{\rm max} = 0.1527$, at $r/a_1 = 1.697$ and $r/R_0 = 2.724$. By comparison, Table XVIII of Ch69 gives $\bar{\Omega}^2_{\rm max} = 0.1413$, with the maximum occurring at the Roche limit. From the other values listed in that table, we calculate that $r_{\rm lim}/a_1 = 1.710$ and $r_{\rm lim}/R_0 = 2.662$.

To better illustrate some of our results, we have plotted curves of E, J, and Ω^2 as a function of binary separation r along equilibrium sequences corresponding to $p = 1$ (Fig. 10) and $p = 0.1$ (Fig. 11), and for polytropes with $n = 0$, 1, 1.5, and 2.5. For convenience, we have subtracted the quantity $E_\infty \equiv -[(3-n)/(5-n)]GM^2/R_0$, equal to E when $r \to \infty$ (cf. eq. [7.11]). For Ω^2, the fractional deviation from Ω_K^2 is shown. The Roche limit is clearly apparent in these plots, as the point where r reaches a minimum, and where the curves of $E(r)$ and $J(r)$ have infinite slope.

Most importantly, we note in Figures 10 and 11 that, before reaching the Roche limit, *all sequences must pass through a point where both E and J are minimum*. We will see in § 10 that the existence of this minimum is neither a peculiarity of the Roche model, nor an artifact of our (approximate) ellipsoidal method. Indeed, this important feature is also exhibited in detailed numerical models of more realistic binary systems (see § 10.3). As was shown in § 2.3, the existence of such a turning point along an equilibrium sequence indicates the onset of instability, and we will return to this interpretation in great detail when discussing the stability properties of Roche binaries in § 9. For now, we merely wish to emphasize that the points where the equilibrium $E(r)$ and $J(r)$ curves have either infinite or zero slope *coincide*. This is in agreement with the general result that, for uniformly rotating configurations, $dE = \Omega dJ$ all along an equilibrium sequence (see Ostriker & Gunn 1969 and Appendix D). As a check on our numerical procedure, we have verified that this result holds to high numerical accuracy not only at the Roche limit and at the minimum of E and J, but also at various points all along the sequences that we have calculated. In contrast, one can show that the numerical results presented in Ch69 (§ 56) fail to satisfy $dE = \Omega dJ$, and this inconsistency can again be traced to the use of the unmodified Kepler's law (Ch69, eq. [8.5]). As shown in Figures 10 and 11, the deviation of Ω^2 from the Keplerian value can be large for small binary separation: as much as 13% near the Roche limit of the sequence with $p = 1$ and $n = 0$ (one of the cases studied in Ch69). Figure 12 illustrates the variation of the axis ratios a_2/a_1 and a_3/a_1 along the compressible Roche sequences. Each curve terminates at the Roche limit. Also shown in Figure 12 are the curves obtained by setting $\delta = 0$ in the equilibrium structure equations, reproducing the results of Ch69.

In the astrophysically important limit where the mass ratio $p \to 0$, the equilibrium Roche solutions exhibit an interesting behavior which can be studied analytically. We defer our discussion of these limiting solutions until § 8.3, when the $p \to 0$ limit of the more general Roche-Riemann solutions is explored. Note that the $p \to \infty$ limit is unphysical for the Roche problem. Indeed, as $M' \to 0$, the orbiting companion becomes a test mass, and the assumption of synchronized rotation can no longer be valid.

8. COMPRESSIBLE ROCHE-RIEMANN ELLIPSOIDS

In this section we consider a generalization of the Roche problem to the case where the assumption of synchronized rotation is relaxed. Specifically, we use our energy variational method to construct the compressible analogues of the incompressible "Roche-Riemann" ellipsoids of type S first explored by Aizenman (1968).

8.1. *Equilibrium Conditions*

The equilibrium problem considered here is an adaptation of the Roche problem to Riemann-S ellipsoids. As in the Roche problem, the polytrope is in a circular orbit about a

[10] Note that, to determine this minimum correctly, it is important to measure r in a unit that remains constant along the sequence, as we have done here by calculating the ratio r/R_0. Other ratios, such as r/a_1 or $r/(a_1a_2a_3)^{1/3}$ do not, in general, reach a minimum at the same point, and may even never reach a minimum at any point along the sequence.

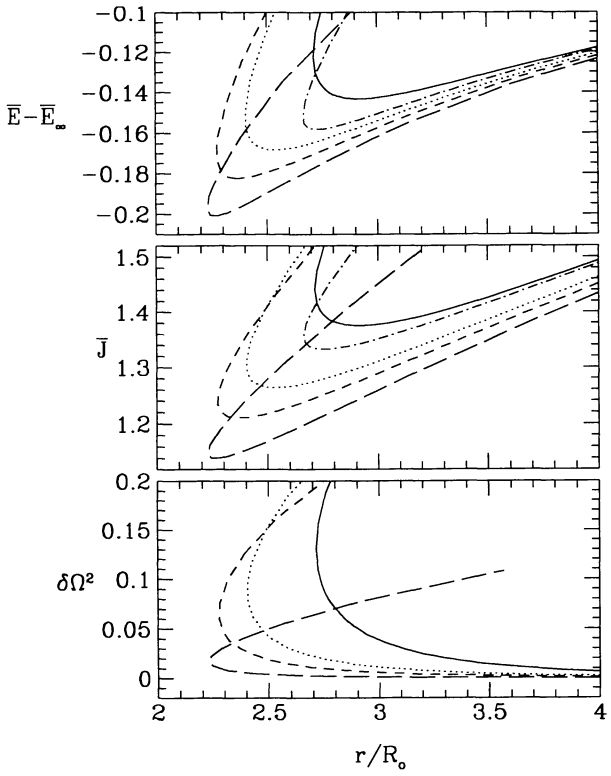

FIG. 10.—Equilibrium curves of total energy, total angular momentum, and orbital angular frequency as a function of binary separation along the compressible Roche sequences with $p = M/M' = 1$ and $n = 0$ (*solid lines*), $n = 1$ (*dotted lines*), $n = 1.5$ (*short-dashed lines*), and $n = 2.5$ (*long-dashed lines*). The units for E and J are defined as before in eq. (3.26). The quantity $\bar{E}_\infty \equiv -(3-n)/(5-n)$ has been subtracted from $\bar{E}$ for convenience. For Ω, the fractional deviation $\delta\Omega^2 \equiv (\Omega^2 - \Omega_K^2)/\Omega_K^2$ from the Keplerian value $\Omega_K^2 = G(M+M')/r^3$ is shown. The binary separation r is given in units of the radius R_0 of a spherical polytrope with the same mass and entropy (eq. [3.24]). For comparison, we also show the results obtained by Ch69 using the TV method for $n = 0$ (dotted-dashed lines for E and J; recall that $\delta\Omega^2 = 0$ in Ch69).

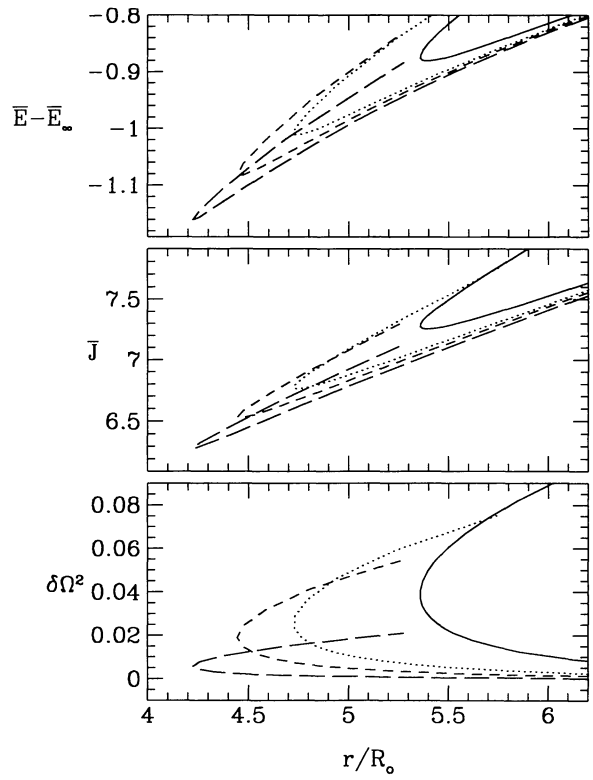

FIG. 11.—Equilibrium curves of total energy, total angular momentum, and orbital angular frequency as a function of binary separation along compressible Roche sequences with $p = M/M' = 0.1$. Conventions are as in Fig. 10 (but the results of Ch69 are not shown).

point-mass companion, and its *equilibrium figure* is rotating at the orbital angular frequency Ω. However, the fluid itself is not, in general, corotating with the binary. Instead, as in the Riemann-S case, internal fluid motions are allowed that have uniform vorticity $\zeta \mathbf{e}_3$, parallel to $\boldsymbol{\Omega}$. The notations and conventions in this section are identical to those introduced in §§ 5 and 7.

It is straightforward to write the total energy $E(\rho_c, \lambda_1, \lambda_2, r; M, M', J, \mathscr{C}) = U + T + W + W_i$ for Roche-Riemann configurations. The expressions for U, W, and W_i are identical to those used for the Roche problem (eqs. [3.1], [4.6], and [7.4]). The total kinetic energy of the binary can be written (cf. eqs. [5.6], [5.11], and [7.2]–[7.3])

$$T = \frac{1}{2} I(\Lambda^2 + \Omega^2) - \frac{2}{5} \kappa_n M a_1 a_2 \Lambda\Omega + \frac{1}{2} M r_{\rm cm}^2 \Omega^2 (1+p)$$

$$= T_+ + T_- + \frac{M r^2 \Omega^2}{2(1+p)}, \qquad (8.1)$$

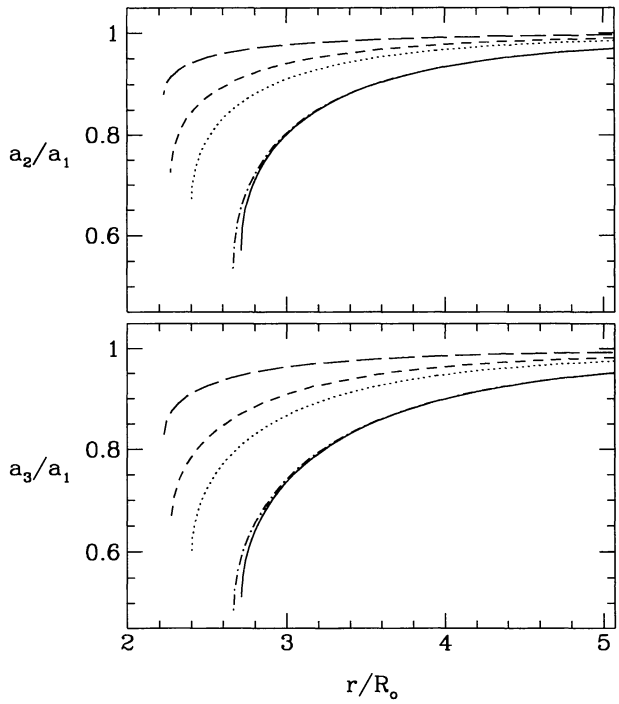

FIG. 12.—Variation of the axis ratios along the same compressible Roche sequences as shown in Fig. 10. Conventions are as in Fig. 10.

where

$$T_{\pm} = \frac{1}{20}\kappa_n M(a_1 \mp a_2)^2(\Omega \pm \Lambda)^2 = \frac{1}{2}k_3\left[J \pm \mathscr{C} - \frac{Mr^2\Omega}{(1+p)}\right]^2 M^{-5/3}\rho_c^{2/3}h_{\pm} . \quad (8.2)$$

The quantities Λ, $\mathscr{C}$, and $h_{\pm}$ were defined in § 5 (eqs. [5.3], [5.10], and [5.12]).

The equilibrium conditions are the same as in the Roche problem (eq. [7.5]), but holding M, M', J, *and* $\mathscr{C}$ constant. From the condition $\partial E/\partial\rho_c = 0$ we find expressions for the virial relation and the total equilibrium energy identical to those of § 7 (eqs. [7.8] and [7.11]) but with the "spin" kinetic energy (i.e., the kinetic energy of the star excluding its center-of-mass motion) now defined by $T_s \equiv T_+ + T_-$. The total angular momentum of the binary is (cf. eqs. [5.5] and [7.12])

$$J = \left[\frac{Mr^2}{(1+p)} + I\right]\Omega - \frac{2}{5}\kappa_n M a_1 a_2 \Lambda = \left[\frac{Mr^2}{(1+p)} + I + 2\frac{I_{11}I_{22}}{I}f_R\right]\Omega , \quad (8.3)$$

with f_R defined as before by equation (5.9). As in § 7, the equilibrium condition $\partial E/\partial r = 0$ gives the modified Kepler's law for the binary, equation (7.6) (or [7.17]). Note that in the TV treatment of the problem (Aizenman 1968), the unmodified Kepler's law $\Omega^2 = \Omega_K^2 = (1+p)\mu$ is used instead.

Following the notations of § 7, the two equilibrium conditions $\partial E/\partial\lambda_1 = \partial E/\partial\lambda_2 = 0$ together with the virial relation can be written in the form (cf. eq. [7.16])

$$\mathscr{M}_{11} + I_{11}(\Omega^2 + 2\mu + 2\Omega Q_2) + I_{22}Q_1^2 = \mathscr{M}_{22} + I_{22}(\Omega^2 - \mu - 2\Omega Q_1) + I_{11}Q_2^2 = \mathscr{M}_{33} - \mu I_{33} = -\frac{U}{n} , \quad (8.4)$$

with Q_1 and Q_2 defined as in § 5 (cf. eq. [5.2]). These equations are the compressible generalizations of those given by Aizenman[11] (1968; cf. his eqs. [46]–[48]), only now Ω^2 is again given by equation (7.17). As in the case of the Roche problem, the conditions (8.4), together with the definition of $\mathscr{M}_{ij}$ (eq. [7.14]), can be combined to give

$$q_n\tilde{\mu}\left\{\frac{Q_1^2a_2^2}{\mu} + \left[2 + (1+p)(1+\delta) + \frac{2Q_2\Omega}{\mu}\right]a_1^2 + a_3^2\right\} = 2(a_1^2 - a_3^2)B_{13} , \quad (8.5)$$

and

$$q_n\tilde{\mu}\left\{\frac{Q_2^2a_1^2}{\mu} + \left[(1+p)(1+\delta) - 1 - \frac{2Q_1\Omega}{\mu}\right]a_2^2 + a_3^2\right\} = 2(a_2^2 - a_3^2)B_{23} , \quad (8.6)$$

[11] Note that the quantities Q_1 and Q_2 are called Q_{12} and Q_{21} in Aizenman (1968).

where, as before, $\tilde{\mu} \equiv \mu/(\pi G\bar{\rho})$. Taking the ratio of these last two expressions we get an equation for the principal axes,

$$\frac{Q_1^2a_2^2 + \{[2 + (1+p)(1+\delta)]\mu + 2Q_2\Omega\}a_1^2 + \mu a_3^2}{Q_2^2a_1^2 + \{[(1+p)(1+\delta) - 1]\mu - 2Q_1\Omega\}a_2^2 + \mu a_3^2} = \frac{(a_1^2 - a_3^2)B_{13}}{(a_2^2 - a_3^2)B_{23}} . \quad (8.7)$$

Equation (8.7) reduces to equation (50) of Aizenman (1968) when $n = 0$ *and* $\delta = 0$. It also reduces to the equation determining the axis ratios of Roche ellipsoids, equation (7.20), when $Q_1 = Q_2 = \zeta = 0$, as expected.

8.2. *Constructing Equilibrium Sequences*

The procedure for constructing Roche-Riemann sequences is very similar to that described for Roche binaries (cf. § 7.2). Here, for given f_R and r/a_1, the axis ratios are obtained by solving equations (8.5) and (8.6) by iteration. The quantity Λ is calculated from Ω (eq. [7.17]) as $\Lambda = -f_R\Omega a_1a_2/(a_1^2 + a_2^2)$. The "spin" kinetic energy T_s is obtained from equation (8.2), the total angular momentum J from equation (8.3), and the circulation $\mathscr{C}$ from equation (5.10). Expression (7.21) for R/R_0 still applies. The Roche sequences considered in § 7 are a particular case of the more general Roche-Riemann sequences, corresponding to $\Lambda = f_R = 0$. Also of astrophysical interest are the *irrotational* Roche-Riemann sequences (see, e.g., Kochanek 1992b), for which $\mathscr{C} = 0$ and $f_R = -2$. In Table 7 we present selected results for these irrotational Roche-Riemann sequences when $p = 1$ and 0.1, and for $n = 0$, 1, 1.5, and 2.5. The *Roche-Riemann limit* along each sequence, where the binary separation r is minimum, is indicated by a double asterisk. Note that, just like the irrotational Riemann-S ellipsoids, all irrotational Roche-Riemann ellipsoids have $a_1 > a_3 > a_2$ while Roche ellipsoids have $a_1 > a_2 > a_3$.

The results for $p = 1$ are illustrated in Figure 13, where we show curves of E, J, and Ω^2 as a function of r along the irrotational Roche-Riemann sequences for $n = 0$ and 1. The corresponding curves for the Roche sequences (with $f_R = 0$) are also shown for comparison. The Roche-Riemann limit is clearly identified as the point where both $E(r)$ and $J(r)$ have infinite slopes, and where r reaches a minimum. Similarly, the stability limit corresponds to the point where $E(r)$ and $J(r)$ have zero slope and where E and J simultaneously reach a minimum (see § 9 for a more detailed discussion of stability). Note that, for a given separation, the irrotational Roche-Riemann configurations have lower energy and angular momentum than the corresponding Roche configurations. This is because the fluid in a Roche-Riemann ellipsoid with $\mathscr{C} = 0$ rotates far slower than is necessary to maintain synchronization.

8.3. *The Limiting Solutions for $p \to 0$ and $p \to \infty$*

Our equilibrium Roche-Riemann solutions become particularly simple in the $p \to 0$ and $p = \infty$ limits. The $p \to 0$ limit is of great astrophysical interest, since it corresponds to the case of a star in orbit around a much more massive pointlike object, such as a massive black hole. We show below that, in this limit, the compressible Roche-Riemann sequences satisfy scaling

relations such that we can again construct a "universal" sequence, independent of n, as we have done in §§ 3–5.

In the $p \to 0$ limit, we expect the binary separation to grow according to $r \propto p^{-1/3} \to \infty$ if $\tilde{\Omega}$ is to remain finite in the equilibrium structure equations (see below). Therefore we can set $\delta = 0$ in all the results of § 8.1. In particular, we now have $\Omega^2 = \Omega_K^2 = \mu$, and equations (8.5) and (8.6) become

$$q_n\tilde{\mu}[\hat{Q}_1^2 f_R^2 a_2^2 + (3 + 2\hat{Q}_2 f_R)a_1^2 + a_3^2] = 2(a_1^2 - a_3^2)B_{13}\,,$$

$$q_n\tilde{\mu}[\hat{Q}_2^2 f_R^2 a_1^2 - 2\hat{Q}_1 f_R a_2^2 + a_3^2] = 2(a_2^2 - a_3^2)B_{23}\,, \tag{8.8}$$

where $\hat{Q}_1 \equiv -a_1^2/(a_1^2 + a_2^2)$ and $\hat{Q}_2 \equiv a_2^2/(a_1^2 + a_2^2)$. Clearly, in the $p \to 0$ limit, the polytropic index n and the mass ratio p enter the equations only through the quantity $q_n\tilde{\mu}$. For a given value of $q_n\tilde{\mu} = q_n\tilde{\Omega}^2$, the two axis ratios a_2/a_1 and a_3/a_1 are uniquely determined. Since $\tilde{\Omega}^2 \propto p^{-1}(R/r)^3$, it is natural to rescale the binary separation according to

$$\hat{r} \equiv r\left(\frac{p}{q_n}\right)^{1/3}. \tag{8.9}$$

For a given value of $\hat{r}/a_1$, or $\hat{r}/R$, the universal variables $\hat{\Omega}^2$, $\hat{W}$, and $\hat{R}$ defined in equation (3.27), as well as the axis ratios and $T_s/|W|$, are all determined independent of n. For $\hat{\Omega}^2 = q_n\tilde{\Omega}^2$ and $\hat{W}$, this is immediately apparent. For $\hat{R}$, we first use equation (7.21) to write

$$\hat{R} = \left[f(\lambda_1, \lambda_2)\left(1 - 2\frac{T_s}{|W|}\right) - \left(\frac{5-n}{3p}\right)g_t\right]^{-1}, \tag{8.10}$$

and then notice that the quantity

$$\left(\frac{5-n}{3p}\right)g_t = \frac{5}{3}\frac{q_n R^3}{pr^3}\frac{\delta I}{\kappa_n M R^2} \tag{8.11}$$

is independent of n for given $\hat{r}/R$.

The universal Roche and irrotational Roche-Riemann sequences in the $p \to 0$ limit are given in Tables 8 and 9. These tables apply to all polytropic indices. Other equilibrium quantities can be calculated easily for any n using these tables and the results of §§ 7.1 and 8.1. Note, however, that no universal Roche limit can be defined. This is because the Roche limit corresponds to the point where r/R_0 (rather than r/R) reaches a minimum. Therefore, it depends explicitly on n through $R/R_0 = \hat{R}^{n/(3-n)}$.

As noted above, in the $p \to 0$ limit, Ω is simply given by Kepler's law, and our results for $n = 0$ should be directly comparable to those of Ch69 or Aizenman (1968). For the Roche limit, when $p \to 0$ we find $r_{\rm lim}/R \to 2.455p^{-1/3}$, $\tilde{\Omega} \to 0.3002$, $a_2/a_1 \to 0.5114$, and $a_3/a_1 \to 0.4826$. This agrees with the result of Ch69 (see his Table XVIII) to within our numerical accuracy, and is also very close to the result quoted in Aizenman (1968). For the irrotational Roche-Riemann limit we find $r_{\rm lim}/R \to 2.502p^{-1/3}$, $\tilde{\Omega} \to 0.2917$, $a_2/a_1 \to 0.4819$, and $a_3/a_1 \to 0.5214$. Note that this irrotational Roche-Riemann limit is different from the type-S_+ Roche-Riemann limit[12] studied by Aizenman (1968), which is defined in terms of the *absolute* minimum binary separation (or maximum of $\Omega = \Omega_K$) for *all* type-S Roche-Riemann binaries (i.e., for all f_R). For this absolute Roche-Riemann limit, which we denote by r_{rr}, we find $r_{rr}/R \to 2.438p^{-1/3}(r_{rr}/a_1 \to 1.548p^{-1/3})$, $\tilde{\Omega} \to 0.3034$, $a_2/a_1 \to 0.5065$, and $a_3/a_1 \to 0.5060$, with the absolute minimum occurring for the sequence with $f_R \simeq -0.66$. This also corresponds to the minimum binary separation along an equilibrium sequence with constant $\mathscr{C}/(GM^3R)^{1/2} \simeq -0.088$. These results are in very good agreement with those obtained by Aizenman (1968).

The $p \to \infty$ limit is less astrophysically relevant, since, in this limit, the point-mass companion becomes a test particle. For the Roche problem, as already noted in § 7.2, this limit is unphysical because the assumption of synchronized rotation must break down. In fact, as shown by Ch69, the Roche sequence tends to the combined Maclaurin-Jacobi sequence when $p \to \infty$. Similarly, the Roche-Riemann sequence tends to the Riemann-S sequence in this limit (see Aizenman 1968).

9. STABILITY OF BINARY CONFIGURATIONS

In this section we study the stability properties of compressible Roche and Roche-Riemann binaries, using the formalism developed in § 2. We found in §§ 7 and 8 that the equilibrium energy curves $E_{\rm eq}(r)$ exhibit a minimum along all Roche and Roche-Riemann sequences. This minimum always occurs before the Roche limit (minimum binary separation) is reached and coincides with the minimum in the equilibrium $J(r)$ curve. According to our general turning-point condition (cf. eq. [2.20]), such a minimum should correspond to the onset of instability along the sequence. The existence of this instability can have a profound effect on the evolution of a binary system undergoing secular decay via some dissipative mechanism such as the emission of gravitational radiation. The astrophysical implications are presently being explored for the particular cases of coalescing neutron-star binaries (Lai, Rasio, & Shapiro 1993a) and the formation of blue stragglers in globular clusters (Rasio 1993). Here we evaluate the determinant appearing in equation (2.15), to confirm the onset of an instability at the minimum of $E_{\rm eq}(r)$, and to further elucidate its nature. As demonstrated in § 6 for single star configurations, both secular and dynamical instabilities can be identified with our method.

9.1. *Secular Instability of Roche Binaries*

The energy function for the Roche problem was given in § 7.1. Here, for convenience when taking derivatives, we rewrite the kinetic and gravitational interaction terms as

$$T = T_s + T_0 = \frac{1}{2I_s}\left[J - \frac{Mr^2\Omega}{(1+p)}\right]^2 h + \frac{1}{2}\frac{Mr^2\Omega^2}{(1+p)}\,,$$

$$W_i = -\frac{GMM'}{r} - \frac{1}{2}\frac{GM'\delta I}{r^3}\,, \tag{9.1}$$

[12] Also quoted as the "stationary" Roche-Riemann limit by Luminet & Carter (1986).

TABLE 7

COMPRESSIBLE ROCHE-RIEMANN SEQUENCES WITH $\mathscr{C} = 0$[a]

$rp^{1/3}/a_1$ [b]	$rp^{1/3}/R_o$	a_2/a_1	a_3/a_1	$T_s/\|W\|$	$\bar{\Omega}$	J	$\bar{E}$	R/R_o
			$p = 1, \quad n = 0$					
5.0	5.103	0.9693	0.9705	0.492(-5)	0.1418	1.599	-0.6979	1.
4.0	4.165	0.9391	0.9431	0.372(-4)	0.1925	1.446	-0.7197	1.
3.5	3.722	0.9080	0.9161	0.125(-3)	0.2284	1.370	-0.7334	1.
3.0	3.315	0.8522	0.8696	0.495(-3)	0.2729	1.301	-0.7484	1.
2.7	3.104	0.7976	0.8253	0.123(-2)	0.3028	1.269	-0.7565	1.
2.5	2.985	0.7483	0.7852	0.232(-2)	0.3229	1.255	-0.7601	1.
2.361*	2.916	0.7068	0.7510	0.363(-2)	0.3362	1.252	-0.7610	1.
2.2	2.853	0.6513	0.7041	0.608(-2)	0.3500	1.257	-0.7594	1.
2.0	2.806	0.5716	0.6331	0.114(-1)	0.3635	1.282	-0.7517	1.
1.893**	2.799	0.5248	0.5889	0.158(-1)	0.3683	1.307	-0.7439	1.
1.5	2.950	0.3375	0.3896	0.478(-1)	0.3576	1.517	-0.6773	1.
1.0	5.362	0.0790	0.0822	0.162	0.1662	2.881	-0.3767	1.
			$p = 1, \quad n = 1$					
5.0	5.053	0.9841	0.9844	0.695(-6)	0.1438	1.590	-0.5989	1.0001
4.0	4.085	0.9687	0.9698	0.524(-5)	0.1979	1.430	-0.6223	1.0002
3.0	3.159	0.9241	0.9299	0.711(-4)	0.2917	1.261	-0.6575	1.0012
2.5	2.745	0.8667	0.8816	0.367(-3)	0.3618	1.182	-0.6798	1.0036
2.2	2.536	0.8042	0.8307	0.112(-2)	0.4097	1.146	-0.6918	1.0078
2.1	2.479	0.7761	0.8079	0.165(-2)	0.4253	1.138	-0.6945	1.0103
1.958*	2.412	0.7283	0.7689	0.290(-2)	0.4456	1.134	-0.6962	1.0155
1.9	2.391	0.7061	0.7504	0.366(-2)	0.4528	1.135	-0.6959	1.0184
1.8	2.365	0.6638	0.7148	0.545(-2)	0.4630	1.141	-0.6933	1.0248
1.693**	2.355	0.6134	0.6709	0.831(-2)	0.4697	1.157	-0.6869	1.0345
1.5	2.398	0.5110	0.5755	0.173(-1)	0.4658	1.219	-0.6617	1.0633
1.0	3.766	0.2039	0.2288	0.932(-1)	0.2619	1.979	-0.4251	1.3557
			$p = 1, \quad n = 1.5$					
5.0	5.036	0.9892	0.9893	0.222(-6)	0.1445	1.587	-0.5278	1.0001
4.0	4.058	0.9787	0.9793	0.167(-5)	0.1999	1.425	-0.5517	1.0002
3.0	3.108	0.9486	0.9515	0.226(-4)	0.2986	1.249	-0.5891	1.0011
2.5	2.664	0.9097	0.9175	0.118(-3)	0.3770	1.159	-0.6150	1.0034
2.2	2.425	0.8660	0.8810	0.372(-3)	0.4356	1.111	-0.6320	1.0073
2.0	2.289	0.8213	0.8445	0.858(-3)	0.4771	1.086	-0.6420	1.0130
1.9	2.232	0.7922	0.8209	0.133(-2)	0.4970	1.077	-0.6456	1.0177
1.767*	2.173	0.7451	0.7826	0.241(-2)	0.5203	1.072	-0.6477	1.0272
1.7	2.152	0.7173	0.7597	0.326(-2)	0.5295	1.074	-0.6470	1.0340
1.582**	2.137	0.6612	0.7126	0.558(-2)	0.5395	1.086	-0.6415	1.0512
1.3	2.272	0.4966	0.5613	0.190(-1)	0.5069	1.196	-0.5911	1.1419
1.0	3.204	0.2906	0.3343	0.611(-1)	0.3217	1.656	-0.4283	1.4728
			$p = 1, \quad n = 2.5$					
5.0	5.014	0.9958	0.9958	0.131(-7)	0.1454	1.583	-0.2997	1.0000
4.0	4.023	0.9918	0.9918	0.983(-7)	0.2024	1.418	-0.3243	1.0001
3.0	3.042	0.9803	0.9808	0.132(-5)	0.3079	1.234	-0.3643	1.0008
2.5	2.564	0.9657	0.9670	0.689(-5)	0.3981	1.133	-0.3947	1.0025
2.0	2.113	0.9317	0.9365	0.521(-4)	0.5329	1.031	-0.4356	1.0097
1.8	1.953	0.9054	0.9139	0.135(-3)	0.6010	0.993	-0.4541	1.0185
1.6	1.820	0.8640	0.8793	0.389(-3)	0.6701	0.963	-0.4706	1.0382
1.5	1.774	0.8346	0.8553	0.686(-3)	0.6985	0.954	-0.4758	1.0568
1.440*	1.756	0.8131	0.8379	0.977(-3)	0.7106	0.953	-0.4769	1.0732
1.379**	1.749	0.7881	0.8176	0.141(-2)	0.7167	0.955	-0.4755	1.0956
1.2	1.842	0.6907	0.7377	0.426(-2)	0.6718	1.001	-0.4478	1.2257
1.0	2.454	0.5395	0.6032	0.143(-1)	0.4481	1.219	-0.3433	1.6879

TABLE 7—*Continued*

$rp^{1/3}/a_1$ [b]	$rp^{1/3}/R_o$	a_2/a_1	a_3/a_1	$T_s/\|W\|$	Ω	J	E	R/R_o
			$p = 0.1, \quad n = 0$					
5.0	5.100	0.9704	0.9710	0.252(-5)	0.1052	9.996	-1.0549	1.
4.0	4.157	0.9429	0.9450	0.180(-4)	0.1430	9.027	-1.1580	1.
3.5	3.705	0.9160	0.9202	0.570(-4)	0.1699	8.526	-1.2256	1.
3.0	3.280	0.8704	0.8791	0.209(-3)	0.2042	8.030	-1.3057	1.
2.5	2.904	0.7895	0.8081	0.894(-3)	0.2456	7.575	-1.3939	1.
2.2	2.721	0.7133	0.7414	0.228(-2)	0.2716	7.357	-1.4427	1.
2.0	2.626	0.6475	0.6827	0.429(-2)	0.2872	7.256	-1.4671	1.
1.778*	2.556	0.5596	0.6012	0.860(-2)	0.3003	7.210	-1.4788	1.
1.7	2.544	0.5253	0.5681	0.109(-1)	0.3031	7.217	-1.4769	1.
1.622**	2.539	0.4894	0.5326	0.138(-1)	0.3047	7.239	-1.4709	1.
1.3	2.658	0.3260	0.3590	0.348(-1)	0.2888	7.605	-1.3763	1.
1.0	3.364	0.1573	0.1670	0.754(-1)	0.2083	8.991	-1.0798	1.
			$p = 0.1, \quad n = 1$					
5.0	5.053	0.9844	0.9846	0.368(-6)	0.1066	9.948	-0.9593	1.0001
4.0	4.083	0.9698	0.9704	0.268(-5)	0.1468	8.944	-1.0683	1.0002
3.0	3.149	0.9298	0.9328	0.334(-4)	0.2168	7.859	-1.2363	1.0011
2.5	2.719	0.8820	0.8895	0.158(-3)	0.2705	7.309	-1.3516	1.0030
2.2	2.488	0.8327	0.8459	0.448(-3)	0.3094	7.001	-1.4288	1.0062
2.0	2.354	0.7857	0.8048	0.942(-3)	0.3366	6.821	-1.4790	1.0103
1.8	2.246	0.7233	0.7502	0.204(-2)	0.3619	6.682	-1.5212	1.0178
1.7	2.206	0.6853	0.7166	0.302(-2)	0.3724	6.635	-1.5360	1.0237
1.564*	2.171	0.6259	0.6630	0.516(-2)	0.3823	6.609	-1.5446	1.0354
1.485**	2.165	0.5871	0.6271	0.702(-2)	0.3847	6.620	-1.5410	1.0450
1.3	2.210	0.4854	0.5286	0.142(-1)	0.3755	6.758	-1.4954	1.0802
1.0	2.681	0.2939	0.3229	0.409(-1)	0.2862	7.697	-1.2272	1.2230
			$p = 0.1, \quad n = 1.5$					
5.0	5.036	0.9893	0.9894	0.119(-6)	0.1072	9.932	-0.8894	1.0001
4.0	4.057	0.9792	0.9795	0.874(-6)	0.1482	8.915	-1.0006	1.0002
3.0	3.103	0.9514	0.9529	0.111(-4)	0.2216	7.799	-1.1761	1.0010
2.5	2.652	0.9175	0.9215	0.541(-4)	0.2807	7.213	-1.3027	1.0030
2.2	2.401	0.8815	0.8890	0.160(-3)	0.3260	6.869	-1.3929	1.0062
2.0	2.249	0.8460	0.8575	0.350(-3)	0.3599	6.654	-1.4566	1.0105
1.8	2.118	0.7968	0.8144	0.804(-3)	0.3944	6.467	-1.5175	1.0186
1.6	2.020	0.7287	0.7550	0.192(-2)	0.4243	6.335	-1.5643	1.0345
1.458*	1.984	0.6664	0.6997	0.362(-2)	0.4370	6.300	-1.5773	1.0549
1.406**	1.981	0.6404	0.6763	0.456(-2)	0.4386	6.306	-1.5751	1.0655
1.2	2.052	0.5208	0.5637	0.113(-1)	0.4187	6.486	-1.5079	1.1363
1.0	2.379	0.3833	0.4221	0.258(-1)	0.3391	7.120	-1.3007	1.2960
			$p = 0.1, \quad n = 2.5$					
5.0	5.014	0.9958	0.9958	0.716(-8)	0.1079	9.910	-0.6628	1.0000
4.0	4.022	0.9918	0.9919	0.530(-7)	0.1501	8.876	-0.7769	1.0001
3.0	3.041	0.9808	0.9810	0.694(-6)	0.2283	7.719	-0.9630	1.0008
2.5	2.562	0.9669	0.9677	0.350(-5)	0.2954	7.085	-1.1056	1.0024
2.0	2.106	0.9364	0.9389	0.248(-4)	0.3964	6.426	-1.3010	1.0089
1.7	1.863	0.8987	0.9044	0.100(-3)	0.4768	6.048	-1.4435	1.0227
1.5	1.733	0.8565	0.8668	0.283(-3)	0.5319	5.840	-1.5344	1.0462
1.4	1.688	0.8272	0.8410	0.494(-3)	0.5540	5.768	-1.5683	1.0681
1.291*	1.664	0.7870	0.8059	0.926(-3)	0.5667	5.735	-1.5842	1.1068
1.277**	1.663	0.7808	0.8005	0.101(-2)	0.5670	5.735	-1.5838	1.1137
1.0	1.933	0.6202	0.6579	0.540(-2)	0.4555	6.241	-1.3606	1.4336

[a] $p = M/M'$; $\bar{\Omega}$, $\bar{J}$, and $\bar{E}$ are defined in eq. (3.26); R_0 is given by eq. (3.24); T_s and W are the kinetic energy (excluding the center-of-mass motion) and the self-gravitational energy of the ellipsoid.

[b] One asterisk marks the dynamical instability limit, two the irrotational Roche-Riemann limit.

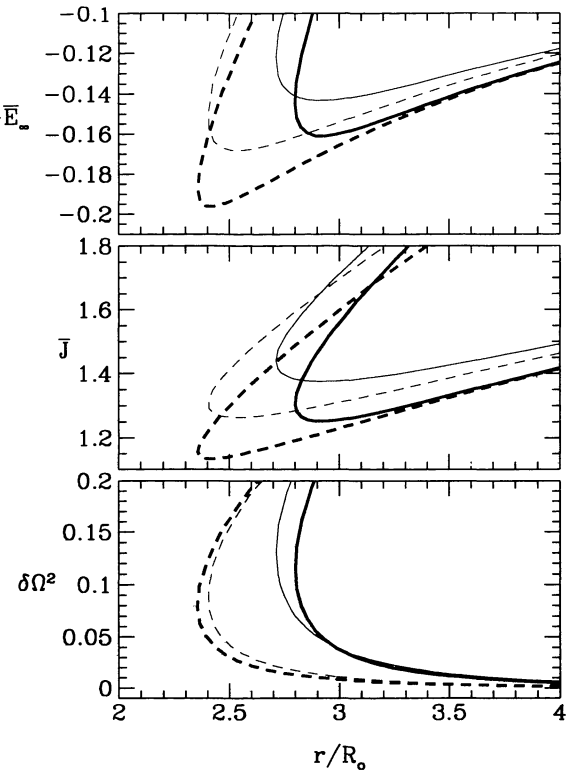

FIG. 13.—Equilibrium curves of total energy, total angular momentum, and orbital angular frequency as a function of binary separation along irrotational Roche-Riemann sequences with $p = 1$ and $n = 0$ (*thick solid lines*) and $n = 1$ (*thick dashed lines*). Also shown for comparison are the corresponding Roche sequences (*thinner lines*). Other conventions are as in Fig. 10.

where $I_s = (2/5)\kappa_n MR^2$ (eq. [3.13]) and we have defined $\delta I \equiv 2I_{11} - I_{22} - I_{33}$. Notice that, with T written in this form, we have $\partial E/\partial\Omega = 0$, so that all first derivatives of E can be evaluated at constant Ω. Using the results of Appendix A, we find

$$\begin{aligned}
\frac{\partial E}{\partial r} &= -\frac{M}{1+p} r\Omega^2 + \frac{GMM'}{r^2}\left(1 + \frac{3\delta I}{2Mr^2}\right), \\
\frac{\partial E}{\partial \rho_c} &= \frac{1}{n\rho_c} U + \frac{1}{3\rho_c} W + \frac{2}{3\rho_c} T_s + \frac{1}{3\rho_c}\frac{GM'\delta I}{r^3}, \\
\frac{\partial E}{\partial \lambda_1} &= \frac{h_{(1)}}{\lambda_1} T_s + \frac{\mathcal{I}_{(1)}}{\lambda_1} W + \frac{GM'}{2r^3\lambda_1}(4I_{11} + I_{22} + I_{33}), \\
\frac{\partial E}{\partial \lambda_2} &= \frac{h_{(2)}}{\lambda_2} T_s + \frac{\mathcal{I}_{(2)}}{\lambda_2} W - \frac{GM'}{2r^3\lambda_2}(2I_{11} + 2I_{22} - I_{33}).
\end{aligned} \tag{9.2}$$

The equilibrium conditions given in § 7.1 are recovered by setting these first derivatives equal to zero.

For the second derivatives, we first write $\Omega = J/I_{\rm cm}$, with $I_{\rm cm}$ given by equation (7.3), and we calculate the four derivatives $\partial\Omega/\partial r$, $\partial\Omega/\partial\rho_c$, $\partial\Omega/\partial\lambda_1$, and $\partial\Omega/\partial\lambda_2$. We then use relations like

$$\frac{\partial^2 E}{\partial r^2} = \frac{\partial}{\partial r}\bigg|_\Omega\left(\frac{\partial E}{\partial r}\right) + \left(\frac{\partial\Omega}{\partial r}\right)\frac{\partial}{\partial\Omega}\left(\frac{\partial E}{\partial r}\right) \tag{9.3}$$

to calculate the 10 matrix elements needed to evaluate the determinant in condition (2.15). Using again the results of Appendix A we find

$$\begin{aligned}
r^2\left(\frac{\partial^2 E}{\partial r^2}\right)_{\rm eq} &= \left(-2 + \frac{8Mr^2}{(1+p)I_{\rm cm}}\right)T_0 \\
&\quad - \frac{2GMM'}{r} - \frac{6GM'\delta I}{r^3}, \\
\rho_c^2\left(\frac{\partial^2 E}{\partial \rho_c^2}\right)_{\rm eq} &= \frac{W}{3}\left[\left(\frac{1}{3} - \frac{1}{n}\right) - 2\left(\frac{2}{3} - \frac{1}{n}\right)\frac{T_s}{|W|}\right] \\
&\quad - \frac{1}{3}\left(\frac{2}{3} + \frac{1}{n}\right)\frac{GM'\delta I}{r^3} \\
&\quad - \frac{8Mr^2}{9(1+p)I_{\rm cm}} T_s, \\
\lambda_1^2\left(\frac{\partial^2 E}{\partial \lambda_1^2}\right)_{\rm eq} &= h_{(11)}T_s + \mathcal{I}_{(11)}W - \frac{6GM'I_{11}}{r^3} \\
&\quad - \frac{2Mr^2}{(1+p)I_{\rm cm}} h_{(1)}^2 T_s, \\
\lambda_2^2\left(\frac{\partial^2 E}{\partial \lambda_2^2}\right)_{\rm eq} &= h_{(22)}T_s + \mathcal{I}_{(22)}W + \frac{3GM'I_{22}}{r^3} \\
&\quad - \frac{2Mr^2}{(1+p)I_{\rm cm}} h_{(2)}^2 T_s, \\
\rho_c r\left(\frac{\partial^2 E}{\partial \rho_c \partial r}\right)_{\rm eq} &= -\frac{GM'\delta I}{r^3} - \frac{8Mr^2}{3(1+p)I_{\rm cm}} T_s, \\
r\lambda_1\left(\frac{\partial^2 E}{\partial r \partial \lambda_1}\right)_{\rm eq} &= -\frac{4Mr^2}{(1+p)I_{\rm cm}} h_{(1)}T_s \\
&\quad - \frac{3GM'}{2r^3}(4I_{11} + I_{22} + I_{33}), \\
r\lambda_2\left(\frac{\partial^2 E}{\partial r \partial \lambda_2}\right)_{\rm eq} &= -\frac{4Mr^2}{(1+p)I_{\rm cm}} h_{(2)}T_s \\
&\quad + \frac{3GM'}{2r^3}(2I_{11} + 2I_{22} - I_{33}), \\
\rho_c\lambda_1\left(\frac{\partial^2 E}{\partial \rho_c \partial \lambda_1}\right)_{\rm eq} &= \frac{2h_{(1)}}{3} T_s + \frac{\mathcal{I}_{(1)}}{3} W \\
&\quad - \frac{GM'}{3r^3}(4I_{11} + I_{22} + I_{33}) \\
&\quad - \frac{4Mr^2}{3(1+p)I_{\rm cm}} h_{(1)}T_s, \\
\rho_c\lambda_2\left(\frac{\partial^2 E}{\partial \rho_c \partial \lambda_2}\right)_{\rm eq} &= \frac{2h_{(2)}}{3} T_s + \frac{\mathcal{I}_{(2)}}{3} W \\
&\quad + \frac{GM'}{3r^3}(2I_{11} + 2I_{22} - I_{33}) \\
&\quad - \frac{4Mr^2}{3(1+p)I_{\rm cm}} h_{(2)}T_s,
\end{aligned} \tag{9.4}$$

TABLE 8

COMPRESSIBLE ROCHE SEQUENCE IN THE $p \to 0$ LIMIT[a]

$\hat{r}/a_1$	$\hat{r}/R$	a_2/a_1	a_3/a_1	$T_s/\lvert W\rvert$	$\hat{\Omega}$	$\hat{W}$	$\hat{R}$
6.0	6.080	0.9830	0.9777	0.150(-2)	0.0770	1.000	1.0032
5.0	5.114	0.9712	0.9624	0.253(-2)	0.0998	1.000	1.0055
4.5	4.640	0.9610	0.9495	0.341(-2)	0.1155	1.000	1.0077
4.0	4.175	0.9456	0.9303	0.473(-2)	0.1354	1.000	1.0112
3.5	3.724	0.9214	0.9010	0.676(-2)	0.1607	0.999	1.0171
3.2	3.464	0.9002	0.8758	0.852(-2)	0.1791	0.999	1.0228
3.0	3.296	0.8819	0.8547	0.100(-1)	0.1929	0.998	1.0281
2.8	3.135	0.8593	0.8291	0.118(-1)	0.2080	0.997	1.0352
2.6	2.981	0.8311	0.7981	0.140(-1)	0.2243	0.996	1.0449
2.4	2.838	0.7959	0.7603	0.168(-1)	0.2416	0.994	1.0584
2.2	2.707	0.7516	0.7143	0.201(-1)	0.2593	0.991	1.0777
2.0	2.594	0.6961	0.6585	0.242(-1)	0.2764	0.986	1.1064
1.9	2.546	0.6633	0.6263	0.266(-1)	0.2842	0.983	1.1260
1.8	2.507	0.6267	0.5910	0.292(-1)	0.2910	0.978	1.1506
1.7	2.476	0.5859	0.5522	0.322(-1)	0.2963	0.972	1.1818
1.6	2.458	0.5407	0.5098	0.355(-1)	0.2996	0.963	1.2221
1.5	2.457	0.4909	0.4637	0.393(-1)	0.2999	0.952	1.2753
1.4	2.477	0.4364	0.4136	0.436(-1)	0.2961	0.937	1.3469
1.2	2.629	0.3149	0.3019	0.547(-1)	0.2708	0.885	1.5897
1.0	3.121	0.1835	0.1793	0.708(-1)	0.2094	0.779	2.1628

[a] Here $\hat{r} \equiv r(p/q_n)^{1/3}$, with $p = M/M'$ and q_n given by eq. (4.18); $\hat{\Omega}$, $\hat{W}$, and $\hat{R}$ are defined in eq. (3.27); T_s and W are the spin kinetic energy and the self-gravitational energy of the ellipsoid.

$$\lambda_1\lambda_2\left(\frac{\partial^2 E}{\partial\lambda_1\lambda_2}\right)_{\rm eq} = h_{(12)}T_s + \mathcal{I}_{(12)}W + \frac{GM'}{2r^3}(4I_{11} - 2I_{22} + I_{33}) - \frac{2Mr^2}{(1+p)I_{\rm cm}}h_{(1)}h_{(2)}T_s\,.$$

Here the explicit form of condition (2.15) for the onset of instability is too complicated to be solved analytically (as we did in § 6 for single stars). Instead, we evaluate the determinant numerically along the equilibrium Roche sequences (calculated as in § 7.2).

We find that the determinant is always positive at large separation. As r decreases, the value of the determinant decreases and, before the Roche limit is reached, changes sign at a certain critical separation. We denote this critical separation by $r_{\rm sec}$ and identify it with the point of onset of secular instability. The numerical values of $r_{\rm sec}$ are given in Table 10 for several different values of the mass ratio p and polytropic index n. Also

TABLE 9

COMPRESSIBLE $\mathcal{C} = 0$ ROCHE-RIEMANN SEQUENCE IN THE $p \to 0$ LIMIT[a]

$\hat{r}/a_1$	$\hat{r}/R$	a_2/a_1	a_3/a_1	$T_s/\lvert W\rvert$	$\hat{\Omega}$	$\hat{W}$	$\hat{R}$
6.0	6.069	0.9828	0.9830	0.451(-6)	0.0772	1.000	1.0001
5.0	5.100	0.9705	0.9710	0.228(-5)	0.1003	1.000	1.0004
4.5	4.623	0.9598	0.9608	0.575(-5)	0.1162	1.000	1.0007
4.0	4.156	0.9433	0.9452	0.161(-4)	0.1363	1.000	1.0014
3.5	3.703	0.9169	0.9206	0.507(-4)	0.1620	0.999	1.0030
3.2	3.443	0.8930	0.8988	0.108(-3)	0.1807	0.999	1.0051
3.0	3.277	0.8722	0.8800	0.184(-3)	0.1947	0.998	1.0072
2.8	3.117	0.8461	0.8567	0.322(-3)	0.2098	0.998	1.0106
2.6	2.967	0.8132	0.8275	0.576(-3)	0.2259	0.996	1.0158
2.4	2.829	0.7718	0.7910	0.105(-2)	0.2426	0.995	1.0241
2.2	2.708	0.7200	0.7451	0.196(-2)	0.2592	0.991	1.0375
2.0	2.607	0.6563	0.6879	0.367(-2)	0.2743	0.986	1.0598
1.9	2.567	0.6197	0.6544	0.502(-2)	0.2808	0.982	1.0762
1.8	2.535	0.5800	0.6172	0.685(-2)	0.2861	0.976	1.0977
1.7	2.513	0.5373	0.5763	0.929(-2)	0.2899	0.969	1.1260
1.6	2.503	0.4918	0.5313	0.125(-1)	0.2917	0.960	1.1637
1.5	2.508	0.4437	0.4823	0.168(-1)	0.2908	0.948	1.2145
1.4	2.533	0.3933	0.4292	0.223(-1)	0.2864	0.932	1.2844
1.2	2.687	0.2862	0.3112	0.382(-1)	0.2622	0.879	1.5267
1.0	3.165	0.1726	0.1827	0.621(-1)	0.2050	0.775	2.1076

[a] Here $\hat{r} \equiv r(p/q_n)^{1/3}$, with $p = M/M'$ and q_n given by eq. (4.18); $\hat{\Omega}$, $\hat{W}$, and $\hat{R}$ are defined in eq. (3.27); T_s and W are the kinetic energy (excluding the center-of-mass motion) and the self-gravitational energy of the ellipsoid.

TABLE 10

CRITICAL POINTS ALONG THE ROCHE SEQUENCES[a]

p [b]	$\hat{r}/a_1$	$\hat{r}/R_0$	a_2/a_1	a_3/a_1	$T_s/\|W\|$	$\hat{\Omega}$	J	E	R/R_0
				$n = 0$					
100.	10.980	10.983	1.0000	0.9990	0.252(-3)	0.0317	0.044	-0.6003	1.
	1.4551	1.6859	0.9641	0.6668	0.993(-1)	0.5502	0.260	-0.5362	1.
	1.3195	1.6402	0.8937	0.5825	0.123	0.5888	0.297	-0.5180	1.
10.	3.5981	3.6478	0.9925	0.9669	0.702(-2)	0.1659	0.244	-0.6090	1.
	1.5709	1.8579	0.8708	0.6941	0.701(-1)	0.4753	0.340	-0.5783	1.
	1.3298	1.7823	0.7365	0.5639	0.985(-1)	0.5275	0.394	-0.5548	1.
5.	2.6935	2.8080	0.9667	0.9130	0.160(-1)	0.2464	0.406	-0.6235	1.
	1.6117	1.9495	0.8229	0.6866	0.606(-1)	0.4423	0.462	-0.6053	1.
	1.3461	1.8704	0.6778	0.5500	0.869(-1)	0.4907	0.519	-0.5819	1.
2.	2.0746	2.3547	0.8662	0.7895	0.299(-1)	0.3248	0.808	-0.6716	1.
	1.6580	2.0963	0.7507	0.6591	0.496(-1)	0.3960	0.830	-0.6646	1.
	1.3869	2.0249	0.6089	0.5277	0.702(-1)	0.4317	0.888	-0.6434	1.
1.	1.8887	2.3144	0.7715	0.7044	0.341(-1)	0.3358	1.375	-0.7432	1.
	1.6764	2.2088	0.6960	0.6281	0.436(-1)	0.3648	1.386	-0.7399	1.
	1.4292	2.1532	0.5708	0.5123	0.588(-1)	0.3886	1.441	-0.7218	1.
0.5	1.7927	2.3488	0.6944	0.6403	0.349(-1)	0.3286	2.322	-0.8607	1.
	1.6742	2.3026	0.6468	0.5943	0.398(-1)	0.3408	2.328	-0.8590	1.
	1.4708	2.2659	0.5459	0.5010	0.503(-1)	0.3545	2.375	-0.8447	1.
0.2	1.7088	2.4002	0.6222	0.5799	0.351(-1)	0.3166	4.497	-1.1311	1.
	1.6464	2.3835	0.5948	0.5541	0.375(-1)	0.3208	4.500	-1.1302	1.
	1.5103	2.3670	0.5279	0.4920	0.435(-1)	0.3263	4.534	-1.1207	1.
0.1	1.6606	2.4251	0.5855	0.5484	0.355(-1)	0.3103	7.260	-1.4799	1.
	1.6183	2.4171	0.5661	0.5302	0.371(-1)	0.3122	7.262	-1.4793	1.
	1.5266	2.4095	0.5209	0.4883	0.409(-1)	0.3147	7.286	-1.4727	1.
0.01	1.5725	2.4523	0.5289	0.4985	0.369(-1)	0.3019	33.927	-4.9214	1.
	1.5520	2.4514	0.5188	0.4891	0.377(-1)	0.3021	33.930	-4.9207	1.
	1.5404	2.4513	0.5130	0.4837	0.381(-1)	0.3022	33.934	-4.9196	1.
0.	1.5400	2.4552	0.5114	0.4826	0.377(-1)	0.3002	∞	$-\infty$	1.
	1.5244	2.4554	0.5035	0.4753	0.383(-1)	0.3001	∞	$-\infty$	1.
	1.5400	2.4552	0.5114	0.4826	0.377(-1)	0.3002	∞	$-\infty$	1.
				$n = 1$					
100.	8.8799	8.8850	1.0000	0.9990	0.249(-3)	0.0436	0.040	-0.5004	1.0002
	1.1730	1.5281	0.9643	0.6673	0.992(-1)	0.6377	0.249	-0.4203	1.1247
	1.1348	1.5249	0.9508	0.6397	0.108	0.6443	0.264	-0.4123	1.1386
10.	2.9466	3.0057	0.9928	0.9685	0.669(-2)	0.2218	0.220	-0.5110	1.0068
	1.2710	1.6280	0.8731	0.6971	0.694(-1)	0.5792	0.318	-0.4708	1.0855
	1.1679	1.6110	0.8180	0.6344	0.837(-1)	0.5990	0.346	-0.4568	1.1085
5.	2.2389	2.3615	0.9698	0.9201	0.146(-1)	0.3194	0.368	-0.5284	1.0155
	1.3098	1.6958	0.8281	0.6925	0.594(-1)	0.5445	0.429	-0.5030	1.0756
	1.1927	1.6761	0.7639	0.6254	0.726(-1)	0.5644	0.458	-0.4891	1.0986
2.	1.7629	2.0283	0.8852	0.8143	0.262(-1)	0.4050	0.739	-0.5850	1.0316
	1.3631	1.8169	0.7639	0.6726	0.475(-1)	0.4894	0.767	-0.5735	1.0676
	1.2451	1.7991	0.7003	0.6098	0.572(-1)	0.5041	0.795	-0.5615	1.0882
1.	1.6247	2.0087	0.8063	0.7420	0.295(-1)	0.4131	1.264	-0.6683	1.0418
	1.3967	1.9182	0.7189	0.6506	0.407(-1)	0.4490	1.281	-0.6617	1.0661
	1.2950	1.9057	0.6656	0.5990	0.473(-1)	0.4579	1.305	-0.6522	1.0831
0.5	1.5628	2.0496	0.7438	0.6898	0.298(-1)	0.4008	2.143	-0.8040	1.0499
	1.4168	2.0077	0.6815	0.6277	0.362(-1)	0.4166	2.156	-0.7997	1.0677
	1.3424	2.0012	0.6433	0.5911	0.401(-1)	0.4209	2.174	-0.7930	1.0800
0.2	1.5167	2.1055	0.6888	0.6442	0.293(-1)	0.3833	4.173	-1.1139	1.0588
	1.4214	2.0893	0.6450	0.6017	0.331(-1)	0.3892	4.183	-1.1105	1.0722
	1.3866	2.0879	0.6275	0.5849	0.347(-1)	0.3901	4.192	-1.1073	1.0781

TABLE 10—*Continued*

p [b]	$\hat{r}/a_1$	$\hat{r}/R_0$	a_2/a_1	a_3/a_1	$T_s/\|W\|$	Ω	J	E	R/R_0
				$n = 1$					
0.1	1.4912	2.1325	0.6625	0.6219	0.292(-1)	0.3747	6.759	-1.5115	1.0641
	1.4147	2.1248	0.6262	0.5869	0.322(-1)	0.3775	6.770	-1.5081	1.0758
	1.4053	2.1247	0.6214	0.5824	0.326(-1)	0.3776	6.773	-1.5071	1.0774
0.01	1.4426	2.1619	0.6247	0.5887	0.297(-1)	0.3643	31.787	-5.4179	1.0737
	1.3881	2.1628	0.5973	0.5626	0.318(-1)	0.3642	31.813	-5.4097	1.0833
	1.4227	2.1614	0.6150	0.5793	0.305(-1)	0.3644	31.791	-5.4169	1.0770
0.	1.4235	2.1651	0.6137	0.5786	0.302(-1)	0.3625	∞	$-\infty$	1.0770
	1.3744	2.1680	0.5885	0.5547	0.320(-1)	0.3617	∞	$-\infty$	1.0861
	1.4235	2.1651	0.6137	0.5786	0.302(-1)	0.3625	∞	$-\infty$	1.0770
				$n = 1.5$					
100.	7.8597	7.8661	1.0000	0.9991	0.246(-3)	0.0523	0.037	-0.4290	1.0005
	1.0345	1.5150	0.9644	0.6676	0.991(-1)	0.6462	0.250	-0.3379	1.2646
	1.1024	1.5038	0.9783	0.7162	0.833(-1)	0.6466	0.221	-0.3539	1.2116
10.	2.6381	2.7061	0.9932	0.9699	0.639(-2)	0.2596	0.208	-0.4409	1.0130
	1.1245	1.5579	0.8750	0.6995	0.688(-1)	0.6185	0.312	-0.3932	1.1763
	1.1172	1.5578	0.8716	0.6950	0.699(-1)	0.6193	0.314	-0.3920	1.1798
5.	2.0294	2.1618	0.9723	0.9261	0.135(-1)	0.3645	0.349	-0.4601	1.0286
	1.1631	1.6086	0.8323	0.6973	0.585(-1)	0.5889	0.417	-0.4284	1.1536
	1.1393	1.6076	0.8201	0.6834	0.612(-1)	0.5914	0.424	-0.4251	1.1634
2.	1.6244	1.8891	0.8990	0.8332	0.234(-1)	0.4496	0.704	-0.5213	1.0561
	1.2214	1.7112	0.7742	0.6832	0.459(-1)	0.5344	0.741	-0.5052	1.1331
	1.1908	1.7098	0.7581	0.6666	0.485(-1)	0.5370	0.748	-0.5016	1.1437
1.	1.5095	1.8790	0.8310	0.7697	0.262(-1)	0.4551	1.210	-0.6110	1.0725
	1.2635	1.8032	0.7358	0.6674	0.386(-1)	0.4913	1.235	-0.6007	1.1259
	1.2412	1.8025	0.7243	0.6559	0.401(-1)	0.4926	1.240	-0.5983	1.1331
0.5	1.4633	1.9211	0.7775	0.7249	0.262(-1)	0.4401	2.058	-0.7567	1.0845
	1.2945	1.8872	0.7054	0.6511	0.338(-1)	0.4558	2.078	-0.7490	1.1248
	1.2892	1.8872	0.7027	0.6485	0.340(-1)	0.4560	2.080	-0.7484	1.1265
0.2	1.4339	1.9766	0.7320	0.6873	0.256(-1)	0.4201	4.020	-1.0879	1.0964
	1.3136	1.9656	0.6773	0.6329	0.303(-1)	0.4254	4.040	-1.0808	1.1282
	1.3340	1.9650	0.6874	0.6428	0.295(-1)	0.4253	4.033	-1.0832	1.1219
0.1	1.4182	2.0033	0.7112	0.6698	0.253(-1)	0.4105	6.524	-1.5120	1.1032
	1.3160	2.0001	0.6633	0.6226	0.292(-1)	0.4125	6.547	-1.5039	1.1318
	1.3531	1.9982	0.6816	0.6405	0.277(-1)	0.4127	6.533	-1.5089	1.1203
0.01	1.3862	2.0320	0.6825	0.6446	0.255(-1)	0.3995	30.784	-5.6696	1.1149
	1.3050	2.0377	0.6427	0.6059	0.284(-1)	0.3980	30.851	-5.6462	1.1402
	1.3714	2.0317	0.6756	0.6379	0.260(-1)	0.3996	30.786	-5.6689	1.1190
0.	1.3727	2.0351	0.6746	0.6373	0.257(-1)	0.3977	∞	$-\infty$	1.1190
	1.2965	2.0431	0.6366	0.6004	0.285(-1)	0.3954	∞	$-\infty$	1.1436
	1.3726	2.0351	0.6746	0.6373	0.258(-1)	0.3977	∞	$-\infty$	1.1190
				$n = 2.5$					
100.	5.8318	5.8473	1.0000	0.9991	0.235(-3)	0.0817	0.032	-0.2006	1.0024
	(0.7577)	(2.8191)	(0.9650)	(0.6689)	(0.987(-1))	(0.2547)	(0.347)	(-0.0875)	(3.2154)
	1.1793	1.6345	0.9962	0.8982	0.276(-1)	0.5559	0.116	-0.1692	1.3355
10.	2.1043	2.2333	0.9948	0.9767	0.493(-2)	0.3462	0.182	-0.2157	1.0511
	(0.8351)	(2.1234)	(0.8829)	(0.7102)	(0.664(-1))	(0.3880)	(0.363)	(-0.1396)	(2.1764)
	1.1805	1.6502	0.9674	0.8796	0.264(-1)	0.5491	0.226	-0.1965	1.3247
5.	1.7158	1.9235	0.9823	0.9509	0.889(-2)	0.4336	0.313	-0.2380	1.0959
	(0.8784)	(1.9893)	(0.8499)	(0.7184)	(0.543(-1))	(0.4264)	(0.457)	(-0.1758)	(1.9212)
	1.1881	1.6685	0.9444	0.8655	0.251(-1)	0.5408	0.343	-0.2246	1.3131
2.	1.4659	1.7891	0.9455	0.9026	0.134(-1)	0.4846	0.653	-0.3048	1.1577
	0.9582	1.9013	0.8141	0.7268	0.393(-1)	0.4527	0.762	-0.2579	1.6658
	1.2179	1.7164	0.9062	0.8433	0.219(-1)	0.5187	0.669	-0.2978	1.2885

TABLE 10—*Continued*

p [b]	$\hat{r}/a_1$	$\hat{r}/R_0$	a_2/a_1	a_3/a_1	$T_s/\|W\|$	$\bar{\Omega}$	$\bar{J}$	$\bar{E}$	R/R_0
				$n = 2.5$					
1.	1.3991	1.7959	0.9112	0.8685	0.146(-1)	0.4825	1.140	-0.4009	1.1873
	1.0267	1.8971	0.7966	0.7312	0.308(-1)	0.4510	1.238	-0.3605	1.5432
	1.2560	1.7691	0.8804	0.8289	0.192(-1)	0.4951	1.150	-0.3969	1.2681
0.5	1.3822	1.8329	0.8836	0.8444	0.144(-1)	0.4678	1.958	-0.5570	1.2027
	1.0861	1.9218	0.7856	0.7334	0.253(-1)	0.4396	2.058	-0.5174	1.4724
	1.2964	1.8227	0.8623	0.8190	0.169(-1)	0.4725	1.964	-0.5546	1.2521
0.2	1.3821	1.8785	0.8612	0.8258	0.139(-1)	0.4502	3.856	-0.9103	1.2132
	1.1372	1.9592	0.7770	0.7337	0.216(-1)	0.4246	3.982	-0.8624	1.4286
	1.3365	1.8755	0.8490	0.8118	0.150(-1)	0.4515	3.859	-0.9091	1.2396
0.1	1.3829	1.9001	0.8519	0.8180	0.136(-1)	0.4420	6.284	-1.3607	1.2182
	1.1570	1.9792	0.7731	0.7329	0.202(-1)	0.4170	6.455	-1.2972	1.4155
	1.3543	1.8989	0.8440	0.8092	0.143(-1)	0.4426	6.286	-1.3600	1.2348
0.01	1.3786	1.9233	0.8409	0.8084	0.134(-1)	0.4332	29.868	-5.7593	1.2267
	1.1732	2.0036	0.7676	0.7303	0.191(-1)	0.4076	30.524	-5.5205	1.4082
	1.3723	1.9232	0.8391	0.8065	0.135(-1)	0.4332	29.869	-5.7591	1.2304
0.	1.3742	1.9259	0.8385	0.8061	0.135(-1)	0.4320	∞	$-\infty$	1.2299
	1.1727	2.0083	0.7659	0.7290	0.190(-1)	0.4057	∞	$-\infty$	1.4102
	1.3742	1.9259	0.8385	0.8061	0.135(-1)	0.4320	∞	$-\infty$	1.2299

[a] Here $\hat{r} \equiv r/(1 + 1/p)^{1/3}$ with $p = M/M'$; $\bar{\Omega}$, $\bar{J}$, and $\bar{E}$ are defined in eq. (3.26); R_0 is given by eq. (3.24); T_s and W are the spin kinetic energy and the self-gravitational energy of the ellipsoid.

[b] For each value of p, the first line gives the secular instability limit, the second line the dynamical instability limit, and the third line the Roche limit. Data in parentheses indicate that the two stars overlap.

given in the table are the dynamical instability limits (see § 9.2 below) and the Roche limits (cf. § 7.2). The approximate scaling $r_{sec} \propto (1 + 1/p)^{1/3}$ (see below) has been factored out for convenience. In Table 6 we have also marked by an asterisk the point of onset of secular instability along the equilibrium sequences. As expected from the general results of § 2.3, we find that, to within our numerical accuracy, the point where the equilibrium energy curve $E_{eq}(r)$ has a minimum coincides with $r = r_{sec}$.

The *identification of a turning point prior to the Roche limit along a binary equilibrium sequence is one of the most significant results to be revealed by our energy variational approach.* The consequences are very important for the final orbital evolution of any close binary system. All configurations with binary separation $r < r_{sec}$ are secularly unstable. In the presence of internal viscous dissipation (but with no loss of angular momentum from the system), the orbit of an unstable configuration at r_{sec} will decay on the viscous dissipation timescale. Although orbital angular momentum is continually transferred to spin angular momentum during the evolution, the configuration will evolve more and more out of synchronization. Eventually, merging of the two components must occur.

It is surprising that this important instability was not identified in the TV treatment of the problem by Ch69 (§§ 57–59). There it is found that the Roche solutions remain stable (both secularly and dynamically) all the way to the Roche limit, and that they become secularly unstable precisely at the Roche limit. This appears to be in conflict with the existence of a minimum of E and J before the Roche limit in the TV equilibrium solutions themselves (see Fig. 10). The secular instability has been identified in other studies of close binary configurations such as those of van't Veer (1979), based on the Roche model, and Hachisu & Eriguchi (1984a, b), using a fully numerical solution.

The secular instability can also affect drastically the orbital decay of a system losing energy and angular momentum, for example, because of gravitational radiation. This can be seen as follows. Even if the energy loss rate $\dot{E}$ were infinitesimally small, one would naively predict that the secular rate of change of the binary separation $\dot{r} = \dot{E}/(dE_{eq}/dr) \to \infty$ as $r \to r_{sec}$. In a forthcoming paper we will show how the orbital decay actually proceeds through $r = r_{sec}$, and discuss some of the astrophysical implications of the instability for coalescing binaries (Lai et al. 1993a).

The limiting behavior of the secular instability limit r_{sec} as $p \to 0$ or $p \to \infty$ can be understood easily. When $p \to 0$, we see from Table 10 that $r_{sec} \propto p^{-1/3}$, in agreement with our discussion of § 8.3. The constant of proportionality for various polytropic indices can be read off the table. Using expressions (9.4) in the $p \to \infty$ limit, one can show that, in this limit, $r_{sec}/a_1 = r_{sec}/R_0 = Dp^{1/2}$, where the proportionality constant D is close to unity ($D = 1.0954$ for $n = 0$, $D = 0.8855$ for $n = 1$, $D = 0.7834$ for $n = 1.5$, and $D = 0.5791$ for $n = 2.5$). The limiting scaling $r_{sec} \propto p^{1/2}$ can be understood as follows. As $M' \to 0$, tidal forces become negligible, and the minimum of $\bar{E}_{eq} \equiv E_{eq}/(GM^2/R_0)$ is determined from a balance between the orbital energy of two point masses $\bar{E}_{orb} = -(R_0/r)/(2p) \propto (rp)^{-1}$, and the spin kinetic energy $\bar{T}_s = (1/2)I\Omega_K^2/(GM^2/R_0) \propto r^{-3}$. Therefore, in the $p \to \infty$ limit, we have $dE_{eq}/dr = 0$ at $r = r_{sec} \propto p^{1/2}$. Recall, however, that the Roche problem in this limit is somewhat unphysical because of the assumption of synchronized rotation (cf. § 8.3).

9.2. *Dynamical Instability of Roche Binaries*

Motivated by the results of § 6.3 for Maclaurin spheroids, we can tentatively identify the onset of *dynamical* instability by considering perturbations which not only conserve M and J,

but also conserve $\mathscr{C}$. That is, we now substitute the energy function of Roche-Riemann binaries (§ 8.1) in the determinant of condition (2.15) before evaluating it along the equilibrium Roche sequence (where $\Lambda = f_R = \zeta = 0$).

As in § 9.1, we rewrite the kinetic energy term

$$T = T_s + T_0 = T_+ + T_- + \frac{1}{2}\frac{Mr^2\Omega^2}{(1+p)}, \tag{9.5}$$

where

$$T_\pm = \frac{1}{4I_s}\left[J \pm \mathscr{C} - \frac{Mr^2\Omega}{(1+p)}\right]^2 h_\pm, \tag{9.6}$$

so that $\partial E/\partial\Omega = 0$. The first derivatives can then be evaluated at constant Ω, giving

$$\begin{aligned}\frac{\partial E}{\partial\lambda_1} &= \frac{h_{+(1)}}{\lambda_1}T_+ + \frac{h_{-(1)}}{\lambda_1}T_- + \frac{\mathscr{I}_{(1)}}{\lambda_1}W \\ &\quad + \frac{GM'}{2r^3\lambda_1}(4I_{11} + I_{22} + I_{33}), \\ \frac{\partial E}{\partial\lambda_2} &= \frac{h_{+(2)}}{\lambda_2}T_+ + \frac{h_{-(2)}}{\lambda_2}T_- \\ &\quad + \frac{\mathscr{I}_{(2)}}{\lambda_2}W - \frac{GM'}{2r^3\lambda_2}(2I_{11} + 2I_{22} - I_{33}),\end{aligned} \tag{9.7}$$

while the expressions for $\partial E/\partial r$ and $\partial E/\partial\rho_c$ are identical to those obtained in § 9.1. Setting these first derivatives equal to zero again yields the equilibrium conditions for a general Roche-Riemann binary (§ 8.1).

Now turn to the second derivatives. From the relation

$$J \pm \mathscr{C} - \frac{Mr^2\Omega}{(1+p)} = \frac{I_s}{h_\pm}(\Omega \pm \Lambda) \tag{9.8}$$

(cf. eqs. [3.13], [5.12], [8.2] and [9.6]), we get

$$\Omega = \frac{(J+\mathscr{C})h_+ + (J-\mathscr{C})h_-}{2I_e}, \tag{9.9}$$

where we have defined

$$I_e \equiv I_s + \frac{Mr^2}{2(1+p)}(h_+ + h_-). \tag{9.10}$$

As in § 9.1, we first evaluate the partial derivatives of Ω, using expression (9.9), and then use the relations like equation (9.3) as well as the results of Appendix A to calculate the second derivatives of E. We find

$$\begin{aligned}r^2\left(\frac{\partial^2 E}{\partial r^2}\right)_{\rm eq} &= \left[-2 + \frac{4Mr^2}{(1+p)I_e}(h_+ + h_-)\right]T_0 \\ &\quad - \frac{2GMM'}{r} - \frac{6GM'\delta I}{r^3}, \\ \rho_c^2\left(\frac{\partial^2 E}{\partial\rho_c^2}\right)_{\rm eq} &= \frac{W}{3}\left[\left(\frac{1}{3} - \frac{1}{n}\right) - 2\left(\frac{2}{3} - \frac{1}{n}\right)\frac{T_s}{|W|}\right] \\ &\quad - \frac{1}{3}\left(\frac{2}{3} + \frac{1}{n}\right)\frac{GM'\delta I}{r^3} - \frac{8I_s}{9I_e}T_0, \\ \lambda_1^2\left(\frac{\partial^2 E}{\partial\lambda_1^2}\right)_{\rm eq} &= h_{+(11)}T_+ + h_{-(11)}T_- + \mathscr{I}_{(11)}W \\ &\quad - \frac{6GM'I_{11}}{r^3} - \frac{I_sMr^2}{4(1+p)I_e}\Sigma_1^2, \\ \lambda_2^2\left(\frac{\partial^2 E}{\partial\lambda_2^2}\right)_{\rm eq} &= h_{+(22)}T_+ + h_{-(22)}T_- + \mathscr{I}_{(22)}W \\ &\quad + \frac{3GM'I_{22}}{r^3} - \frac{I_sMr^2}{4(1+p)I_e}\Sigma_2^2, \\ \rho_c r\left(\frac{\partial^2 E}{\partial\rho_c\partial r}\right)_{\rm eq} &= -\frac{GM'\delta I}{r^3} - \frac{8I_s}{3I_e}T_0, \\ r\lambda_1\left(\frac{\partial^2 E}{\partial r\partial\lambda_1}\right)_{\rm eq} &= -\frac{I_sMr^2}{(1+p)I_e}\Omega\Sigma_1 \\ &\quad - \frac{3GM'}{2r^3}(4I_{11} + I_{22} + I_{33}), \\ r\lambda_2\left(\frac{\partial^2 E}{\partial r\partial\lambda_2}\right)_{\rm eq} &= -\frac{I_sMr^2}{(1+p)I_e}\Omega\Sigma_2 \\ &\quad + \frac{3GM'}{2r^3}(2I_{11} + 2I_{22} - I_{33}), \\ \rho_c\lambda_1\left(\frac{\partial^2 E}{\partial\rho_c\partial\lambda_1}\right)_{\rm eq} &= \frac{2}{3}(h_{+(1)}T_+ + h_{-(1)}T_-) + \frac{\mathscr{I}_{(1)}}{3}W \\ &\quad - \frac{GM'}{3r^3}(4I_{11} + I_{22} + I_{33}) \\ &\quad - \frac{I_sMr^2}{3(1+p)I_e}\Omega\Sigma_1, \\ \rho_c\lambda_2\left(\frac{\partial^2 E}{\partial\rho_c\partial\lambda_2}\right)_{\rm eq} &= \frac{2}{3}(h_{+(2)}T_+ + h_{-(2)}T_-) + \frac{\mathscr{I}_{(2)}}{3}W \\ &\quad + \frac{GM'}{3r^3}(2I_{11} + 2I_{22} - I_{33}) \\ &\quad - \frac{I_sMr^2}{3(1+p)I_e}\Omega\Sigma_2, \\ \lambda_1\lambda_2\left(\frac{\partial^2 E}{\partial\lambda_1\lambda_2}\right)_{\rm eq} &= h_{+(12)}T_+ + h_{-(12)}T_- + \mathscr{I}_{(12)}W \\ &\quad + \frac{GM'}{2r^3}(4I_{11} - 2I_{22} + I_{33}) \\ &\quad - \frac{I_sMr^2}{4(1+p)I_e}\Sigma_1\Sigma_2,\end{aligned} \tag{9.11}$$

where we have introduced

$$\Sigma_i \equiv h_{+(i)}(\Omega + \Lambda) + h_{-(i)}(\Omega - \Lambda), \quad i = 1, 2. \tag{9.12}$$

We then evaluate the matrix coefficients *along an equilibrium Roche sequence,* and calculate the determinant of condition (2.15) as a function of r.

When $n < 3$ ($\Gamma > 4/3$), and for sufficiently large r, we find that the determinant remains always positive. As r decreases, the value of the determinant decreases, and a change of sign occurs at a certain critical separation r_{dyn}, which we tentatively identify as the point of onset of dynamical instability. The values of r_{dyn} for different mass ratios and polytropic indices are listed in Table 10, and the corresponding points are also noted by a double asterisk in the sequences of Table 6. In the limit where $p \to 0$, we have $r_{dyn} \propto p^{-1/3}$ (cf. § 8.3). For some equilibrium sequences, the dynamical instability limit is reached only when $r_{dyn}/a_1 < 1$. These configurations are clearly unphysical since the point-mass companion would be located inside the star. The corresponding entries in Table 10 (those with $n = 2.5$ and $p \geq 5$) have been placed in parentheses. When $n \gtrsim 1.7$, the configurations remain dynamically stable all the way to the Roche limit. For $n \lesssim 1.7$, the dynamical stability limit is reached before the Roche limit when p exceeds a minimum value, p_{min}. In particular, for $n = 0$, we find $p_{min} \simeq 4 \times 10^{-3}$; for $n = 1$, $p_{min} \simeq 0.07$; and for $n = 1.5$, $p_{min} \simeq 0.4$. Note that the point $r = r_{dyn}$ does *not* correspond to any minimum (or maximum) of the equilibrium energy curve $E_{eq}(r)$ for Roche binaries (see Fig. 14). The reason is that the perturbations considered here allow for internal motions of the fluid body (a new degree of freedom) so as to maintain the conservation of $\mathscr{C}$. These perturbations do not take one equilibrium Roche configuration into a neighboring Roche configuration since they do not preserve the synchronized rotation state of the binary.

Does a dynamical instability really set in at $r = r_{dyn}$ as determined here? The answer to that question may be of little astrophysical relevance since *the secular instability limit is always encountered first* along the sequence (see Tables 6 and 10, and Fig. 14). As discussed in § 9.1, the system must evolve out of synchronization as $r \to r_{sec}$, even if the dissipation is infinitesimally small. Synchronized configurations that are dynamically unstable may therefore never be encountered (the situation is different for nonsynchronized binaries, see § 9.3). Nevertheless, we reemphasize here that conservation of M, J, and $\mathscr{C}$ is a necessary but not sufficient condition for the existence of physically realizable dynamical perturbations.

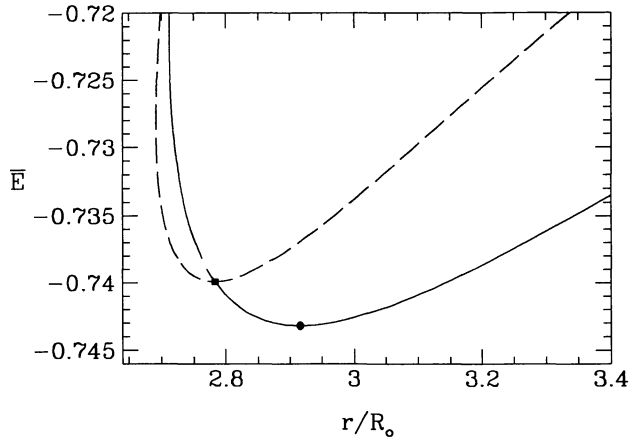

FIG. 14.—Secular instability limit (*filled circle*) and dynamical instability limit (*filled square*) along the equilibrium Roche sequence with $p = 1$ and $n = 0$ (*solid line*). The dynamical instability limit is also the point where the total equilibrium energy E is minimum along a Roche-Riemann sequence with constant $\mathscr{C}/(GM^3R_0)^{1/2} = -0.15268$ (*dashed line*). See text for discussion (§ 9.3).

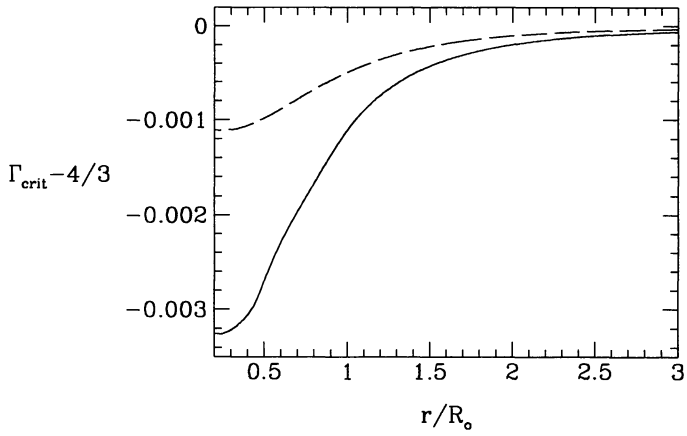

FIG. 15.—Variation of the critical adiabatic exponent for the onset of radial instability in a compressible Roche ellipsoid as a function of binary separation. The solid line is for $p = 1$, the dashed line for $p = 0.1$.

As we showed analytically in § 6.2 for Maclaurin spheroids, condition (2.15) can also become realized at *any* separation r when the adiabatic index Γ falls below a certain critical value Γ_{crit}. Motivated by the results of § 6.3, we identify this as the onset of *radial collapse.* Because of the complexity of equations (9.4), it is not possible to obtain a closed-form expression of Γ_{crit} for compressible Roche ellipsoids. Instead, we have evaluated Γ_{crit} numerically as a function of r for two selected values of the mass ratio. The results are shown in Figure 15. We see that $\Gamma_{crit} < 4/3$ everywhere for all mass ratios. Indeed, we can use a simple argument to show that tidal effects, just like rotation, tend to *stabilize* the star against radial collapse. Using the virial relation (eq. [7.8]), we find that for Roche ellipsoids (cf. eq. [3.22]):

$$M(\rho_c; J) = M(\rho_c; 0)\left[f(\lambda_1, \lambda_2)\left(1 - 2\frac{T_s}{|W|}\right) - \left(\frac{5-n}{3p}\right)g_t\right]^{-3/2}, \tag{9.13}$$

where g_t is given by equation (7.22) and $M(\rho_c; 0)$ is the mass of an unperturbed spherical polytrope, given by expression (2.13). For Roche ellipsoids, we have $g_t > 0$ since $a_1 > a_2 > a_3$. Recall that an isolated spherical polytrope of index $n = 3$ is marginally stable against radial collapse. For a given K, $M_0 \equiv (k_1K/k_2)^{3/2}$ is the only mass at which an $n = 3$ equilibrium configuration can exist (cf. eq. [2.13]). But if we evaluate equation (9.13) for the same value of K and $n = 3$, we see that the equilibrium mass actually increases above M_0. Hence, tidal forces, just like rotation, increase the maximum allowable mass of the star, that is, both rotation and tidal forces have a stabilizing effect with respect to radial collapse.

9.3. *Stability of Roche-Riemann Binaries*

It is straightforward to extend the results of the previous section to study the stability properties of Roche-Riemann binaries. In Figure 13 we see that the equilibrium energy curve $E_{eq}(r)$ for the irrotational ($\mathscr{C} = 0, f_R = -2$) Roche-Riemann sequence also exhibits a minimum before the Roche-Riemann limit is reached. According to our conventions (§ 2.4), since the equilibrium model allows for nonuniform rotation and $\mathscr{C}$ is fixed along this sequence, we refer to the corresponding instability as dynamical. As before, we can locate the minimum of E_{eq} at $r = r_{dyn}$ by calculating the determinant of condition (2.15). The matrix elements have already been written in § 9.2, expressions (9.11). Here we evaluate the determinant along an irrotational Roche-Riemann equilibrium sequence, calculated as in § 8.2. The values of r_{dyn} for sequences with different p and n are listed in Table 11, together with the corresponding irrotational Roche-Riemann limits. The instability points are also noted by an asterisk in the sequences of Table 7.

Similarly, one can locate the onset of instability along any Roche-Riemann sequence with constant $\mathscr{C} \neq 0$. Note, however, that a minimum of $E_{eq}(r)$ along a sequence with constant f_R does *not* indicate the onset of instability except when $f_R = 0$ or $f_R = -2$. For $f_R = 0$, the Roche sequence is recovered, and the minimum corresponds to the onset of *secular instability* (cf. § 9.1), while for $f_R = -2$, $\mathscr{C} = 0$ is fixed along the sequence, and the minimum corresponds to the onset of dynamical instability as discussed above.

It is interesting to note that the point $r = r_{dyn}$ along the Roche sequence (§ 9.2) also corresponds to the minimum of the equilibrium energy curve for an appropriate Roche-Riemann sequence of constant $\mathscr{C}$, with the value of $\mathscr{C}$ calculated at $r = r_{dyn}$ for the Roche ellipsoid. This is illustrated in Figure 14, where we show a blowup of the $E_{eq}(r)$ curve for the $n = 0$ Roche sequence near the location of the secular and dynamical instability points. The value of $\mathscr{C}$ at the dynamical instability point is given by $\mathscr{C}/(GM^3R_0)^{1/2} = -0.15268$. We have constructed a Roche-Riemann sequence corresponding to that particular value of $\mathscr{C}$. The resulting energy curve is also shown in Figure 14. Clearly this curve has a minimum located precisely at its point of intersection with the Roche energy curve, which coincides with $r = r_{dyn}$ as determined in § 9.2.

9.4. *Dependence on the Mass Ratio*

The variation of the critical separations r_{sec}, r_{dyn} and r_{lim} along Roche and irrotational Roche-Riemann sequences is plotted in Figure 16 as a function of the mass ratio. When $p \ll 1$, we see that all three critical separations are approximately equal and scale like $(1 + 1/p)^{1/3}$, as expected from simple tidal breakup considerations, and in agreement with the discussion of § 8.3. More precisely, for Roche binaries, one can show that $|r_{sec} - r_{lim}| \to 0$ but $r_{dyn} \gtrsim r_{lim}$ as $p \to 0$ (see Table 10). For irrotational Roche-Riemann binaries, $|r_{dyn} - r_{lim}| \to 0$ as $p \to 0$ (see Table 11). In the (less important) $p \to \infty$ limit, r_{lim} and r_{dyn} approach constant values, while r_{sec} for Roche binaries increases as $p^{1/2}$ (see § 9.1).

In the limit of very high compressibility (large n), where our ellipsoidal approximation is expected to be poor, the Roche limit may be better determined from standard Roche lobe considerations (Kopal 1959; Paczyński 1971). In Figure 16*a*, we show this approximate limiting behavior of the Roche limit, as predicted by setting the mean radius of the Roche lobe equal to the spherical equilibrium radius R_0. Here we have used Eggleton's (1983) fitting formula for the mean Roche lobe radius R_L,

$$\frac{R_L}{r} \simeq \frac{0.49p^{2/3}}{0.6p^{2/3} + \ln(1 + p^{1/3})}. \tag{9.14}$$

We emphasize that no direct comparison between the two approaches is possible since they are expected to be valid in opposite limits. However, we see clearly from Figure 16 that the Roche lobe theory should not be trusted when applied to configurations with small polytropic indices.

10. COMPRESSIBLE DARWIN ELLIPSOIDS

The classical Darwin problem treats a binary system consisting of two identical incompressible stars in circular orbit about each other, where the mutual tidal interactions are incorporated to quadrupole order. We now use our energy variational method to solve this problem for two identical compressible configurations. Note, however, that our method can also be used to construct more general binaries containing two polytropes of different masses and entropies. Other generalizations, such as the construction of "Darwin-Riemann" configurations, where both stars have internal fluid motions of uniform vorticity, are also possible (see § 10.4).

10.1. *Equilibrium Conditions*

Consider two identical polytropes, each of mass M, in circular orbit about each other. The system is assumed to be rotating uniformly with angular velocity Ω. The notations and definitions of § 4 and § 7 are used throughout this section.

Here we write the total energy *per star* in the binary system as $E(\rho_c, \lambda_1, \lambda_2, r; M, J) = U + T + W + W_i$, where W is the gravitational potential self-energy of one star, and W_i is one-half of the gravitational interaction energy of the binary. Both U and W retain the same form they had for isolated configurations (§ 4). The kinetic energy per star is given by equation (7.2) with now

$$\begin{aligned} I_{cm} &= Mr_{cm}^2 + I \\ &= \frac{1}{4}Mr^2 + \frac{M^{5/3}\rho_c^{-2/3}}{2k_3h(\lambda_1, \lambda_2)}. \end{aligned} \tag{10.1}$$

The gravitational potential energy is obtained from equation (B7) with $M = M'$,

$$W_i = -\frac{1}{2}\frac{GM^2}{r} - \frac{1}{2}\frac{GM}{r^3}(2I_{11} - I_{22} - I_{33}) \tag{10.2}$$

(where we have divided eq. [B7] by 2 to obtain the energy per star).

As in § 7, the equilibrium condition, $\partial E/\partial r = \partial T/\partial r + \partial W_i/\partial r = 0$, provides the *modified Kepler's law* for the binary. Using equations (7.2) and (10.1) for T and (10.2) for W_i, we find

TABLE 11

CRITICAL POINTS ALONG THE $\mathscr{C} = 0$ ROCHE-RIEMANN SEQUENCES[a]

p [b]	$\hat{r}/a_1$	$\hat{r}/R_0$	a_2/a_1	a_3/a_1	$T_s/\lvert W\rvert$	Ω	J	E	R/R_0
				$n = 0$					
100.	1.8098	1.8408	0.9687	0.9811	0.545(-4)	0.4644	0.014	-0.6026	1.
	1.6270	1.7647	0.8551	0.9165	0.156(-2)	0.5043	0.018	-0.6009	1.
10.	1.8755	2.0121	0.8835	0.9165	0.656(-3)	0.4107	0.142	-0.6228	1.
	1.5053	1.8889	0.6642	0.7620	0.957(-2)	0.4710	0.169	-0.6120	1.
5.	1.8896	2.0948	0.8374	0.8764	0.122(-2)	0.3883	0.282	-0.6422	1.
	1.4813	1.9661	0.6091	0.7021	0.129(-1)	0.4467	0.321	-0.6277	1.
2.	1.8917	2.2210	0.7646	0.8082	0.241(-2)	0.3573	0.676	-0.6921	1.
	1.4809	2.1045	0.5530	0.6301	0.155(-1)	0.4030	0.727	-0.6746	1.
1.	1.8737	2.3141	0.7068	0.7510	0.363(-2)	0.3362	1.252	-0.7610	1.
	1.5021	2.2217	0.5248	0.5889	0.158(-1)	0.3683	1.307	-0.7439	1.
0.5	1.8373	2.3893	0.6528	0.6965	0.506(-2)	0.3198	2.214	-0.8743	1.
	1.5300	2.3260	0.5071	0.5613	0.152(-1)	0.3395	2.266	-0.8594	1.
0.2	1.7720	2.4517	0.5936	0.6360	0.711(-2)	0.3061	4.417	-1.1375	1.
	1.5592	2.4203	0.4944	0.5407	0.143(-1)	0.3149	4.456	-1.1267	1.
0.1	1.7223	2.4763	0.5596	0.6012	0.860(-2)	0.3003	7.210	-1.4788	1.
	1.5715	2.4600	0.4894	0.5326	0.138(-1)	0.3047	7.239	-1.4709	1.
0.01	1.6191	2.5001	0.5016	0.5416	0.119(-1)	0.2932	34.137	-4.8541	1.
	1.5805	2.4989	0.4834	0.5234	0.134(-1)	0.2935	34.145	-4.8520	1.
0.	1.5790	2.5023	0.4819	0.5214	0.133(-1)	0.2917	∞	$-\infty$	1.
	1.5790	2.5023	0.4819	0.5214	0.133(-1)	0.2917	∞	$-\infty$	1.
				$n = 1$					
100.	1.4584	1.4834	0.9689	0.9811	0.541(-4)	0.6420	0.012	-0.5033	1.0001
	1.3247	1.4249	0.8721	0.9268	0.119(-2)	0.6931	0.015	-0.5016	1.0019
10.	1.5150	1.6269	0.8853	0.9176	0.632(-3)	0.5648	0.127	-0.5282	1.0020
	1.2778	1.5445	0.7254	0.8090	0.566(-2)	0.6287	0.141	-0.5209	1.0120
5.	1.5315	1.7002	0.8416	0.8793	0.114(-2)	0.5308	0.254	-0.5522	1.0041
	1.2789	1.6204	0.6813	0.7618	0.731(-2)	0.5875	0.272	-0.5429	1.0182
2.	1.5484	1.8194	0.7762	0.8171	0.209(-2)	0.4811	0.610	-0.6130	1.0095
	1.3064	1.7555	0.6357	0.7039	0.841(-2)	0.5198	0.633	-0.6029	1.0279
1.	1.5540	1.9145	0.7283	0.7689	0.290(-2)	0.4456	1.134	-0.6962	1.0155
	1.3437	1.8689	0.6134	0.6709	0.831(-2)	0.4697	1.157	-0.6869	1.0345
0.5	1.5504	1.9972	0.6875	0.7267	0.368(-2)	0.4170	2.013	-0.8316	1.0222
	1.3832	1.9690	0.5999	0.6491	0.784(-2)	0.4303	2.033	-0.8240	1.0395
0.2	1.5327	2.0716	0.6471	0.6848	0.459(-2)	0.3927	4.035	-1.1431	1.0304
	1.4219	2.0592	0.5906	0.6332	0.727(-2)	0.3979	4.050	-1.1379	1.0434
0.1	1.5152	2.1033	0.6259	0.6630	0.516(-2)	0.3823	6.609	-1.5446	1.0354
	1.4386	2.0974	0.5871	0.6272	0.702(-2)	0.3847	6.620	-1.5410	1.0450
0.01	1.4730	2.1360	0.5928	0.6297	0.628(-2)	0.3709	31.492	-5.4965	1.0441
	1.4542	2.1356	0.5833	0.6207	0.675(-2)	0.3710	31.495	-5.4956	1.0467
0.	1.4547	2.1395	0.5824	0.6195	0.673(-2)	0.3690	∞	$-\infty$	1.0470
	1.4547	2.1395	0.5824	0.6195	0.673(-2)	0.3690	∞	$-\infty$	1.0470
				$n = 1.5$					
100.	1.2859	1.3080	0.9690	0.9812	0.536(-4)	0.7754	0.012	-0.4323	1.0002
	1.1756	1.2583	0.8827	0.9330	0.982(-3)	0.8338	0.014	-0.4307	1.0033
10.	1.3390	1.4391	0.8869	0.9187	0.610(-3)	0.6787	0.120	-0.4605	1.0038
	1.1574	1.3758	0.7564	0.8315	0.417(-2)	0.7434	0.129	-0.4547	1.0184
5.	1.3577	1.5091	0.8454	0.8820	0.107(-2)	0.6344	0.239	-0.4875	1.0079
	1.1693	1.4509	0.7185	0.7907	0.522(-2)	0.6883	0.251	-0.4805	1.0277
2.	1.3841	1.6272	0.7860	0.8246	0.184(-2)	0.5681	0.575	-0.5555	1.0174
	1.2100	1.5845	0.6797	0.7407	0.579(-2)	0.6014	0.589	-0.5484	1.0417
1.	1.4026	1.7244	0.7451	0.7827	0.241(-2)	0.5202	1.072	-0.6477	1.0272
	1.2553	1.6958	0.6612	0.7126	0.558(-2)	0.5395	1.086	-0.6415	1.0512

TABLE 11—*Continued*

p [b]	$\hat{r}/a_1$	$\hat{r}/R_0$	a_2/a_1	a_3/a_1	$T_s/\|W\|$	$\bar{\Omega}$	$\bar{J}$	$\bar{E}$	R/R_0
				$n = 1.5$					
0.5	1.4148	1.8102	0.7123	0.7480	0.287(-2)	0.4822	1.909	-0.7969	1.0373
	1.3004	1.7936	0.6503	0.6943	0.518(-2)	0.4920	1.920	-0.7920	1.0581
0.2	1.4176	1.8883	0.6817	0.7156	0.334(-2)	0.4502	3.839	-1.1383	1.0486
	1.3437	1.8815	0.6431	0.6812	0.475(-2)	0.4538	3.848	-1.1351	1.0634
0.1	1.4128	1.9218	0.6665	0.6998	0.362(-2)	0.4370	6.300	-1.5773	1.0549
	1.3624	1.9186	0.6404	0.6763	0.456(-2)	0.4386	6.306	-1.5751	1.0655
0.01	1.3927	1.9563	0.6438	0.6769	0.414(-2)	0.4229	30.114	-5.8918	1.0650
	1.3806	1.9561	0.6376	0.6712	0.437(-2)	0.4230	30.115	-5.8913	1.0677
0.	1.3820	1.9602	0.6370	0.6703	0.435(-2)	0.4207	∞	$-\infty$	1.0681
	1.3820	1.9602	0.6370	0.6703	0.435(-2)	0.4207	∞	$-\infty$	1.0681
				$n = 2.5$					
100.	(0.9411)	(0.9579)	(0.9695)	(0.9815)	(0.516(-4))	(1.2373)	(0.010)	(-0.2050)	(1.0011)
	(0.8786)	(0.9281)	(0.9146)	(0.9514)	(0.491(-3))	(1.3094)	(0.011)	(-0.2041)	(1.0085)
10.	0.9951	1.0761	0.8967	0.9250	0.485(-3)	1.0483	0.103	-0.2430	1.0161
	(0.9160)	(1.0520)	(0.8372)	(0.8865)	(0.152(-2))	(1.0956)	(0.105)	(-0.2408)	(1.0398)
5.	1.0268	1.1504	0.8664	0.8966	0.725(-3)	0.9504	0.207	-0.2783	1.0299
	.9524	1.1326	0.8158	0.8614	0.169(-2)	0.9809	0.210	-0.2761	1.0573
2.	1.0882	1.2835	0.8317	0.8597	0.939(-3)	0.8062	0.505	-0.3641	1.0547
	1.0270	1.2738	0.7961	0.8325	0.161(-2)	0.8195	0.508	-0.3623	1.0813
1.	1.1429	1.3939	0.8131	0.8379	0.976(-3)	0.7106	0.953	-0.4769	1.0732
	1.0948	1.3886	0.7881	0.8177	0.141(-2)	0.7167	0.955	-0.4755	1.0955
0.5	1.1917	1.4899	0.8009	0.8228	0.960(-3)	0.6411	1.713	-0.6562	1.0880
	1.1564	1.4872	0.7840	0.8086	0.122(-2)	0.6436	1.714	-0.6553	1.1048
0.2	1.2343	1.5754	0.7912	0.8110	0.934(-3)	0.5874	3.478	-1.0629	1.1009
	1.2128	1.5745	0.7816	0.8026	0.107(-2)	0.5882	3.479	-1.0624	1.1114
0.1	1.2511	1.6116	0.7870	0.8059	0.926(-3)	0.5666	5.735	-1.5842	1.1068
	1.2368	1.6112	0.7808	0.8005	0.101(-2)	0.5670	5.735	-1.5838	1.1138
0.01	1.2646	1.6485	0.7814	0.7997	0.933(-3)	0.5461	27.599	-6.7014	1.1145
	1.2613	1.6485	0.7800	0.7984	0.952(-3)	0.5461	27.599	-6.7013	1.1161
0.	1.2641	1.6528	0.7799	0.7982	0.944(-3)	0.5434	∞	$-\infty$	1.1164
	1.2641	1.6528	0.7799	0.7982	0.944(-3)	0.5434	∞	$-\infty$	1.1164

[a] Here $\hat{r} \equiv r/(1 + 1/p)^{1/3}$ with $p = M/M'$; $\bar{\Omega}$, $\bar{J}$, and $\bar{E}$ are defined in eq. (3.26); R_0 is given by eq. (3.24); T_s and W are the kinetic energy (excluding the center-of-mass motion) and the self-gravitational energy of the ellipsoid.

[b] For each value of p, the first line gives the dynamical instability limit and the second line gives the irrotational Roche-Riemann limit. Data in parentheses indicate that the stars overlap.

$$\Omega^2 = \frac{4}{M}\left(\frac{1}{r}\frac{\partial W_i}{\partial r}\right) = \frac{2GM}{r^3}\left[1 + 3\frac{(2I_{11} - I_{22} - I_{33})}{Mr^2}\right] = \frac{2GM}{r^3}(1 + 2\delta), \quad (10.3)$$

with δ defined by equation (7.7). As already observed for Roche binaries, our result does not agree with the expression for Ω^2 used in the standard TV treatment of Ch69. In that treatment, Ω^2 is determined by the requirement that certain terms linear in the coordinates disappear from the fluid equation of motion, to lowest order (Ch69, § 61). This requirement leads to the following expression for Ω^2 (cf. Ch69, eq. [8.111])

$$\Omega^2 = \Omega^2_{\rm Ch} \equiv \frac{2}{r}\frac{\partial \Phi^{\rm ext}}{\partial r} = \frac{2GM}{r^3}\left[1 + \frac{3}{2}\frac{(2I_{11} - I_{22} - I_{33})}{Mr^2}\right] = \frac{2GM}{r^3}(1 + \delta), \quad (10.4)$$

where we have expanded the result to quadrupole order, using equation (B5) for $\Phi^{\rm ext}$. The gradient of the gravitational *potential* appears in expression (10.4), whereas the gradient of the *potential energy* appears in our result, equation (10.3). Expression (10.4) ignores the fact that the tidal potential is not constant over the interior of the stars and contains a factor of 2 error in the (leading-order) quadrupole correction to Kepler's law.[13] The energy variational method is clearly superior here, in that it provides naturally a self-consistent equilibrium rotation law (but see Appendix C).

As before the condition $\partial E/\partial \rho_c = 0$ leads to the virial relation (7.8), where now

$$W_t \equiv W_i + \frac{1}{2}\frac{GM^2}{r} = -\frac{1}{2}\frac{GM}{r^3}(2I_{11} - I_{22} - I_{33}). \quad (10.5)$$

[13] Note that instead of expanding expression (10.4) to quadrupole order, as we have done, Ch69 proceeds to evaluate $\Phi_{\rm ext}$ *exactly* for a homogeneous ellipsoid. This does not, of course, remove the discrepancy.

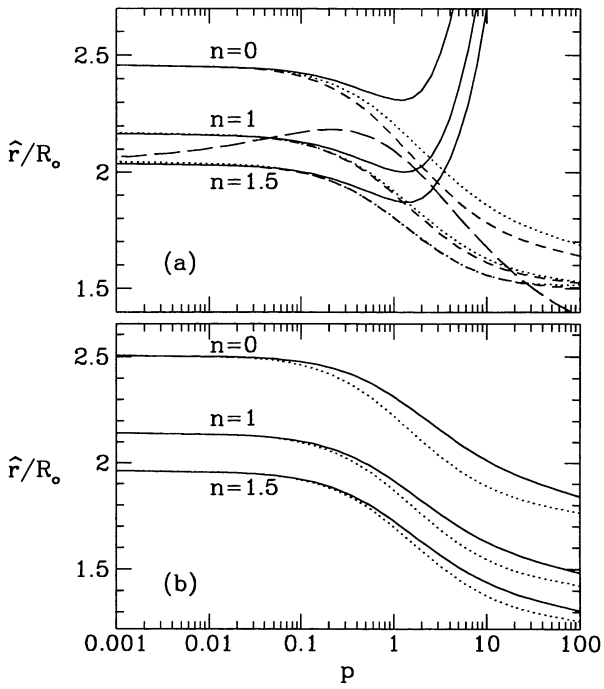

FIG. 16.—Plots of the instability and Roche limits as a function of the mass ratio $p = M/M'$ for Roche (*a*) and Roche-Riemann (*b*) systems with $n = 0$, 1, and 1.5. The critical binary separations are given in terms of the reduced quantity $\hat{r} \equiv r/(1 + 1/p)^{1/3}$, as in Tables 10 and 11. In (*a*) the solid lines show the secular instability limits $\hat{r}_{\rm sec}$, the dotted lines show the dynamical instability limits $\hat{r}_{\rm dyn}$, and the short-dashed lines give the Roche limits $\hat{r}_{\rm lim}$. Also shown (*long-dashed line*) is the Roche limit calculated from a simple Roche-lobe–type argument (cf. eq. [9.14]). In (*b*) the solid lines show the dynamical instability limits $\hat{r}_{\rm dyn}$, and the dotted lines show the Roche-Riemann limits $\hat{r}_{\rm lim}$.

The total equilibrium energy per star can be written

$$E_{\rm eq} = \frac{3-n}{3} W\left(1 - \frac{3-2n}{3-n}\frac{T_s}{|W|}\right) + \frac{1}{8} Mr^2\Omega^2 - \frac{1}{2}\frac{GM^2}{r} - \frac{2n+3}{6}\frac{M}{r^3}(2I_{11} - I_{22} - I_{33}), \quad (10.6)$$

and the total angular momentum per star is given by $J = I_{\rm cm}\Omega$ with $I_{\rm cm}$ obtained from equation (10.1).

Following Ch69 (§ 61), we now introduce the quantities

$$\beta_{11} \equiv \Omega^2 - \Phi^{\rm ext}_{,11}(P), \quad (10.7)$$

$$\beta_{22} \equiv \Omega^2 - \Phi^{\rm ext}_{,22}(P), \quad (10.8)$$

$$\beta_{33} \equiv -\Phi^{\rm ext}_{,33}(P) = \Phi^{\rm ext}_{,11}(P) + \Phi^{\rm ext}_{,22}(P). \quad (10.9)$$

After manipulations similar to those described in § 4.1, the two equilibrium conditions $\partial E/\partial\lambda_1 = \partial E/\partial\lambda_2 = 0$ can be written

$$0 = \mathcal{M}_{11} - \tfrac{1}{2}\mathcal{M}_{22} - \tfrac{1}{2}\mathcal{M}_{33} + \beta_{11}I_{11} - \tfrac{1}{2}\beta_{22}I_{22} - \tfrac{1}{2}\beta_{33}I_{33} = (1 \leftrightarrow 2) \quad (10.10)$$

where $\mathcal{M}_{ij}$ are the components of the potential-energy tensor, defined by equation (7.14). Together with the virial relation (7.8), these two conditions can be rewritten in the symmetric form

$$\mathcal{M}_{11} + \beta_{11}I_{11} = \mathcal{M}_{22} + \beta_{22}I_{22} = \mathcal{M}_{33} + \beta_{33}I_{33} = -\frac{U}{n}. \quad (10.11)$$

These equations are the compressible equivalents of the conditions (8.118) of Ch69. To proceed further and still follow Ch69 (§ 62) we must also introduce the quantities

$$\alpha_1 \equiv \frac{1}{2r}\Phi^{\rm ext}_{,1}(P) = \frac{1}{4}\Omega^2_{\rm Ch}, \quad \alpha_2 \equiv \frac{1}{2}\Phi^{\rm ext}_{,22}(P), \quad \alpha_3 \equiv \frac{1}{2}\Phi^{\rm ext}_{,33}(P). \quad (10.12)$$

However, to be consistent with our form of Kepler's law, equation (10.3), we must replace α_1 by

$$\alpha_1^* \equiv \frac{1}{Mr}\left(\frac{\partial W_i}{\partial r}\right) = \frac{1}{4}\Omega^2. \quad (10.13)$$

To quadrupole order, we have $\alpha_2 = \alpha_3 = GM/(2r^3)$. Using the definitions (10.12) and (10.13) we can rewrite the first two conditions (10.11) in the form

$$q_n\tilde{\alpha}_1^* = \frac{A_1a_1^2 - A_3a_3^2}{(2 + \alpha_2/\alpha_1^*)a_1^2 + (a_1^2 + a_3^2)\alpha_3/\alpha_1^*} = \frac{A_2a_2^2 - A_3a_3^2}{(2 - \alpha_2/\alpha_1^*)a_2^2 + a_3^2\alpha_3/\alpha_1^*}, \quad (10.14)$$

where $\tilde{\alpha}_1^* \equiv \alpha_1^*/(\pi G\bar{\rho})$. Equation (10.14) reduces to equation (8.143) of Ch69 for $n = 0$ *only* when we replace α_1^* by α_1.

10.2. *Constructing Equilibrium Sequences*

All equilibrium equations obtained for Roche ellipsoids in § 7.1 can be used to calculate Darwin ellipsoids as well, except that now we use $\Omega^2 = (1 + p)\mu(1 + 2\delta)$ instead of equation (7.17), and replace δ in equations (7.18)–(7.20) by 2δ. We also let the mass ratio $p = 1$ everywhere. The numerical procedure for calculating sequences of Darwin binaries is then identical to that used in § 7.2 for Roche binaries. Alternatively, we can use equation (10.14) explicitly, as done by Ch69. We have verified that the numerical results of Ch69 (cf. his Table XXV) are recovered exactly when we replace α_1^* by α_1 in equation (10.14) and use his expression (8.136) for α_i (this is equivalent to using the exact form of $\Phi_{\rm ext}$ for a homogeneous ellipsoid in the definitions [10.12]). As an additional check, we have also verified that the relation $dE = \Omega dJ$ (cf. Appendix D) is satisfied to high numerical accuracy along all our calculated equilibrium sequences (but only when we use α_1^* and not when we use α_1).

Representative results are given in Table 12 for $n = 0$, 1, 1.5, and 2.5. No "Roche limit" is ever reached along the compressible Darwin sequences. Instead, all sequences terminate when

TABLE 12

COMPRESSIBLE DARWIN SEQUENCES[a]

r/a_1 [b]	r/R_0	a_2/a_1	a_3/a_1	$T_*/\|W\|$	$\bar{\Omega}$	$\bar{J}$	$\bar{E}$	R/R_0
				$n = 0$				
6.0	6.092	0.9829	0.9722	0.299(-2)	0.1087	1.823	-1.2784	1.
5.0	5.131	0.9707	0.9532	0.507(-2)	0.1408	1.704	-1.2911	1.
4.5	4.661	0.9602	0.9373	0.683(-2)	0.1628	1.647	-1.2985	1.
4.0	4.202	0.9441	0.9137	0.948(-2)	0.1906	1.595	-1.3065	1.
3.8	4.023	0.9352	0.9011	0.109(-1)	0.2037	1.576	-1.3098	1.
3.5	3.761	0.9183	0.8777	0.136(-1)	0.2260	1.551	-1.3144	1.
3.2	3.510	0.8951	0.8469	0.172(-1)	0.2519	1.532	-1.3182	1.
3.0	3.350	0.8747	0.8210	0.203(-1)	0.2713	1.525	-1.3199	1.
2.859*	3.242	0.8573	0.7995	0.229(-1)	0.2861	1.523	-1.3203	1.
2.7	3.128	0.8338	0.7716	0.264(-1)	0.3037	1.526	-1.3196	1.
2.324**	2.895	0.7556	0.6853	0.374(-1)	0.3488	1.560	-1.3098	1.
2.0	2.769	0.6494	0.5802	0.519(-1)	0.3860	1.646	-1.2822	1.
				$n = 1$				
6.0	6.058	0.9910	0.9852	0.159(-2)	0.1095	1.791	-1.0801	1.0016
5.0	5.083	0.9845	0.9748	0.271(-2)	0.1426	1.661	-1.0942	1.0028
4.0	4.130	0.9701	0.9523	0.517(-2)	0.1950	1.531	-1.1129	1.0055
3.5	3.669	0.9559	0.9310	0.754(-2)	0.2332	1.470	-1.1241	1.0082
3.2	3.401	0.9429	0.9121	0.966(-2)	0.2617	1.437	-1.1311	1.0108
3.0	3.229	0.9314	0.8958	0.115(-1)	0.2835	1.418	-1.1356	1.0132
2.8	3.062	0.9166	0.8755	0.139(-1)	0.3077	1.403	-1.1396	1.0163
2.6	2.904	0.8975	0.8501	0.168(-1)	0.3345	1.392	-1.1426	1.0205
2.5	2.828	0.8858	0.8350	0.186(-1)	0.3489	1.389	-1.1436	1.0231
2.405*	2.760	0.8731	0.8190	0.205(-1)	0.3629	1.388	-1.1439	1.0260
2.2	2.624	0.8387	0.7774	0.256(-1)	0.3948	1.394	-1.1419	1.0344
2.0	2.516	0.7932	0.7256	0.322(-1)	0.4258	1.416	-1.1341	1.0463
				$n = 1.5$				
6.0	6.046	0.9938	0.9898	0.109(-2)	0.1099	1.778	-0.9379	1.0022
5.0	5.067	0.9894	0.9825	0.187(-2)	0.1432	1.644	-0.9526	1.0038
4.0	4.104	0.9794	0.9667	0.359(-2)	0.1966	1.506	-0.9726	1.0075
3.5	3.636	0.9695	0.9513	0.528(-2)	0.2360	1.439	-0.9851	1.0113
3.2	3.363	0.9604	0.9376	0.680(-2)	0.2656	1.400	-0.9934	1.0148
3.0	3.185	0.9522	0.9255	0.815(-2)	0.2884	1.377	-0.9990	1.0180
2.8	3.013	0.9417	0.9103	0.986(-2)	0.3140	1.356	-1.0045	1.0223
2.6	2.847	0.9280	0.8911	0.121(-1)	0.3425	1.338	-1.0096	1.0280
2.4	2.691	0.9099	0.8664	0.149(-1)	0.3740	1.325	-1.0135	1.0358
2.3	2.618	0.8985	0.8514	0.167(-1)	0.3908	1.322	-1.0147	1.0409
2.200*	2.548	0.8854	0.8344	0.187(-1)	0.4080	1.320	-1.0152	1.0470
2.0	2.425	0.8515	0.7925	0.238(-1)	0.4431	1.327	-1.0126	1.0634
				$n = 2.5$				
6.0	6.039	0.9976	0.9960	0.429(-3)	0.1100	1.759	-0.4818	1.0043
5.0	5.056	0.9958	0.9931	0.740(-3)	0.1436	1.618	-0.4971	1.0075
4.0	4.088	0.9919	0.9866	0.143(-2)	0.1976	1.470	-0.5188	1.0147
3.0	3.159	0.9809	0.9691	0.333(-2)	0.2912	1.319	-0.5500	1.0352
2.8	2.983	0.9766	0.9623	0.407(-2)	0.3173	1.291	-0.5574	1.0436
2.6	2.814	0.9709	0.9535	0.504(-2)	0.3466	1.265	-0.5650	1.0548
2.4	2.653	0.9632	0.9419	0.632(-2)	0.3788	1.241	-0.5723	1.0703
2.3	2.578	0.9584	0.9346	0.713(-2)	0.3959	1.231	-0.5757	1.0803
2.2	2.506	0.9527	0.9262	0.807(-2)	0.4134	1.223	-0.5786	1.0924
2.1	2.439	0.9459	0.9163	0.918(-2)	0.4310	1.216	-0.5810	1.1072
2.0	2.377	0.9378	0.9047	0.105(-1)	0.4483	1.212	-0.5825	1.1253

[a] Here $p = 1$, $\bar{\Omega}$, $\bar{J}$, and $\bar{E}$ are defined in eq. (3.26); R_0 is given by eq. (3.24); J and E are the total angular momentum and total equilibrium energy (2 times eq. [10.6]) of the system.

[b] One asterisk marks the secular instability limit, two the dynamical instability limit.

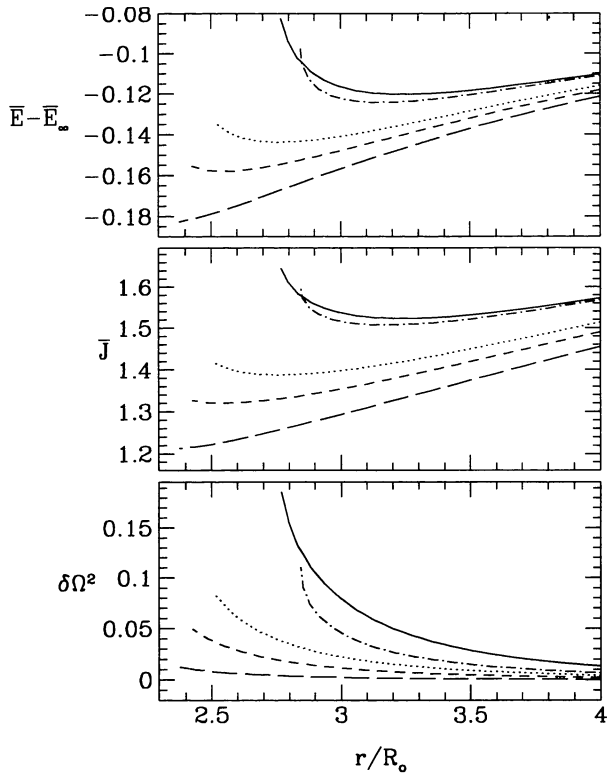

FIG. 17.—Equilibrium curves of total energy ($2 \times$ eq. [10.6]), total angular momentum, and orbital angular frequency as a function of binary separation along the compressible Darwin sequences with $n = 0$ (*solid lines*), $n = 1$ (*dotted lines*), $n = 1.5$ (*short-dashed lines*), and $n = 2.5$ (*long-dashed lines*). The units for E and J are defined in eq. (3.26). The quantity $\bar{E}_\infty \equiv -2(3-n)/(5-n)$ has been subtracted from $\bar{E}$ for convenience. For Ω, the fractional deviation $\delta\Omega^2 \equiv (\Omega^2 - \Omega_K^2)/\Omega_K^2$ from the Keplerian value $\Omega_K^2 = 2GM/r^3$ is shown. The binary separation r is given in units of the radius R_0 of a spherical polytrope with the same mass and entropy (eq. [3.24]). For comparison, we also show the results obtained by Ch69 using the TV method for $n = 0$ (*dotted-dashed lines*).

the surfaces of the two stars are in contact. The last entry for each sequence in Table 12 corresponds to this point of contact.[14] As in the cases of Roche and Roche-Riemann binaries, we see that, for a given separation r, more compressible stars have a smaller deformation.

Figure 17 shows the variation of E, J, and Ω^2 along several Darwin sequences. The curves terminate at the point where the stellar surfaces are in contact. In contrast to the results of §§ 7.2 and 8.2 for Roche and Roche-Riemann binaries, we note here that *not all* equilibrium $E(r)$ and $J(r)$ curves exhibit a minimum. There exists a critical polytropic index $n_{\rm crit} \approx 2.0$ such that the minimum coincides with the point of contact (see § 10.4). As a consequence (cf. §§ 9 and 10.4), when $n > n_{\rm crit}$ (i.e., for sufficiently high compressibility, with $\Gamma \lesssim \frac{3}{2}$), *stable* Darwin configurations can exist all the way until the stars are in contact. For comparison, Figure 17 also shows the curves obtained for $n = 0$ when $\Omega^2 = \Omega_{\rm Ch}^2$ (eq. [10.4]) is used (this reproduces the results of Ch69). We note that the resulting equilibria do not exactly satisfy the relation $dE = \Omega dJ$. In particular, the minima of the equilibrium $J(r)$ and $E(r)$ curves do not coincide when $\Omega^2 = \Omega_{\rm Ch}^2$.

10.3. *Comparison with Other Work*

Recent numerical calculations involving polytropes in synchronized circular binaries have been performed by Hachisu (1986b), using a three-dimensional self-consistent-field method, and by Rasio & Shapiro (1992, 1993), using SPH. To assess the accuracy of our approximations, we have made some detailed comparisons of these numerical treatments with the results of § 10.2.

In Figure 18 we show our predicted variation of $\bar{E}$, $\bar{J}$ and $\bar{\Omega}^2$ as a function of r near the end (point of contact) of the $n = 1$ sequence, compared to the results of SPH simulations. Figure 19 shows equilibrium curves of $\tilde{\Omega}^2$ versus $\tilde{E}$ and $\tilde{J}$ for $n = 0$ and 0.5, compared to the numerical results of Hachisu (1986b). In both cases the agreement is clearly excellent. Most importantly, both numerical treatments, which make no simplifying assumptions concerning the internal structure of the stars or the gravitational field, *confirm the existence of a minimum of $E(r)$ and $J(r)$*. This provides reassurance that the minimum identified here is real, and not the result of our use of the ellipsoidal approximation, or the quadrupole approximation. However, we note that the minimum occurs slightly earlier

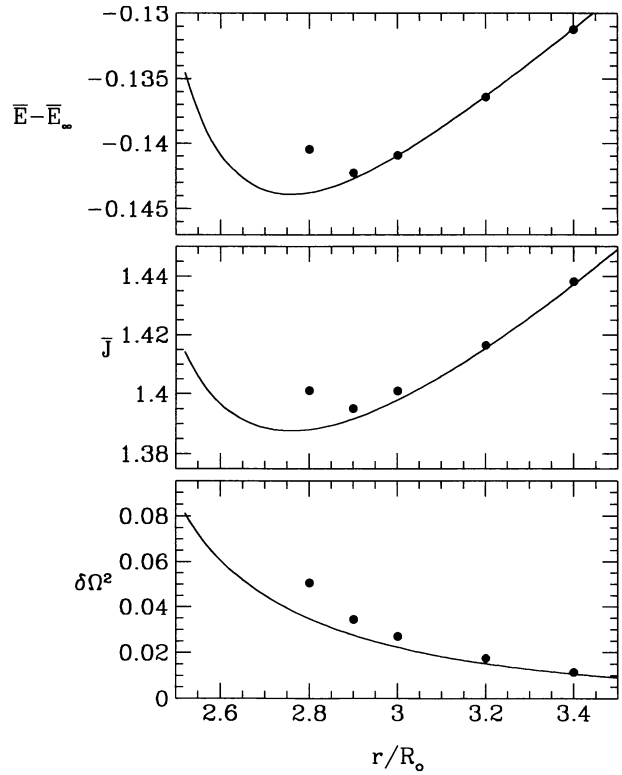

FIG. 18.—Comparison of our predicted equilibrium curves (*solid lines*) for the $n = 1$ Darwin sequence with the results of SPH calculations (*dots*). All quantities are defined as in Fig. 17.

[14] If we formally extend our results past this point, they become incorrect, since expression (10.2) for W_i was written for a detached configuration (cf. Appendix B). However, it is physically possible to construct equilibrium configurations for two overlapping stars and to extend the Darwin sequence smoothly past the point of contact (see Hachisu 1986b).

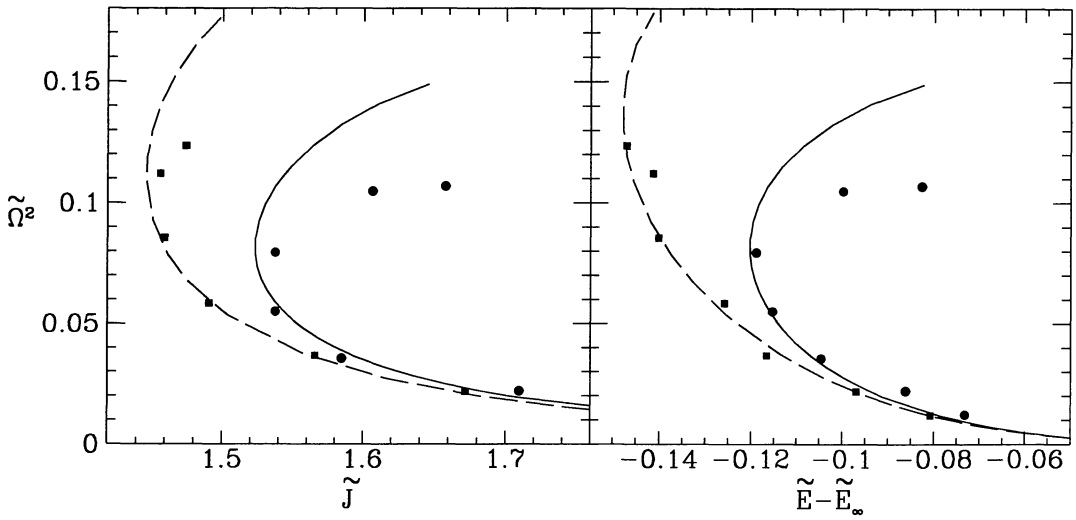

FIG. 19.—Comparison of our predicted equilibrium curves for the $n = 0$ (*solid lines*) and $n = 0.5$ (*dashed lines*) Darwin sequences with the numerical results of Hachisu (1986b) for $n = 0$ (*filled circles*) and $n = 0.5$ (*filled squares*). Here units based on the mean radius R (rather than R_0) have been used, as in Fig. 8, and we have subtracted $\tilde{E}_\infty \equiv -2(3 - n)/(5 - n)$ from $\tilde{E}$ for convenience.

along the sequence in the numerical solutions. This is because the quadrupole approximation underestimates the magnitude of the gravitational interaction energy when the stars are near contact (cf. eq. [10.6]).

10.4. *Stability of Darwin Binaries*

The secular stability of compressible Darwin binaries can be studied exactly as we did in § 9.1 for Roche binaries. As expected from our discussion in § 2.3, we find that the point of onset of secular instability along a Darwin sequence corresponds to the minimum of $E_{eq}(r)$ identified in § 10.2. We can also identify the onset of *dynamical* instability along a Darwin sequence by using the energy function of a "Darwin-Riemann" ellipsoid (the analogue of the Roche-Riemann ellipsoids considered in §§ 8 and 9.2) in condition (2.15). The details will be given elsewhere (Lai, Rasio, & Shapiro 1993b). As in the case of Roche binaries, we find that, when both instabilities occur along a compressible Darwin sequence, $r_{sec} > r_{dyn}$. The values of r_{sec} and r_{dyn}, as well as the corresponding equilibrium parameters, are listed in Table 13. In Table 14 we also give the values of r_{dyn} for the irrotational ($\mathscr{C} = 0$) Darwin-Riemann sequences.

As already noted in § 10.2, there exists a critical polytropic index $n_{crit} \approx 2.0$ such that the secular instability of Darwin binaries disappears when $n > n_{crit}$. For comparison here, the

TABLE 13

STABILITY LIMITS ALONG THE DARWIN SEQUENCES[a]

n [b]	r/a_1	r/R_0	a_2/a_1	a_3/a_1	$T_s/\|W\|$	$\bar{\Omega}$	$\bar{J}$	$\bar{E}$	R/R_0
Secular Stability Limits									
0.0	2.8586	3.2422	0.8573	0.7995	0.229(-1)	0.2861	1.523	-1.3203	1.
0.1	2.8104	3.1905	0.8585	0.8010	0.227(-1)	0.2930	1.510	-1.3061	1.0020
0.5	2.6250	2.9922	0.8641	0.8078	0.219(-1)	0.3221	1.455	-1.2425	1.0112
0.7	2.5357	2.8973	0.8674	0.8119	0.214(-1)	0.3379	1.428	-1.2059	1.0166
0.8	2.4918	2.8508	0.8692	0.8142	0.211(-1)	0.3460	1.415	-1.1863	1.0195
1.0	2.4055	2.7600	0.8731	0.8190	0.205(-1)	0.3629	1.388	-1.1439	1.0260
1.5	2.2004	2.5484	0.8854	0.8344	0.187(-1)	0.4080	1.320	-1.0152	1.0470
2.0	2.0228	2.3782	0.9029	0.8571	0.160(-1)	0.4509	1.256	-0.8397	1.0794
(2.1)	(1.9938)	(2.3540)	(0.9074)	(0.8631)	(0.153(-1))	(0.4575)	(1.244)	(-0.7965)	(1.0883)
Dynamical Stability Limits									
0.0	2.3245	2.8946	0.7556	0.6853	0.374(-1)	0.3488	1.560	-1.3098	1.
0.1	2.2816	2.8495	0.7566	0.6863	0.373(-1)	0.3570	1.547	-1.2953	1.0038
0.5	2.1146	2.6772	0.7609	0.6909	0.367(-1)	0.3916	1.495	-1.2298	1.0218
0.7	2.0329	2.5953	0.7635	0.6936	0.363(-1)	0.4099	1.470	-1.1921	1.0329
(0.8)	(1.9925)	(2.5556)	(0.7650)	(0.6951)	(0.361(-1))	(0.4194)	(1.457)	(-1.1717)	(1.0391)

[a] $\bar{\Omega}$, $\bar{J}$, and $\bar{E}$ are defined in eq. (3.26); R_0 is given by eq. (3.24); J and E are the total angular momentum and total equilibrium energy (2 times eq. [10.6]) of the system.

[b] Data in parentheses indicate that the stars overlap.

TABLE 14

STABILITY LIMITS ALONG THE $\mathscr{C} = 0$ DARWIN-RIEMANN SEQUENCES[a]

n [b]	r/a_1	r/R_0	a_2/a_1	a_3/a_1	$T_s/\|W\|$	$\bar{\Omega}$	$\bar{J}$	$\bar{E}$	R/R_0
0.0	2.5820	3.0368	0.7671	0.8013	0.189(-2)	0.3191	1.291	-1.3521	1.
0.1	2.5334	2.9802	0.7678	0.8019	0.187(-2)	0.3282	1.278	-1.3387	1.0008
0.5	2.3441	2.7592	0.7716	0.8049	0.178(-2)	0.3681	1.228	-1.2790	1.0042
0.7	2.2515	2.6511	0.7738	0.8067	0.173(-2)	0.3907	1.203	-1.2447	1.0063
0.8	2.2056	2.5975	0.7751	0.8077	0.170(-2)	0.4027	1.190	-1.2263	1.0075
1.0	2.1146	2.4913	0.7779	0.8100	0.164(-2)	0.4285	1.165	-1.1866	1.0100
1.2	2.0244	2.3862	0.7812	0.8126	0.157(-2)	0.4569	1.139	-1.1425	1.0130
(1.3)	(1.9798)	(2.3342)	(0.7830)	(0.8141)	(0.153(-2))	(0.4721)	(1.126)	(-1.1186)	(1.0147)

[a] $\bar{\Omega}$, $\bar{J}$, and $\bar{E}$ are defined in eq. (3.26); R_0 is given by eq. (3.24); J and E are the total angular momentum and total equilibrium energy of the system.

[b] Data in parentheses indicate that the stars overlap.

numerical results of Hachisu (1986b) appear to indicate that $n_{\rm crit} \approx 1.5$ (see his Fig. 10). Similarly, we find that the *dynamical* instability of Darwin binaries disappears for sufficiently compressible configurations with $n > n_{\rm dyn} \approx 0.7$. This is in agreement with the results of recent three-dimensional hydrodynamic simulations of polytropes in binaries using SPH (Rasio & Shapiro 1993), which indicate that $n_{\rm dyn} \approx 1$. For $n = 0$, our result $r_{\rm dyn}/R_0 = 2.8946$ (Table 13) is also in remarkable agreement with that of Tassoul (1975), who finds $r_{\rm dyn}/R_0 = 2.8956$ using a TV treatment.[15] This is in contrast to the case of Roche binaries (§ 9), where our result for the dynamical stability limit along an $n = 0$ sequence differs fundamentally from that of Ch69. For the irrotational ($\mathscr{C} = 0$) Darwin-Riemann sequences, we find that the dynamical instability does not exist when $n \gtrsim 1.2$ (see Table 14).

[15] Tassoul (1975) pointed out an error in the original calculation by Ch69, which was corrected in the revised (1987) Dover edition of his work; see also Chandrasekhar (1975).

This work was supported by NSF grant AST 90-15451 and NASA grant NAGW-2364 to Cornell University. Partial support was also provided by NASA through grant HF-1037.01-92A awarded by the Space Telescope Science Institute which is operated by the Association of Universities for Research in Astronomy, Inc., for NASA under contract NAS5-26555. Computations were performed on the Cornell National Supercomputer Facility, a resource of the Center for Theory and Simulation in Science and Engineering at Cornell University, which receives major funding from the NSF and from the IBM Corporation, with additional support from New York State and members of its Corporate Research Institute.

APPENDIX A
SOME USEFUL EXPRESSIONS

Here, for convenience, we give some useful expressions needed to evaluate the determinant appearing in the stability condition (2.15). These are the derivatives of h (eq. [4.10]), $h_\pm$ (eq. [5.12]), and $\mathscr{I}$ (eq. [4.2]) with respect to $\lambda_1 = (a_3/a_1)^{2/3}$ and $\lambda_2 = (a_3/a_2)^{2/3}$.

Consider first

$$h = \frac{2R^2}{a_1^2 + a_2^2} = \frac{2\lambda_1^2\lambda_2^2}{\lambda_1^3 + \lambda_2^3}, \qquad R \equiv (a_1 a_2 a_3)^{1/3}. \tag{A1}$$

Defining

$$h_{(i)} \equiv \frac{\lambda_i}{h}\frac{\partial h}{\partial \lambda_i}, \qquad h_{(ij)} \equiv \frac{\lambda_i \lambda_j}{h}\frac{\partial^2 h}{\partial \lambda_i \partial \lambda_j}, \tag{A2}$$

we have

$$\begin{aligned} h_{(1)} &= 2 - \frac{3\lambda_1^3}{\lambda_1^3 + \lambda_2^3} = \frac{2a_1^2 - a_2^2}{a_1^2 + a_2^2}, \\ h_{(2)} &= \frac{2a_2^2 - a_1^2}{a_1^2 + a_2^2}, \\ h_{(11)} &= h_{(22)} = 2\frac{\lambda_1^6 - 7\lambda_1^3\lambda_2^3 + \lambda_2^6}{(\lambda_1^3 + \lambda_2^3)^2} = 2\frac{a_1^4 - 7a_1^2a_2^2 + a_2^4}{(a_1^2 + a_2^2)^2}, \\ h_{(12)} &= h_{(1)}h_{(2)} + \frac{9\lambda_1^3\lambda_2^3}{(\lambda_1^3 + \lambda_2^3)^2} = h_{(1)}h_{(2)} + \frac{9a_1^2a_2^2}{(a_1^2 + a_2^2)^2}. \end{aligned} \tag{A3}$$

Next, consider

$$h_{\pm} = \frac{2R^2}{(a_1 \mp a_2)^2} = \frac{2}{(\lambda_1^{-1}\lambda_2^{1/2} \mp \lambda_2^{-1}\lambda_1^{1/2})^2} . \tag{A4}$$

We define

$$h_{\pm(i)} \equiv \frac{\lambda_i}{h_{\pm}} \frac{\partial h_{\pm}}{\partial \lambda_i} , \qquad h_{\pm(ij)} \equiv \frac{\lambda_i \lambda_j}{h_{\pm}} \frac{\partial^2 h_{\pm}}{\partial \lambda_i \partial \lambda_j} \tag{A5}$$

and obtain

$$\begin{aligned} h_{\pm(1)} &= \frac{2a_1 \pm a_2}{a_1 \mp a_2} , \\ h_{\pm(2)} &= \frac{2a_2 \pm a_1}{a_2 \mp a_1} , \\ h_{\pm(11)} &= h_{\pm(22)} = \frac{4a_1^2 \pm 19a_1a_2 + 4a_2^2}{2(a_1 \mp a_2)^2} , \\ h_{\pm(12)} &= 1 - \frac{6(a_1 \pm a_2/2)(\pm a_2 + a_1/2)}{(a_1 \mp a_2)^2} . \end{aligned} \tag{A6}$$

Finally, consider

$$\mathcal{I} = a_1^2 A_1 + a_2^2 A_2 + a_3^2 A_3 . \tag{A7}$$

Defining

$$\mathcal{I}_{(i)} \equiv \frac{\lambda_i}{\mathcal{I}} \frac{\partial \mathcal{I}}{\partial \lambda_i} , \qquad \mathcal{I}_{(ij)} \equiv \frac{\lambda_i \lambda_j}{\mathcal{I}} \frac{\partial^2 \mathcal{I}}{\partial \lambda_i \partial \lambda_j} , \tag{A8}$$

we have

$$\begin{aligned} \mathcal{I}_{(1)} &= \frac{1}{2\mathcal{I}} (3a_1^2 A_1 - \mathcal{I}) , \\ \mathcal{I}_{(2)} &= \frac{1}{2\mathcal{I}} (3a_2^2 A_2 - \mathcal{I}) , \\ \mathcal{I}_{(11)} &= \frac{3}{4\mathcal{I}} (-9a_1^2 B_{11} + a_2^2 A_2 + a_3^2 A_3) , \\ \mathcal{I}_{(22)} &= \frac{3}{4\mathcal{I}} (-9a_2^2 B_{22} + a_1^2 A_1 + a_3^2 A_3) , \\ \mathcal{I}_{(12)} &= \frac{1}{4\mathcal{I}} (9a_1^2 a_2^2 A_{12} - 2a_1^2 A_1 - 2a_2^2 A_2 + a_3^2 A_3) . \end{aligned} \tag{A9}$$

To derive expressions (A9), various relations between the index symbols A_i, A_{ij}, and B_{ij} given in chapter 3 of Ch69 have been used.

APPENDIX B
INTERACTION ENERGY

Consider a binary system consisting of two ellipsoidal stars with masses M and M'. By definition their gravitational interaction energy is given by

$$W_i = \frac{1}{2} \int_V \rho \Phi'^{\text{ext}} d^3x + \frac{1}{2} \int_{V'} \rho' \Phi^{\text{ext}} d^3x' , \tag{B1}$$

where $\Phi^{\rm ext}$ and $\Phi'^{\rm ext}$ are the gravitational potentials due to M and M'. Momentarily focus on the star of mass M and introduce two coordinate systems: (x_i), centered on that star, and (X_i) centered on its companion. Both x_1 and X_1 are measured along the axis of the binary, increasing from M' toward M, while x_3 and X_3 are along the rotation axis. To quadrupole order, and denoting by P the center of mass of M, at $\boldsymbol{X} = (r, 0, 0)$, we have

$$\Phi'^{\rm ext}(\mathbf{X}) = \Phi'^{\rm ext}(P) + (X_1 - r)\Phi'^{\rm ext}_{,1}(P) + \tfrac{1}{2}(X_1 - r)^2\Phi'^{\rm ext}_{,11}(P) + \tfrac{1}{2}X_2^2\Phi'^{\rm ext}_{,22}(P) + \tfrac{1}{2}X_3^2\Phi'^{\rm ext}_{,33}(P)\,, \tag{B2}$$

where we are indicating derivatives with respect to X_i by a comma. A similar expression can be written for $\Phi^{\rm ext}(\boldsymbol{X}')$. Insertion into equation (B1) then gives

$$W_i = \tfrac{1}{2}M\Phi'^{\rm ext}(P) + \tfrac{1}{4}\Phi'^{\rm ext}_{,ij}(P)I_{ij} + \tfrac{1}{2}M'\Phi^{\rm ext}(P') + \tfrac{1}{4}\Phi^{\rm ext}_{,ij}(P')I'_{ij}\,, \tag{B3}$$

where

$$I_{ij} = \int_V \rho x_i x_j d^3x = \frac{1}{5}\kappa_n a_i^2 M\delta_{ij} \qquad \text{(no summation)} \tag{B4}$$

is the quadrupole tensor of M (cf. eq. [4.8], where $I = I_{11} + I_{22}$), and a similar expression gives I'_{ij} for M'. Here, in evaluating expression (B1), we have made explicit use of the triplanar symmetry of the two ellipsoidal configurations. We now expand $\Phi'^{\rm ext}(\boldsymbol{X})$, $\Phi^{\rm ext}(\boldsymbol{X}')$ and their derivatives to quadrupole order,

$$\Phi'^{\rm ext}(\boldsymbol{X}) = -\frac{GM'}{r} - \frac{1}{2}G(3I'_{lm} - I'_{kk}\delta_{lm})\frac{X_l X_m}{r^5}\,, \tag{B5}$$

$$\Phi'^{\rm ext}_{,ij}(\boldsymbol{X}) = -\frac{GM'}{r^5}(3X_iX_j - r^2\delta_{ij})\,, \tag{B6}$$

and similar expressions for $\Phi^{\rm ext}(\boldsymbol{X}')$ and $\Phi^{\rm ext}_{,ij}(\boldsymbol{X}')$. Evaluating these expressions at $\boldsymbol{X} = (r, 0, 0)$ we obtain from equation (B3),

$$W_i = -\frac{GMM'}{r} - \frac{1}{2}\frac{GM'}{r^3}(2I_{11} - I_{22} - I_{33}) - \frac{1}{2}\frac{GM}{r^3}(2I'_{11} - I'_{22} - I'_{33})\,. \tag{B7}$$

The dependence of W_i on ρ_c, ρ'_c, and λ_1, λ_2, λ'_1, λ'_2 can be made explicit by writing, in analogy with equations (4.7)–(4.9),

$$I_{jj} = \frac{h_j(\lambda_1, \lambda_2)}{4k_3}M^{5/3}\rho_c^{-2/3}\,, \tag{B8}$$

where

$$h_1 \equiv \frac{\lambda_2}{\lambda_1^2}\,, \qquad h_2 \equiv \frac{\lambda_1}{\lambda_2^2}\,, \qquad h_3 \equiv \lambda_1\lambda_2\,, \tag{B9}$$

and similar expressions for I'_{ij} and h'_j.

APPENDIX C
ROTATION LAW IN THE TENSOR VIRIAL METHOD

In our energy variational method, the orbital angular velocity of a binary system is naturally given by equation (7.6), that is,

$$\Omega^2 = \left(\frac{1+p}{Mr}\right)\frac{\partial W_i}{\partial r}\,, \tag{C1}$$

where $p = M/M'$ is the mass ratio, r is the binary separation, and W_i is the gravitational interaction energy, equation (B1). This result is physically intuitive: it states that the centrifugal force acting on the center of mass of M is the gradient of the interaction energy between M and M'. However, Ω given by equation (C1) is different from the value usually assumed in the tensor virial (TV) treatment (see, e.g., Ch69, § 55, where the Keplerian value is used for the Roche problem). Here we show that, with appropriate application of the TV equations, expression (C1) can also be derived.

Consider the fundamental hydrostatic equilibrium equation governing the fluid elements of M in a rotating coordinate frame centered on M. The component of this equation along the x-axis, pointing from M to M', is given by

$$0 = -\frac{\partial P}{\partial x} + \rho \frac{\partial}{\partial x}\left[-\Phi - \Phi' + \frac{1}{2}\Omega^2(x - r_{\rm cm})^2\right], \tag{C2}$$

where Φ and Φ' are the gravitational potentials due to M and M', respectively, and $r_{\rm cm} = r/(1+p)$ is the distance from the center of mass of the binary to the center of mass of M. Equation (C2) is the x-component of equation (8.1) in Ch69, where we have set the internal velocity in the rotating frame $\boldsymbol{u} = 0$ in seeking a stationary state. In applying the TV method, the self-consistent value of Ω should be determined from the virial equation of the *first* order (Ch69, eq. [2.42]), which is obtained by simply integrating the above equation over the volume occupied by the fluid. Since

$$\int d^3x \frac{\partial P}{\partial x} = 0 = \int d^3x \rho \frac{\partial \Phi}{\partial x}, \tag{C3}$$

we have

$$-\int d^3x \rho \Omega^2 (x - r_{\rm cm}) = M r_{\rm cm} \Omega^2 = \frac{M r \Omega^2}{(1+p)} = -\int d^3x \rho \frac{\partial \Phi'}{\partial x}. \tag{C4}$$

But the last expression in equation (C4) may be rewritten as

$$\int d^3x \rho(\boldsymbol{x}) \frac{\partial}{\partial x} \int d^3x' \frac{G\rho'(\boldsymbol{x}')}{|\boldsymbol{x} - \boldsymbol{x}' - \boldsymbol{r}|} = -\frac{\partial}{\partial r} \int d^3x \int d^3x' \frac{G\rho(\boldsymbol{x})\rho'(\boldsymbol{x}')}{|\boldsymbol{x} - \boldsymbol{x}' - \boldsymbol{r}|} = \frac{\partial}{\partial r} W_i, \tag{C5}$$

where $\rho(\boldsymbol{x})$ and $\rho'(\boldsymbol{x}')$ are the density profiles in M and M', respectively, and $\boldsymbol{r}$ is the separation vector from the center of M to the center of M'. Equating (C4) and (C5) we thus recover equation (C1) within the TV approach. For a single star, the virial equation of the first order simply gives the uniform motion of the center of mass; for a binary, it is the equation from which Ω should be determined self-consistently. The analysis given in Ch69 (§§ 55 and 61) does not take advantage of this point. We note that the use of expression (C1) for Ω does not affect the form of the virial equations of the *second* order, from which the equilibrium configuration is determined: "unwanted" (linear) terms in the equilibrium equation of motion due to the use of expression (C1) vanish when integrated to obtain the second-order virial equations. Thus the structure equations given in Ch69 for incompressible Roche and Darwin ellipsoids are unchanged, except that expression (C1) should be used for Ω in these equations.

Recalling equation (B1) or (B7) for W_i, we note that expression (C1) for Ω is symmetric with respect to exchange of M and M'. This symmetry guarantees the existence of solutions to the Darwin problem for *arbitrary* values of the mass ratio p (in § 10 we solve the Darwin problem for the special case $p = 1$). By contrast, the expression for $\Omega = \Omega_{\rm Ch}$ adopted in the standard TV analysis (eq. [10.4]) is only symmetric when $p = 1$ and in the limiting case where $p \to 0$. Only for these special cases will the Darwin problem yield consistent solutions if $\Omega = \Omega_{\rm Ch}$, as pointed out by Ch69.

APPENDIX D
RELATION BETWEEN E, J, AND $\mathscr{C}$ ALONG EQUILIBRIUM SEQUENCES

Here we show how the general result (Ostriker & Gunn 1969)

$$dE = \Omega dJ \tag{D1}$$

along an equilibrium sequence of uniformly rotating configurations of fixed mass and entropy can be generalized to Riemann-S and Roche-Riemann ellipsoidal configurations. Following Ostriker & Gunn (1969), we write

$$dE = \left.\frac{\partial E}{\partial J}\right|_{\alpha_i, \mathscr{C}} dJ + \left.\frac{\partial E}{\partial \mathscr{C}}\right|_{\alpha_i, J} d\mathscr{C} + \sum_k \left.\frac{\partial E}{\partial \alpha_k}\right|_{\alpha_i \neq \alpha_k, J, \mathscr{C}} d\alpha_k, \tag{D2}$$

where (α_i) denotes the independent variables, $(\lambda_1, \lambda_2, R)$ or $(\lambda_1, \lambda_2, \rho_c)$. Along an equilibrium sequence we have $(\partial E/\partial \alpha_k) = 0$ so that the last term in expression (D2) vanishes. For Riemann-S ellipsoids we recall (§ 5.1) that the kinetic energy can be written $T = T_+ + T_-$ with (cf. eqs. [5.6] and [5.11])

$$T_\pm = \frac{(J \pm \mathscr{C})^2}{\frac{4}{5}\kappa_n M(\alpha_1 \mp a_2)^2} \tag{D3}$$

and

$$J \pm \mathscr{C} = \tfrac{1}{5}\kappa_n M(a_1 \mp a_2)^2(\Omega \pm \Lambda)\,. \tag{D4}$$

Therefore we have

$$\left.\frac{\partial E}{\partial J}\right|_{\alpha_i,\mathscr{C}} = \left.\frac{\partial T}{\partial J}\right|_{\alpha_i,\mathscr{C}} = \frac{2T_+}{(J+\mathscr{C})} + \frac{2T_-}{(J-\mathscr{C})}$$
$$= \frac{1}{2}(\Omega+\Lambda) + \frac{1}{2}(\Omega-\Lambda)$$
$$= \Omega\,, \tag{D5}$$

and

$$\left.\frac{\partial E}{\partial \mathscr{C}}\right|_{\alpha_i,J} = \left.\frac{\partial T}{\partial \mathscr{C}}\right|_{\alpha_i,J} = \frac{2T_+}{(J+\mathscr{C})} - \frac{2T_-}{(J-\mathscr{C})}$$
$$= \frac{1}{2}(\Omega+\Lambda) - \frac{1}{2}(\Omega-\Lambda)$$
$$= \Lambda\,, \tag{D6}$$

Substituting into equation (D2) then gives the desired result,

$$dE = \Omega dJ + \Lambda d\mathscr{C} \tag{D7}$$

along a Riemann-S sequence. Using equations (8.1) and (8.2) it is straightforward to show that the same result holds along Roche-Riemann binary sequences.

REFERENCES

Aizenman, M. L. 1968, ApJ, 153, 511
Bailyn, C. D. 1993, in Dynamics of Globular Clusters: a Workshop in Honor of Ivan R. King, ed. S. Djorgovski & G. Meylan, ASP Conference Series, in press
Bardeen, J. M., Friedman, J. L., Schutz, B. F., & Sorkin, R. 1977, ApJ, 217, L49
Bodenheimer, P., & Ostriker, J. P. 1973, ApJ, 180, 159
Carter, B., & Luminet, J.-P. 1985, MNRAS, 212, 23
Chandrasekhar, S. 1939, An Introduction to the Study of Stellar Structure (Chicago: Univ. Chicago Press)
———. 1969, Ellipsoidal Figures of Equilibrium (New Haven: Yale Univ. Press) (Ch69); Equation numbers given in this paper refer to the revised 1987 Dover edition
———. 1975, ApJ, 202, 809
Chau, W. Y., Cheng, K. S., & Zhang, J. L. 1992, ApJ, 390, 486
Clark, J. P. A., & Eardley, D. M. 1977, ApJ, 215, 311
Colpi, M., Shapiro, S. L., & Teukolsky, S. A. 1991, ApJ, 369, 422
Cook, G. B., Shapiro, S. L., & Teukolsky, S. A. 1992, ApJ, 398, 203
Cox, J. P. 1980, Theory of Stellar Pulsation (Princeton: Princeton Univ. Press)
Eggleton, P. P. 1983, ApJ, 268, 368
Friedman, J. L., Ipser, J. R., & Sorkin, R. D. 1988, ApJ, 325, 722
Hachisu, I. 1986a, ApJS, 61, 479
———. 1986b, ApJS, 62, 461
Hachisu, I., & Eriguchi, Y. 1982, Prog. Theor. Phys., 68, 206
———. 1984a, PASJ, 36, 239
———. 1984b, PASJ, 36, 259
Hachisu, I., Eriguchi, Y., & Sugimoto, D. 1982, Prog. Theor. Phys., 68, 191
Hunter, C. 1977, ApJ, 213, 497
Hurley, M., & Roberts, P. H. 1964, ApJ, 140, 583
———. 1965, ApJS, 11, 95
Ipser, J. R., & Lindblom, L. 1990, ApJ, 355, 226
James, R. A. 1964, ApJ, 140, 552
Kochanek, C. S. 1992a, ApJ, 385, 604
———. 1992b, ApJ, 398, 234
Kopal, Z. 1959, Close Binary Systems (London: Chapman & Hall)
Lai, D., Rasio, F. A., & Shapiro, S. L. 1993a, ApJ, 406, L63
———. 1993b, in preparation
Lebovitz, N. R. 1966, ApJ, 145, 878
Luminet, J.-P., & Carter, B. 1986, ApJS, 61, 219
Martin, P. G. 1970, Ap. & Space Sci., 7, 119
Miller, B. D. 1974, ApJ, 187, 609
Monaghan, J. J., & Roxburgh, I. W. 1965, MNRAS, 131, 13
Nakamura, T., & Oohara, K. 1989, Prog. Theor. Phys., 82, 1066
Naylor, M. D. T., & Anand, S. P. S. 1970, in Stellar Rotation, ed. A. Slettebak (Dordrecht: Reidel)
Ostriker, J. P., & Gunn, J. E. 1969, ApJ, 157, 1395
Ostriker, J. P., & Mark, J. W.-K. 1968, ApJ, 151, 1075
Paczyński, B. 1971, ARA&A, 9, 183
Rasio, F. A. 1993, in Proc. STScI Workshop on Blue Stragglers, ed. M. Livio & R. Saffer, ASP Conference Series, in press
Rasio, F. A., & Shapiro, S. L. 1992, ApJ, 401, 226
———. 1993, in preparation
Riemann, B. 1860, Abh. Königl. Gesell. Wiss. Göttingen, 9, 3
Roberts, P. H. 1963a, ApJ, 137, 1129
———. 1963b, ApJ, 138, 809
Shapiro, S. L., & Teukolsky, S. A. 1983, Black Holes, White Dwarfs, and Neutron Stars (New York: Wiley) (ST)
Shapiro, S. L., Teukolsky, S. A., & Nakamura, T. 1990, ApJ, 357, L17
Tassoul, J.-L. 1970, ApJ, 160, 1031
———. 1978, Theory of Rotating Stars (Princeton: Princeton Univ. Press)
Tassoul, J.-L., & Tassoul, M. 1971, ApJ, 166, 621
Tassoul, M. 1975, ApJ, 202, 803
van't Veer, F. 1979, A&A, 80, 287
Zel'dovich, Y. A. B., & Novikov, I. D. 1971, Relativistic Astrophysics, Vol. 1 (Chicago: Univ. Chicago Press) (ZN)